Design and development of advanced vibration and noise control devices using finite element analysis

Ashwini Gautam

Thesis submitted to the Faculty of the Virginia Polytechnic Institute and State University in partial fulfillment of the requirements for the degree of

Masters of Science
in
Mechanical Engineering

Dr Chris Fuller
Dr Jamie Carneal
Dr Marty Johnson

December 14th 2005
Blacksburg, Virginia

Keywords: Distributed vibration absorbers (DVA's), Heterogeneous blankets (HG) and porous media,

Design and development of advanced vibration and noise control devices using finite element analysis

Ashwini Gautam

Abstract

The high sound pressure levels (SPL's) radiated inside the payload fairing by its vibrating frame causes 40% of the satellite damage in the initial phases of the launch. Numerous experiments conducted on the advanced vibration absorbers such as the distributed vibration absorbers (DVA's) and the heterogeneous blankets (HG blankets) have shown great potential in reducing the vibration levels and the SPL's inside the payload fairings. Despite their good performance, little is known about the detailed mechanisms by which it is achieved. In addition, these vibration absorbers are currently empirically and experimentally designed which is a very cumbersome and time consuming process. To overcome the aforementioned limitations, there is a need for development of numerical techniques to understand the physics behind their functionality and to study the influence of the geometric layout or the choice of materials on their performance.

This work presents the development and validation of the finite element (FE) models to understand the physics behind the functionality of these vibration absorbers. The development of these FE models can be broadly classified in to three stages. In the first stage, the FE models of the individual components was developed and validated. In second stage, the fully coupled 3D-FE models of the advanced vibrations absorbers such

as the DVA's and the HG blankets were validated. Finally, fully coupled 3D-FE models of these vibration absorbers coupled to the structural and acoustics domains were validated

Parametric studies were performed on these fully coupled 3D-FE models in order to understand the effect of the variation in the material properties and geometrical configuration of these vibration absorbers on their response and also on their vibro acoustic attenuation capabilities. The knowledge base built from the parametric studies was later used for the development of the optimized designs of these vibration absorbers.

Acknowledgements

I would like to thank my research advisor, Professor Chris Fuller, for providing me the opportunity to work on a challenging problem. Working with him has been a learning experience that I would cherish for the rest of my life.

I would like to thank my committee member Dr Jamie Carneal as he has advised me whenever I required his help. He has played a pivotal role in the completion of this research. I would also like to thank Professor Marty Johnson for the quality of education and the advice that he provided.

I am also thankful to Dr Rakesh Kapania for his extensive support in the development of the numerical techniques used in this research work

I am indebted to the Boeing Company and NASA for jointly supporting this research work. I would specially like to thank Haisam Osman and Gopal Mathur for there keen interest in my research and for the encouragement provided by them.

I would like to pay homage to my Spiritual Teacher and my parents, who have always been there for me and who have shown the light to me in the times of utter darkness and despair.

This work has been possible by the great support of all these aforementioned people and with a little bit of my effort as well.

INDEX

FIGURES

TABLES

NOMENCLATURE

E	Modulus of elasticity of the plate
ν	Poisson's ratio
ρ_1	Porous media density
ρ_2	Density of Aluminum
η	Porous medium loss factor
φ	Porosity of the porous media
σ	Porous medium flow resistivity
α_∞	Porous medium tortuosity
Λ	Porous medium viscous characteristics dimension
Λ'	Porous medium thermal characteristics dimension
$\{n\}$	Normal component
ω	Frequency (rad/s)
Δ	Gradient
h	Thickness
p	Pressure
c	Velocity of sound
w	Normal displacement
k_s	Tortuosity of the porous media
Ω_p	Number of elements used for the discretization
$[]^T$	Transpose of the matrix
$[N]$	Shape function matrix
$[N']$	Differential of the shape function matrix
a, b	Dimensions of the plate elements
$\sigma_x, \sigma_y, \sigma_z$	Stress in the x,y and the z direction
ρ_1	Density of the solid phase of the porous media
ρ_0	Density of the fluid phase of the porous media

1 Introduction

1.1 Motivation for the research

Over the years there has been marked development in the noise control techniques using various materials and noise control devices for reducing the sound inside the payload fairing. However the control of payload interior noise remains a challenging problem. With the advent of the new composites payload structures promising lighter and more cost effective satellite launches, there comes the bane of high interior noise in the payload fairings causing acoustically induced satellite damage. The primary source of the interior payload noise is the sound radiated by air borne vibration induced in the flexible structures of the payload. These structure being efficient radiators of sound cause the sound pressure level (SPL) to rise in the payload interior. Thus one of the main approaches for sound attenuation in payload fairings is the control of the efficient radiating modes of the payload structure surrounding it. The use of the standard passive treatments such as acoustical blankets, viscoelastic damping and constraining layers are proving ineffective in meeting the sound attenuation requirements posed by the use of new composite payload fairing. To overcome these constraints of the conventional passive treatments there is an impending need for the design and development of optimized light weight devices that combine together in an efficient manner different features of noise control to meet the challenge of reducing interior payload noise.

The techniques used for the vibration control of flexible structures (panels and plates) and noise induced by them into the coupled acoustic cavities can be broadly divided into three categories: passive, reactive and active.

Passive devices use friction to dissipate the vibration energy and acoustic energy into heat. Passive treatments such as acoustic foam blankets and constrained layer damping work well at high frequencies, but are not equally effective at the low frequencies. The passive treatments are not effective at lower frequencies because the acoustic wavelengths are longer at these frequencies and hence thicker foam blanket are required to provide high material damping properties to result in an effective vibration and acoustic attenuation.

Reactive noise control techniques such as the Helmholtz resonators and tuned vibration absorbers, work by creating high impedance in a narrow frequency bandwidth. These devices are good for low frequency noise and vibration attenuation but only in a very narrow frequency range. In addition to the aforementioned problems, the major disadvantage encountered in the use of the reactive devices for vibration control of continuous structures is that they act at a single point and hence a large quantity of these vibration absorbers is required for effectively controlling the dynamics of a large continuous structure

Active control devices work by generating an out of phase signal to cancel the noise field by destructive interference. In an active control mechanism, sensors are used to measure the vibration levels of the structure to be cancelled and the actuators are used to generate a counter signal to cancel the noise field. These systems generally have a high operating and maintenance cost. Furthermore, they require additional equipment for functioning, which increases their mass and space occupancy.

In order to over come the aforementioned constraints encountered in the use of the existing noise and vibration control devices, distributed vibration absorber (DVA) and the heterogeneous blanket (HG) were developed in Vibration and Acoustics Laboratories (VAL) at Virginia Tech. Extensive experiments have indicated that the use of the DVA and the HG blankets can significantly reduce the interior noise in the launch vehicle payload fairings in the 50-200 Hz low frequency bandwidth with only a marginal(less then 10%) increase in the total weight of the payload fairings. Other tests at NASA on the tilt rotor fuselage and on Boeing 757 fuselage section have also shown large increase in the tonal and broad band transmission loss with these lightweight treatments. There are two primary reasons for the improved performance of these vibration absorbers. First, these vibration absorbers are distributed over a surface area and hence provide the reactive force over a distributed area rather then on a point. Second, due to the presence of the foam in these vibration absorbers, they act both as a vibration absorber at the tuned frequency and also provide high damping at all the acoustic modes of the structure. These properties of the advanced vibration absorbers lead to a broadband attenuation of the vibration levels of the base structure and the SPL’s inside the radiating acoustic domain. The physical implementation of these devices is now discussed.

The DVA, shown in Figure 1 a), is made of spatially distributed foam layer attached to a flexible structure (mass layer). The DVA having a spatially distributed mass layer attached to the porous media acts as a spring mass damper system. HG blankets, shown in Figure 1 b), comprise of a foam layer having mass in-homogeneities inside it. The foam acts as a damped spring with distributed mass and the mass in-homogeneities act as the additional point masses inside the foam layer increasing its vibration absorption capabilities.

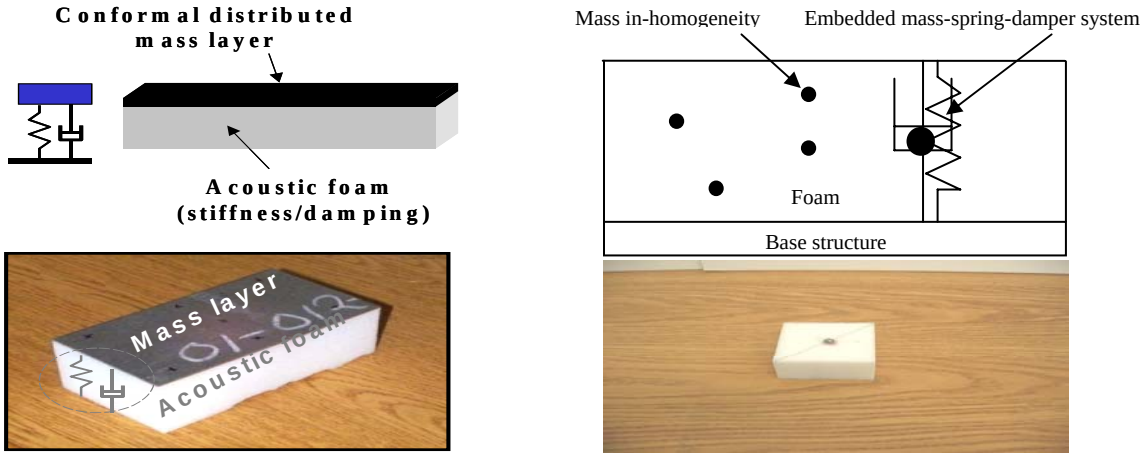

Figure 1. a) Distributed vibration absorber (DVA), b) Heterogeneous Blankets (HG-Blanket)

In spite of the good performance of the DVA and HG blankets in controlling the noise and vibration magnitudes, little is known of the specifics of how it is achieved. The influence of the geometric layout, choice of material and device attachments on the behavior of these devices is also poorly understood. In order to optimize the design of the DVA and the HG blankets and realize their full potential for vibro-acoustic attenuation control, a detailed understanding is required of the physics behind their behavior and the influence of the controlling parameters on their vibro-acoustic attenuation capabilities.

To achieve the aforementioned insight in the functionality of these advanced noise and vibration control devices, detailed finite element (FE) models of the DVA and the HG blankets were developed and validated. Based on the knowledge base built by the validation of these numerical models, advanced fully coupled FE models were developed to study the interaction of these devices with the structural and the acoustic domains. These numerical models would enable the development of advanced designs of these

noise control devices in order to efficiently and effectively control the noise radiated inside the acoustic cavity by the coupled vibrating structures.

1.2 Background on the vibration absorbers

This section presents the mathematical concepts behind the functioning of the dynamic vibration absorbers. The vibration and noise control devices implemented in this research, the distributed vibration absorber (DVA) and the heterogeneous blankets (HG blankets) are distributed versions of the point dynamic vibration absorber. Therefore a review of these fundamental concepts is presented.

The concept of the dynamic vibration absorber was introduced by Frahm [1]. The absorber, for which he filed the first US patent in 1911 entitled “Devices for damping vibration bodies”, is depicted in Figure 1. The inertial and damping affects of the absorber mass reduces the vibration levels of the base structure by applying a reactive force and damping at its point of attachment on the base structure. The mathematical model of the dynamic vibration absorber attached to a single degree of freedom base structure given by Esteve [2] is of the form

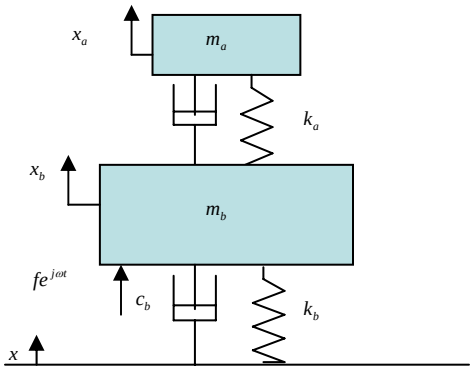

Figure 2. Point dynamic vibration absorber

$$\begin{aligned} m_b\ddot{x}_b + (k_b + k_a)x_b - k_a x_a + (c_b + c_a)\dot{x}_b - c_a\dot{x}_a &= f(t) \\ m_a\ddot{x}_a + k_a(x_a - x_b) + c_a(x_a - x_b) &= 0 \end{aligned} \tag{1}$$

In equation (1) m_b, m_a are the masses of the base structure and the absorber respectively. The stiffness values for the springs attached to the base structure and the absorber are represented by k_b, k_a respectively and c_b, c_a represent the damping ratio values for the base structure and the absorber respectively. The $fe^{j\omega t}$ is the excitation force on the base

structure and x_b, x_a are the displacements of the base structure and the absorber respectively. The natural frequencies and the damping ratio of the second order of system given in Figure 2 are respectively

$$\omega = \sqrt{\frac{k}{m}} \qquad \xi = \frac{c}{2m\omega} \tag{2}$$

In Equation (2) ω represents the resonance frequency and ξ represents the damping ratio of a spring mass system respectively. The impedance of the base structure without the dynamic vibration mass absorber is given by

$$Z_b = \frac{mb({\omega^2}_b - \omega^2 - 2j\omega\omega_b\xi_b)}{-j\omega} \tag{3}$$

The free velocity of the base structure is given by

$$\dot{x}_b = \frac{f}{Z_b} \tag{4}$$

The impedance of the dynamic vibration absorber is defined as the reactive force acting on the base structure due to a unit velocity of its point of attachment on the base structure. The absorber impedance is given by

$$Z_a = m_a \frac{j\omega{\omega^2}_a + 2\xi_a\omega^2\omega_a}{({\omega^2}_a - \omega^2) - 2j\xi_a\omega\omega_a} \tag{5}$$

In Equation (5) ω_a represents the resonance frequency of the absorber.

The resulting response of the base structure is due to the dual affect of the inertial effects of the absorber mass and the external excitation force on the base structure. The resulting velocity of the base structure is given by

$$\begin{aligned} \dot{x}_b &= \frac{f + Z_a\dot{x}_b}{Z_b} = \dot{x}_o + \frac{Z_a\dot{x}_b}{Z_b} \\ \dot{x}_b &= \dot{x}_o\left[1 - \frac{Z_a}{Z_b}\right]^{-1} \end{aligned} \tag{6}$$

From equation (6) it is evident that the effect dynamic vibration absorber on the base structure is due to the mismatch in the absorber and the base structure impedance. Thus

for the optimum effectiveness of the dynamic vibration absorber in controlling the vibration levels of the base structure larger mismatch in the absorber and base structure impedance is desired.

1.3 Literature review

The concept of the Tuned vibration absorbers (TVA's) was presented for the first time by Frahm in 1911[1]. Extensive study was done on the tuned vibration absorber by Den Hartog [3]. The study involved examining the affect of the change of the ratio of the absorber mass and the base structure mass and the addition of damping to the spring on the vibration response of the base structure. It was concluded from this paper that a higher mass ratio provided larger reduction in the vibration levels of the base structure. Furthermore, the addition of the damping to the absorber spring provided broadband attenuation though reducing its vibration attenuation capabilities.

Based on the concept of the TVA, many variants of the vibration absorber were developed such as the adaptive TVA's and the active TVA's. An adaptive TVA tracks the disturbance and tunes the resonance frequency of the TVA to counter the disturbance of the base structure. A robust tuning strategy for the TVA was developed by Franchek et.al [4]. One of the major conclusions of this paper was that in the adaptive TVA design where the controller tracks the optimal tuned frequency, the determination of the tuning direction could be ambiguous and hence care is required to ensure proper convergence of the tuning algorithm.

Active TVA's were developed using an actuator to produce an oscillating control force that interferes with the disturbing force from the vibrating structure. Huang and Lian [5] developed a 2-DOF active TVA. The TVA consisted of 2 DC motors with eccentric masses in order to provide oscillating control forces. Using this approach with a simple PID controller, they enhanced vibration attenuation over a passive TVA. A hybrid TVA combining the adaptive and active concepts was developed by Yasuda et al. [6]. This paper presented the control of the floor vibration using the hybrid TVA.

There is ample literature on the application of the TVA on the vibration and sound radiation control of the flexible structures. Passive TVA's were used for vibration control of the panels by Jolly and Sun [7]. Huang and Fuller [8, 9] developed a model to analyze

the use of the tuned vibration absorbers (TVA's) for interior aircraft noise attenuation. A detuned TVA approach was suggested to reduce the interior noise of the propeller aircraft by Fuller et al. [10]. This paper showed that the globally detuning of the TVA leads to an increase in sound attenuation.

The use of Multiple TVA's tuned to slightly different frequencies was proposed by Joshi and Jangid [11] for controlling the vibration levels of the flexible structures excited by white noise disturbance. The paper presented the optimized values of the damping ratio, the tuned frequencies and the frequency bandwidth to minimize the root mean square displacement of the structure.

A distributed vibration absorber using a beam as the mass layer to control the vibration of the base beam was proposed by Aida et.al. [12]. The boundary conditions of the top layer (beam) were similar to the boundary conditions of the base beam and they were both connected by a set of discrete spring and dampers. Following, they developed similar vibration absorbers for the plates [13]. These vibration absorbers though having distributed mass layers can not be termed distributed vibration absorbers in the true sense as they have the discrete sets of springs and dampers.

All the aforementioned research work on the modified versions of the TVA's resulted in the development of advanced designs of the TVA's to cater to specific noise and vibration control problems. These advanced TVA's had enhanced damping capabilities, but all had the fundamental shortcomings of a dynamic vibration absorbers such as requirements of large quantities, short life spans and limited effective working bandwidths.

To counter the shortcomings of the aforementioned vibration and noise control devices a distributed active vibration absorber (DAVA) was developed by Cambou [14] at the Vibration and Acoustics Laboratories (VAL) in Virginia Tech. DAVA consisted of a sinusoidal PVDF layer with an optimal mass distribution on the top of it. A distributed modal actuator was created and good attenuations were obtained for both the passive and the active versions. However, the sinusoidal PVDF layer acted as a rigid elastic layer having high stiffness and thus large mass layer were required for obtaining attenuations in the low frequency bandwidth.

The successful development of the DAVA's to achieve high frequency broadband attenuation was followed by the development of the DVA's and the HG blankets in order to achieve effective and efficient attenuation at the low frequencies. These vibration absorbers were designed to act as distributed vibration absorbers providing both active and passive damping on their surface of attachment to the base structure. Experimental and analytical models of these vibration absorbers have been developed. These models have shown that these noise control devices exhibit great promise in solving the noise and the vibration control problem in the low frequency bandwidth. These models though effective in demonstrating the utility of the DVA's and the HG blankets as noise control devices are incapable of developing advanced designs for the same as these studies are both cumbersome and expensive to conduct. To overcome the aforementioned shortcomings detailed numerical models (finite element) are required to understand the physics behind functionality of these vibration and noise control devices and to develop advanced designs for the same.

1.4 Advanced Vibration absorbers

After discussing the work done in the past on the development of advanced vibration absorbers, this section would discuss the advanced vibro-acoustic attenuation devices such as the DVA's and the HG blankets individually in greater detail.

DVA's

Distributed vibration absorber (DVA) depicted in Figure 1 a) consists of a thin metal sheet covering a layer of acoustic foam (porous media) that behaves like a spring mass damper system. The foam acts as a damped spring which in combination with the mass sheet provides a high level of reactive force and damping at its attachment surface.

Extensive experimental tests conducted in the Vibration and Acoustics Lab. at Virginia Tech have demonstrated that the DVA treatment on the base structure can reduce the noise radiated to the tune of 10-12 dB with only a marginal increase (less than 10%) in the mass of the base structure [15]. Despite the good performance of the DVA in reducing the noise radiated by the base structure little is known about the detailed mechanism by which it is achieved and the effect of the controlling parameters on its performance. In the present work numerical models (finite element models) of the DVA

have been validated. These numerical models have enabled us to understand the physics behind the functionality of the DVA and conduct parametric studies on the controlling parameters of the DVA to improve its vibration attenuation capabilities.

HG blankets

The HG blankets shown in Figure 1 b) consist of a standard passive matrix material such as urethane, polyurethane or fiberglass embedded with small randomly distributed mass in-homogeneities. These embedded masses have two main effects. First, in conjunction with the surrounding "springiness" of the support matrix material they act like many vibration absorbers (mass-spring-damper system) with different resonant frequencies. Second, it is theorized that the solid shape of the masses leads to increased wave scattering /conversion with the blanket matrix leading to an increased passive damping of the sound waves. The experimental tests have shown that the treatment of the HG blanket have significantly reduced the sound radiated by the base structure with a marginal increase in the overall mass of the base structure

While these tests have unequivocally demonstrated the high potential of the HG blankets, little is known about the detailed mechanism by which it is achieved. In order to fully realize the potential of the HG blankets, comprehensive experimental and numerical modeling of a fundamental nature is required. In the present work numerical models of the HG blankets have been validated by comparing the numerically computed results with the results from the experimental investigation of similar systems. These models have been further used for conducting parametric studies on the controlling parameters of the HG blankets for developing more effective designs.

1.5 Objectives of the research

Experimental and analytical models of the DVA's and the HG blankets have been developed to study the functioning of these vibro-acoustic attenuation devices. To gain a deep insight in the physics behind the functionality of these vibration absorbers and to understand their interaction with the structural and acoustic media, three dimensional fully coupled finite element (3D-FE) modeling of a fundamental nature is required.The main objectives of this research are as follows

- To develop and validate numerical models for the DVA's and the HG blankets to predict their response for different design configurations and excitation conditions.
- To develop fully coupled FE numerical models for predicting the reduction in the vibration levels of the base structure caused by the DVA's and the HG blankets treatment on them.
- To develop the fully coupled 3D-FE numerical model for predicting the reduction in the sound pressure levels (SPL's) inside the radiating acoustic cavities coupled to the elastic structures having a HG treatment on them.

To complete the aforementioned objectives, the following targets had to be achieved.

Reduction of the scale of the system under study

The system under study given in Figure 3 consists of a payload exposed to the airborne excitation in the initial phases of the launch. The large scale physical phenomenon of the sound radiation caused by airborne excitation of the frame of the fairing was reduced into a small scale experimental model. The exterior domain of the fairing, the fairing structure and the interior acoustic domain of the fairing were modeled by an incident acoustic domain, a plate and a radiating acoustic domain respectively. The airborne excitation in the original physical phenomenon was modeled by a volume displacement imparted at one of the corners of the incident acoustic domain. The acoustic treatments on the fairing structure were modeled as DVA and HG blanket treatments on the plate.

Validation of the individual component models:

A methodical approach was followed for the development and validation of the numerical models of the individual components the acoustic domain, the panel and the porous domain of the system under study shown in Figure 3. The finite element (FE) models of these individual components were validated by comparing the numerically computed results with the available experimental and analytical results.

Validation of the DVA and the HG blanket numerical model

DVA and the HG blankets are the vibration absorbing devices used for reducing the base structure vibration and the sound radiated by them into the coupled radiating acoustic field. FE models for the DVA and the HG blankets were validated by comparing

the numerically computed response of these vibration absorbers to their response obtained from the experimental investigation of similar models. These numerical models have been used to understand the physics behind the functionality of these noise control devices and to perform parametric studies on their controlling parametrs. The development of the FE models for an insight in the functionality of these vibration and noise control devices was one of the key deliverables of this research.

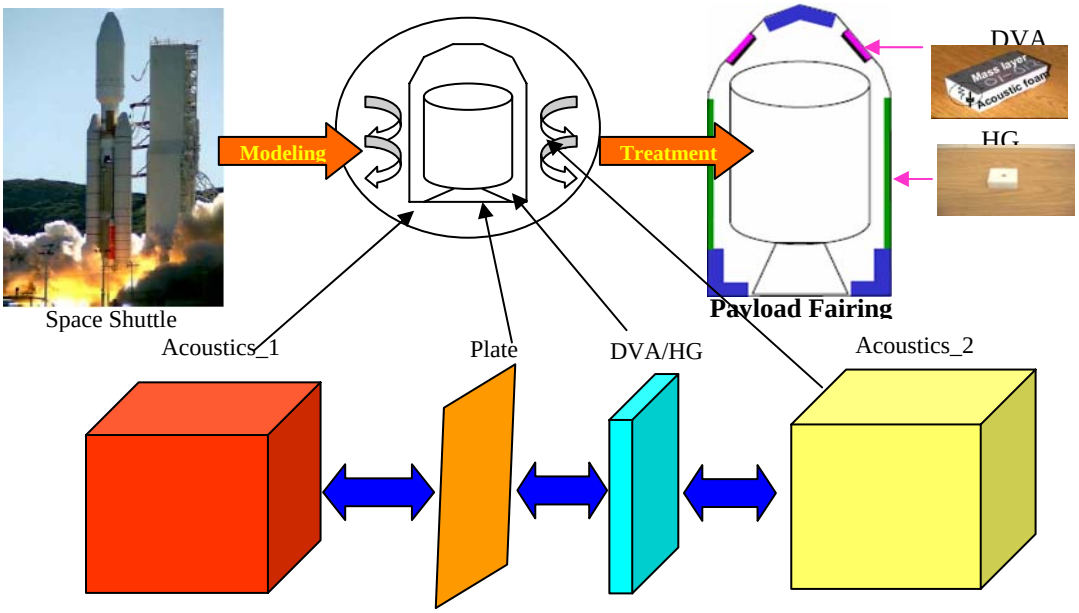

Figure 3. Reduction of the physical phenomenon into a numerical model

Validation of the coupled plate –DVA and plate-HG model

Fully coupled 3D-FE models of the plate-DVA and the plate-HG blankets were developed to understand the interaction of the DVA and the HG blankets with the structural elements. These numerical models have been validated by comparing the numerically computed results with the results obtained from the experimental analysis of similar systems. These models have been used to predict the effectiveness of these devices in controlling the vibration levels of the base plate.

Validation of the coupled plate-DVA-Acoustics and Acoustic-Plate-HG-Acoustics model

Fully coupled 3D-FE models consisting of a coupling between the acoustic domains, the noise control devices (DVA and HG the blanket), and the structural domains were developed. These numerical models were validated by comparing the

numerically computed results with the results obtained from the experimental investigation of similar systems. These models have been used for estimating the effectiveness of these noise control devices in reducing the sound radiated by the plate into the radiating acoustic domain.

1.6 Outline of the thesis

A brief summary of all the chapters is as follows.

Chapter 1 provides an introduction to the research work presented in this thesis along with the literature review of the past work done in this area of vibration and noise control. It also introduces the idea of the distributed vibration absorbers (DVA's) and the heterogeneous blankets (HG blankets). The introduction concludes with the outline of the thesis.

Chapter 2 provides a detailed description of the analytical and finite element formulation, which form the mathematical basis of all the numerical models. The mathematical formulation and the boundary conditions at the interface of the components used in the fully coupled models have been illustrated. The chapter ends with the finite element formulation of the coupled models of the system under study.

Chapter 3 gives a detailed description of the numerically computed results from the individual and fully coupled numerical models. The chapter illustrates the basis of the validation of the numerical models and describes the comparison of the numerically computed results with the available analytical and experimental results. In this chapter the experimental setups, which have been used for the validation of fully coupled models have also been explained in detail.

Chapter 4 explores the possibilities to develop advanced designs of the noise control devices (DVA and HG blanket). In this chapter the validated numerical models are used to predict the behavior of the noise control devices when exposed to varying design configurations and excitation conditions. After performing the parametric studies on the vibration absorbers, the chapter concludes by performing parametric studies on the fully coupled numerical models of the advanced vibration absorbers and the structural and the acoustic media to improve the vibro-acoustic attenuation capabilities of these vibro-acoustic attenuation devices.

Chapter 5 summarizes the major conclusions and findings of this research. The chapter also provides an overview of the different design strategies that can be followed for making the noise control devices more effective. The chapter concludes with a note on the future work that requires to be done for realizing the full potential of these noise control devices.

2 Theory

In this chapter, the analytical and finite element (FE) formulation of the individual components of the numerical models under study shown in Figure 4 such as the acoustic, the plate and the porous media has been described. Furthermore the coupling conditions of the fully coupled models such as the plate-acoustic, acoustic-porous and the plate-porous model along with their respective FE formulations are discussed in detail. The section ends with the FE formulations of the fully coupled models consisting of the incident acoustic domain, the plate, the noise control devices and the radiating acoustic domain.

The configuration of the systems under study shown in Figure 4 consists of an incident acoustic cavity coupled to an elastic structure (plate) having a clamped boundary condition and a noise control device treatment. The plate is further coupled to a radiating acoustic domain. Both the incident and radiating acoustic domains consists of rigid walled boundary conditions. The system is excited by imparting a volume displacement at one of the corners of the incident acoustic domain and the response is measured at the plate and the radiating acoustic domain. The objective of this model is to estimate the transmission loss across the plate with and without the noise control device treatment.

A methodical approach was followed in the development of the finite element (FE) formulation. The development of the (FE) formulation can be divided into two stages. First, the (FE) formulation of the individual components was developed. Second, the FE formulations of the individual components were coupled to capture the interaction between the individual components in the fully coupled models.

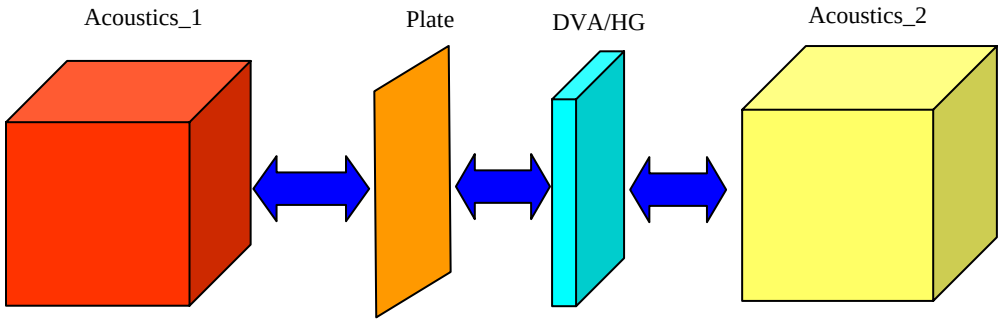

Figure 4. Individual components of the numerical model under study

2.1 Analytical modeling of the acoustic domain

In the present section, the equation for determining the natural frequencies of the standing waves in a rigid walled three dimensional acoustic domain is discussed. The acoustic cavity having rigid walled boundary condition is depicted in Figure 5

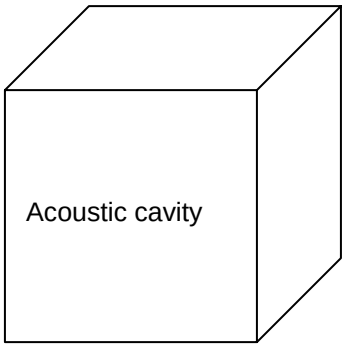

Figure 5. Acoustic cavity

In order to understand the forced response of a completely enclosed acoustic cavity, it is important to examine the natural frequencies and the respective normal modes of the standing waves simulated inside it due to the forcing function. Assuming the pressure to be harmonic in time, the linearized homogenous acoustic wave equation in the rectangular Cartesian coordinates is given by

$$\nabla p^2 = \frac{1}{c^2}\frac{\partial^2 p}{\partial t^2}$$
$$\frac{\partial^2 p}{\partial x^2} + \frac{\partial^2 p}{\partial y^2} + \frac{\partial^2 p}{\partial z^2} + k^2 p = 0 \qquad (7)$$

In equation (7) p, k, c represent the pressure in the acoustic cavity, the acoustic wave number $k = \frac{\omega}{c}$ and the speed of sound. The Cartesian coordinates are represented by x, y, z in equation (7). All the surfaces of the acoustic cavity are perfectly rigid and hence the normal component of the velocity would be zero at the boundaries of the acoustic domain. The equations satisfying these boundary conditions given by Kinsler and Frey [16] is of the form as illustrated in equation (8)

$$\left(\frac{\partial p}{\partial x}\right)_{x=0} = \left(\frac{\partial p}{\partial x}\right)_{x=L_x} = 0$$
$$\left(\frac{\partial p}{\partial y}\right)_{y=0} = \left(\frac{\partial p}{\partial y}\right)_{y=L_y} = 0 \qquad (8)$$
$$\left(\frac{\partial p}{\partial z}\right)_{z=0} = \left(\frac{\partial p}{\partial x}\right)_{z=L_z} = 0$$

In equation (8) L_x, L_y, L_z represent the dimensions of the acoustic cavity in the x, y and the z directions respectively.

As the stimulation of the standing waves are the outcome of the forced analysis of the three dimensional cavities, the assumed solution of the wave equation given in Kinsler and Frey [16] is of the form

$$p(x, y, z, t) = X(x)Y(y)Z(z)e^{j\omega t} \qquad (9)$$

Substitution of the equation (9) into the wave equation (7) and the application of the separation of variables to the resulting expression yields

$$\left(\frac{d^2}{dx^2} + k_x{}^2\right)X = 0$$
$$\left(\frac{d^2}{dy^2} + k_y{}^2\right)Y = 0 \qquad (10)$$
$$\left(\frac{d^2}{dz^2} + k_z{}^2\right)Z = 0$$

Where k_x, k_y, k_z are the acoustic wave numbers in the x, y, z directions respectively. The angular frequencies of the standing waves in the acoustic domain are given by

$$\left(\frac{\omega}{c}\right)^2 = k^2 = k^2{}_x + k^2{}_y + k^2{}_z \qquad (11)$$

Substitution of the boundary condition given in equation (8) in the equation (10) results in the formulation of the pressure in the acoustic cavity of the form

$$p_{lmn} = A_{lmn} \cos k_{xl} x \cos k_{ym} y \cos k_{zn} z \qquad (12)$$

In the equation (12) p_{lmn} is the pressure in the acoustic cavity, A_{lmn} is the scalar term representing the magnitude of the excitation volume displacement. The components of the wavenumber (k) given in Kinsler and Frey [16] are of the form

$$\begin{aligned} k_{xl} &= \frac{l\pi}{L_x} \text{ for } l = 0,1,2,3,..... \\ k_{ym} &= \frac{m\pi}{L_y} \text{ for } m = 0,1,2,3,..... \\ k_{zn} &= \frac{n\pi}{L_z} \text{ for } n = 0,1,2,3,..... \end{aligned} \tag{13}$$

On substituting the values of the components of the wavenumber (k) from the equation (13) into equation (11) we have that the natural frequencies for any standing wave inside the acoustic cavity is of the form given in equation (14)

$$\omega_{lmn} = c\left[\left(\frac{l\pi}{L_x}\right)^2 + \left(\frac{m\pi}{L_y}\right)^2 + \left(\frac{n\pi}{L_z}\right)^2\right]^{21/2} \tag{14}$$

The values of the natural frequencies for the standing waves of the acoustic cavity computed from equation (14) are used as a reference for the validation of the numerical model of the acoustic domain in Section 3.1.

2.2 Finite element formulation of the acoustic domain

In the present section, the finite element formulation for the wave equation of the acoustic domain is derived. In addition, the mass and the stiffness matrices of the acoustic domain are also derived using classical finite element theory of the hexahedral elements The numerical model used for the validation of the acoustic elements consists of a 1m x 1m x 1m three dimensional acoustic cavity. The cavity is discretized using a thousand 8 node hexahedral elements having a single degree of freedom corresponding to the pressure inside the acoustic cavity.

Starting from equation (7) and assuming a harmonic variation of the pressure in the acoustic domain we have that

$$p = \bar{p}e^{j\omega t} \tag{15}$$

Substituting the pressure expression from equation (15) in equation (7) we get

$$\nabla^2 \bar{p} + \frac{\omega^2}{c^2} \bar{p} = 0 \tag{16}$$

The equation 16 can be written in the matrix format using the differential expression

$$\begin{aligned} \nabla.\{\ \} &= [L]^T = \begin{bmatrix} \frac{\partial}{\partial x} & \frac{\partial}{\partial y} & \frac{\partial}{\partial z} \end{bmatrix} \\ \nabla\{\ \} &= [L] \end{aligned} \tag{17}$$

Substituting the equation (17) in equation (7) we have

$$\frac{1}{c^2} \frac{\partial^2 p}{\partial t^2} - [L]^T [L] p = 0 \tag{18}$$

Multiplying the equation (18) with a small perturbation in the pressure represented by $[\delta p]^T$ and integrating the equation with respect to the volume we have

$$\int \frac{1}{c^2} \frac{\partial^2 p}{\partial t^2} [\delta p]^T d\delta p dV - \int [L]^T [L] p [\delta p]^T dV = 0 \tag{19}$$

On minor manipulations we have that the equation (19) can be written as

$$\frac{1}{c^2} \int \frac{\partial^2 p}{\partial t^2} [\delta p]^T dV - \int [L]^T [\delta p]^T [L] p dV = \int \{n\}^T [\delta p]^T (\{L\} p) dS \tag{20}$$

Discritising the acoustic domain and writing the degrees of freedom with the shape functions ($[N]$) of the acoustic domain from the fundamental finite element theory we have that

$$\begin{aligned} p &= [N]^T \{p_e\} \\ u &= [N']^T \{u_e\} \\ \ddot{p} &= [N]^T \{\ddot{p}_e\} \\ \ddot{u} &= [N']^T \{\ddot{u}_e\} \\ [\delta p] &= [N]^T [\delta p_e] \\ [B] &= \{L\}[N]^T \end{aligned} \tag{21}$$

The relationship between the pressure and the particle velocity of the fluid in the acoustic cavity is given by

$$\{n\}.\nabla p = -\rho o\{n\}\frac{\partial^2 u}{\partial t^2} \tag{22}$$

In equation (22) the normal component of the pressure is represented by $\{n\}$. Substituting the values from the equation (21) and equation (22) in equation (20) we have that

$$\int \frac{[\delta pe]^T [N][N]^T}{c^2} dV\{\ddot{p}_e\} - \int [\delta p_e]^T [B]^T [B]\{p_e\}dV + \rho_o [\delta p_e]^T [N]\{n\}[N']^T dS\{\ddot{u}_e\} = 0 \tag{23}$$

In equation (22) [B] matrix represents the differential of the [N]. These matrices are explained in Cook [21]. Substituting the harmonic behavior of the pressure inside the cavity from equation (15) in equation (22) we have that

$$-\frac{\omega^2}{c^2}\left(\int [N][N]^T dV\right)\{p_e\} + \left(\int [B]^T [B]dV\right)\{p_e\} = \omega^2 \rho_o \left(\int [N]\{n\}[N']^T dS\right)\{u_e\} = 0 \tag{24}$$

The equation (23) can be expressed as

$$\left([H] - \frac{\omega^2}{c^2}[Q]\right)\{p_e\} = \rho_o \omega^2 [R] \tag{25}$$

Where

$$\begin{aligned} [Q] &= \int [N]\ [N]^T dV \\ [H] &= \int [B]^T [B]dV \\ [R] &= [N]\{n\}^T [N']^T dS \end{aligned} \tag{26}$$

In equation (26) $[H],[Q]$ and $[R]$ are the mass, the stiffness and the generalized excitation matrices for the acoustic domain. These matrices are square matrices and are sparse in nature. Equation (25) is the finite element formulation followed for the modeling of the acoustic domain in this research work.

2.3 Analytical modeling of the plate

In this section the analytical theory for the thin plate elements derived by Yang [17] is described. In this research work, the plate thickness is small compared to its other dimensions thus thin plate elements given in Yang [17] have been used for modeling of the plate in the numerical model. The rectangular plate element used for the modeling of

the plate is shown in Figure 6 (this figure is based on the plate element in Yang [17] but has not been modified from it)

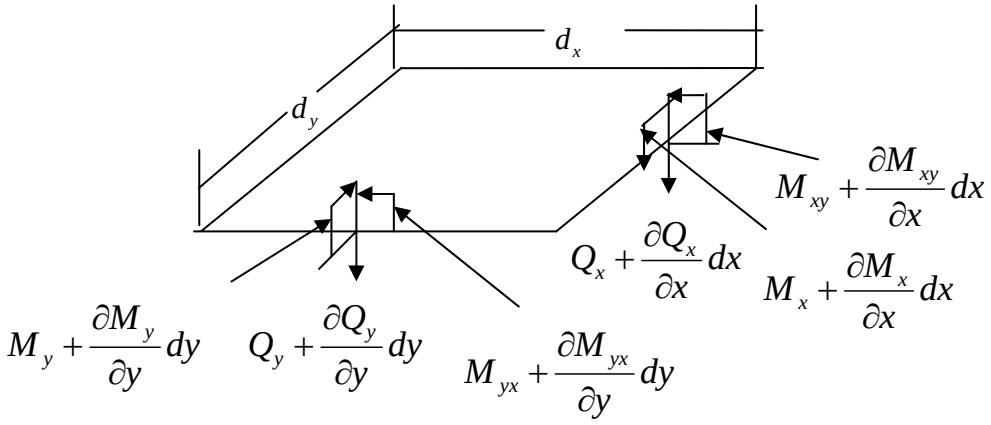

Figure 6. Rectangular plate element

The bending and the twisting moments per unit length from Yang[17] are as follows

$$M_x = \int_{-h/2}^{h/2} \sigma_x z dz = \frac{E}{1-\nu^2} \int_{-h/2}^{h/2} (\varepsilon_x + \nu \varepsilon_y) z dz$$
$$M_y = \int_{-h/2}^{h/2} \sigma_y z dz = \frac{E}{1-\nu^2} \int_{-h/2}^{h/2} (\varepsilon_y + \nu \varepsilon_x) z dz \qquad (27)$$
$$M_{xy} = -\int_{-h/2}^{h/2} \tau_{xy} z dz = \frac{-E}{(1+\nu)} \int_{-h/2}^{h/2} \gamma_{xy} z dz$$

The strains in the expression (27) can be written as

$$\varepsilon_x = -z \frac{\partial^2 w}{\partial x^2}, \varepsilon_y = -z \frac{\partial^2 w}{\partial y^2}, \gamma_{xy} = -2z \frac{\partial^2 w}{\partial x \partial y} \qquad (28)$$

Substituting the values of the strains form equation (28) in the equation (27) we have that the bending and the twisting moments can be written as

$$M_x = -D\left(\frac{\partial^2 w}{\partial x^2} + \nu \frac{\partial^2 w}{\partial y^2} \right)$$
$$M_y = -D\left(\frac{\partial^2 w}{\partial y^2} + \nu \frac{\partial^2 w}{\partial x^2} \right) \qquad (29)$$
$$M_{xy} = D(1-\nu) \frac{\partial^2 w}{\partial x \partial y}$$

Where $D = \frac{Eh^3}{12(1-\nu^2)}$

Now considering that the plate element in Figure 6 is under a distributed load p at its top surface we have that the equilibrium equations of the shearing forces, the bending and the twisting moments on the plate element due to the application of this load is as follows

$$\begin{aligned} &\frac{\partial Q_x}{\partial x} + \frac{\partial Q_y}{\partial y} + p = 0 \\ &\frac{\partial M_{xy}}{\partial x} - \frac{\partial M_y}{\partial y} + Q_y = 0 \\ &\frac{\partial M_{yx}}{\partial y} + \frac{\partial M_x}{\partial x} - Q_x = 0 \end{aligned} \tag{30}$$

On eliminating the shearing forces from the equation (30) and reducing equation (30) in terms of the moments on the plate element we have that

$$\frac{\partial^2 M_x}{\partial x^2} - 2\frac{\partial^2 M_{xy}}{\partial x \partial y} + \frac{\partial^2 M_y}{\partial y^2} = -p \tag{31}$$

Writing the equation (31) in terms of the normal displacement of the plate we have

$$\frac{\partial^4 w}{\partial x^4} + 2\frac{\partial^4 w}{\partial x^2 \partial y^2} + \frac{\partial^4 w}{\partial y^4} = \frac{p}{D} \tag{32}$$

The equation (32) is the differential equation for the small deflection in the thin plates and the finite formulation of the plate model is primarily based on this equation.

2.4 Finite element formulation of the plate

In the present section, the discretization of the strain and the kinetic energy equation from the thin plate theory based on the fundamental principles of the classical finite element theory will be used for deriving the mass and the stiffness matrices of the plate. The numerical model used for the validation of the plate elements consists of a 206 x 308 x 0.794 (mm) plate. The plate is discretized using 150 16-node rectangular plate elements derived in Yang [17]. The stiffness matrix is derived from the strain energy

expression of the plate. The strain energy expression of the plate based on the thin plate theory is given by equation (33)

$$\begin{aligned} dU = &-\frac{1}{2}(M_x dy)(\frac{\partial^2 w}{\partial x^2} dx) + -\frac{1}{2}(M_y dx)(\frac{\partial^2 w}{\partial y^2} dy) \\ &-\frac{1}{2}(M_{xy} dy)(\frac{\partial^2 w}{\partial x \partial y} dx) - \frac{1}{2}(M_{yx} dx)(\frac{\partial^2 w}{\partial y \partial x} dy) \end{aligned} \tag{33}$$

Substituting the values of the respective moments from equation (29) in equation (33) we have that

$$dU = \iint \frac{D}{2}\left[\left(\frac{\partial^2 w}{\partial x^2}\right)^2 + \left(\frac{\partial^2 w}{\partial y^2}\right)^2 + 2\nu\left(\frac{\partial^2 w}{\partial x^2}\right)\left(\frac{\partial^2 w}{\partial y^2}\right) + 2(1-\nu)\left(\frac{\partial^2 w}{\partial x \partial y}\right)\right] dxdy \tag{34}$$

The assumed displacement function used for formulation of the mass and the stiffness matrix of the rectangular plate elements [17] is given in equation (35)

$$w(x, y) = (a_1 + a_2 x + a_3 x^2 + a_4 x^3)(b_1 + b_2 y + b_3 y^2 + b_4 y^3) \tag{35}$$

The displacement function given in equation (35) has 16 constants which can be expressed in a vector $\{c\}$. The plate element consists of 4 degrees of freedom (w, w_x, w_y, w_{xy}) for each node and hence has 16 DOF for each element. The degrees of freedom (DOF's) for the plate element can also be expressed by a vector $\{q\}$.

The relationship between the vector of constants $\{c\}$ and vector of degrees of freedom $\{q\}$ is given by

$$\begin{aligned} &\{q\} = [B]\{c\} \\ &\therefore \{c\} = [B]^{-1}\{q\} = [T]\{q\} \end{aligned} \tag{36}$$

On substituting equation (35) in equation (36) and writing the strain energy in terms of the constant vector we have

$$U = \frac{1}{2}\{c\}^T [\bar{k}]\{c\} \tag{37}$$

The coefficients of the $[\bar{k}]$ can be obtained by applying the conservation of energy theorem to equation (37)

$$\bar{k}_{ij} = \frac{\partial^2 U}{\partial c_i \partial c_j} \tag{38}$$

On substituting the value of the $\{c\}$ from equation (36) in equation (37) we have

$$\begin{aligned} U &= \frac{1}{2}\{q\}^T [T]^T [\bar{k}][T]\{q\} \\ [k] &= [T]^T \bar{k}[T] \end{aligned} \tag{39}$$

Where the $[k]$ is the stiffness matrix for the thin plate element. The 16x16 stiffness matrix of the rectangular plate element given explicitly by Yang [17] is of the form

$$K_{ij} = \frac{Eh^3}{12ab(1-\nu^2)}\left[\alpha_1\left(\frac{b}{a}\right)^2 + \alpha_2\left(\frac{b}{a}\right)^2 + \alpha_3 + \alpha_4\nu\right]a^{\alpha_5}b^{\alpha_6} \tag{40}$$

All the constants in the expression (40) are given in Yang [17] in the form of a Table. The mass matrix of the rectangular plate element [17] is obtained from the kinetic energy expression of the plate. The kinetic energy for the plate elements is given as

$$T = \frac{\rho h}{2}\iint (\dot{w})^2 \, dxdy \tag{41}$$

In equation (41) ρ, h and w represent the density of the plate material, the thickness of the plate and the normal displacement of the plate respectively. On substitution of the shape function from equation (38) in equation (41) and following the same procedure as has been followed for the derivation of the stiffness matrix we have that

$$\begin{aligned} K &= \frac{1}{2}\{\dot{c}\}^T [\bar{m}]\{\dot{c}\} \\ K &= \frac{1}{2}\{\dot{q}\}^T [T]^T [\bar{m}][T]\{\dot{q}\} \\ [m] &= [T]^T [\bar{m}][T] \end{aligned} \tag{42}$$

The 16x16 mass matrix of the rectangular plate element given explicitly by Yang [17] is of the form

$$M_{ij} = \frac{\rho hab}{1225}\alpha_7 a^{\alpha_5} b^{\alpha_6} \tag{43}$$

All the constants in the expression (43) are given in Yang [17]. After the derivation of the mass and the stiffness matrix for the rectangular plate elements, the dynamic equation of the plate in a concise form is given by

$$([K_p] - \omega^2[M_p](1 + i\xi))\{w\} = \{F_p\} \tag{44}$$

In equation (44) $[K_p],[M_p]$ are the global stiffness and the global mass matrix of the plate respectively. These matrices are computed using the explicit expressions for the elements of the stiffness and the mass matrix given in equation (40) and equation (43). The lumped damping ratio of the plate is represented by ξ. In equation (44), the degree of freedom vector (DOF) and the external loading on the plate are represented by $\{w\}$ and $\{F_p\}$ respectively.

2.5 Analytical modeling of the porous domain

In this section, the analytical expressions for the potential, the kinetic and the dissipation energy for the porous media are described. The porous media, shown in Figure 7, consists of both the solid and the fluid phase within the same volume.

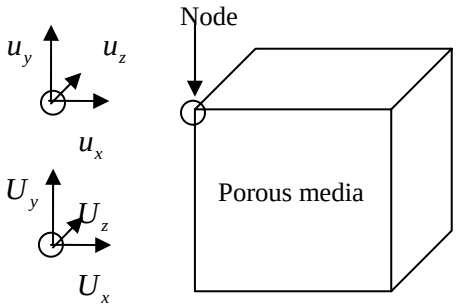

Figure 7. Degrees of freedom of the hexahedral element used for the modeling of the porous media

A detailed illustration of these equations can be found in Panneton et. al. [18]. Kinetic energy of the porous media given by Panneton et. al. [18] is of the form

$$dT = \frac{1}{2}\left(\rho_{11}\{\dot{u}\}^T\{\dot{u}\} + 2\rho_{12}\{\dot{u}\}^T\{\dot{U}\} + \rho_{22}\{\dot{U}\}^T\{\dot{U}\}\right) \tag{45}$$

Equation (45) gives the expressions for the kinetic energy of the porous media. In the equation ρ_{11}, ρ_{22} are the effective densities for the solid and the fluid phase of the porous media respectively. The density term that captures the inertial interaction between the solid and the fluid phase in the porous media is represented by ρ_{12} . These densities are frequency independent and do not include the viscous terms.

The expression for the effective densities of the solid and the fluid phase from Panneton et. al. [18] are given as

$$\begin{aligned} \rho_{11} &= \rho_1 + \rho_a \\ \rho_{22} &= -\rho_a \\ \rho_{12} &= \phi\rho_0 + \rho_a \\ \rho_a &= \phi\rho_0(\alpha_\infty - 1) \end{aligned} \tag{46}$$

The strain energy density for the solid and the fluid phase of the porous media given by Panneton et. al. [18] is of the form

$$dU = \frac{1}{2}\left(\{\sigma_s\}^T\{\varepsilon_s\} + \{\sigma_f\}^T\{\varepsilon_f\}\right) \tag{47}$$

In equation (47) $\{\sigma_s\}$ and $\{\varepsilon_s\}$ are the stress and the strains in the solid phase of the porous media respectively. The stresses and the strains in the fluid phase of the porous media are given by $\{\sigma_f\}$ and $\{\varepsilon_f\}$ respectively. Equation (47) illustrates that both the solid and the fluid phase of the porous media contribute to its effective kinetic energy.

The dissipation of the energy in the porous media is modeled by the use of a complex valued dissipation constant $b(\omega)$ given by Johnson et. al. [19]. The expression for the dissipation mechanism of the porous media given by Panneton et. al. [18] is of the form

$$dD = \frac{1}{2}b(\omega)\left(\{\dot{u}\} - \{\dot{U}\}\right)^T\left(\{\dot{u}\} - \{\dot{U}\}\right) \tag{48}$$

In equation (48) $b(\omega)$ is a frequency dependent dissipation term. This term is calculated from the flowresistivity and the tortuosity of the porous material [18]. The solid phase and the fluid phase velocity vectors of the porous media are given by $\{\dot{u}\}$ and $\{\dot{U}\}$

respectively. It can be observed from equation (48) that the dissipation mechanism at a particular surface in the porous media is proportional to the relative motion of the solid and the fluid phase of the porous media at that surface. In order to achieve the maximum dissipation of the vibration energy by the porous media, the boundary conditions of the mounting of the porous media on the vibrating structure should be such as to allow maximum relative motion of the solid and the fluid phase of the porous media. These material properties have been mentioned in the nomenclature. The expression for the $b(\omega)$ in terms of the material properties of the porous media [18] is as follows

$$\begin{aligned} b(\omega) &= \beta + j\omega\alpha \\ \alpha &= \frac{4\varphi^2\sigma\rho_o\eta k_s{}^2}{2\sigma^2\Lambda^2 h^2} \\ \beta &= \varphi^2\sigma \end{aligned} \tag{49}$$

2.6 Finite element formulation of the porous domain

In the following, the discretized equation of the kinetic, the strain and the dissipation energy are used for the computation of the mass, the stiffness and the damping matrices of the porous media respectively. The porous media is discretized using 8 node hexahedral elements following the mathematical formulation derived by Panneton et. al. [18]. Each node of the hexahedral elements has six degrees of freedom (DOF) accounting for the three displacements components of the solid phase $\{u\}$ and the three displacements components of the fluid phase $\{U\}$.

Writing the macroscopic displacements of the solid and the fluid phase of the porous media with respect to the nodal (DOF's) we have

$$\{u\}^e = [N_u]^e\{\overline{u}\}^e \text{ and } \{U\}^e = [N_U]^e\{\overline{U}\} \tag{50}$$

In equation (50) $\{\overline{u}\}^e$ and $\{\overline{U}\}^e$ are the nodal DOF for the solid and the fluid phase of the porous element respectively. The shape function matrices for the solid and the fluid phase of the porous element are given by $[N_u]^e$ and $[N_U]^e$ respectively. Substituting the discretized values of the solid and the fluid field displacements from equation (50) in the expressions for the kinetic energy, the potential energy and the dissipation energy we obtain the finite element formulation for the porous media

The finite element formulation of dynamic equation of the porous media given by Panneton et. al. [18] is of the form

$$\left(-\omega^2\begin{bmatrix}[M_{ss}] & [M_{sf}]\\ [M_{sf}] & [M_{ff}]\end{bmatrix}+j\omega\begin{bmatrix}[C_{ss}(\omega)] & -[C_{sf}(\omega)]\\ -[C_{sf}(\omega)] & [C_{ff}(\omega)]\end{bmatrix}+\begin{bmatrix}[K_{ss}(\omega)] & -[K_{sf}(\omega)]\\ -[K_{sf}(\omega)] & [K_{ff}(\omega)]\end{bmatrix}\right)\begin{Bmatrix}\{u\}\\ \{U\}\end{Bmatrix}=\begin{Bmatrix}\{F_s\}\\ \{F_f\}\end{Bmatrix} \quad (51)$$

In equation (51) $[M_{ss}],[K_{ss}],[C_{ss}]$ and $[M_{ff}][K_{ff}][C_{ff}]$ are the mass, the stiffness and the damping matrices for the solid and the fluid phase of the porous media respectively. The mass matrix capturing the inertial interaction of the solid and the fluid phase of the porous media is represented by$[M_{sf}]$. The strain and the energy dissipation interaction between the solid and the fluid phase of the porous media is captured by $[K_{sf}]$ and $[C_{sf}]$ respectively.

The finite element formulation of the mass, the stiffness and the damping matrices of the porous media derived by Panneton et. al. [18] is given in equation (52) and equation (53). The number of elements used for the discretization of the porous media is represented by Ω_p.

$$\begin{aligned}
[M_{ss}] &= \sum_{e\in\Omega_p}\int_{\Omega_p}[N_u]^T\rho_{11}[N_u]dV \quad (52)\\
[M_{ff}] &= \sum_{e\in\Omega_p}\int_{\Omega_p}[N_U]^T\rho_{22}[N_U]dV\\
[M_{sf}] &= \sum_{e\in\Omega_p}\int_{\Omega_p}[N_u]^T\rho_{11}[N_U]dV\\
[C_{ss}] &= \sum_{e\in\Omega_p}\int_{\Omega_p}[N_u]^T b(\omega)[N_u]dV\\
[C_{ff}] &= \sum_{e\in\Omega_p}\int_{\Omega_p}[N_U]^T b(\omega)[N_U]dV\\
[C_{sf}] &= \sum_{e\in\Omega_p}\int_{\Omega_p}[N_u]^T b(\omega)[N_U]dV
\end{aligned}$$

$$
\begin{aligned}
\left[K_{ss}\right] &= \sum_{e\in\Omega_p}\int_{\Omega_p}\left[B_u\right]^T\left[Ds\right]\left[B_u\right]dV \\
\left[K_{ff}\right] &= \sum_{e\in\Omega_p}\int_{\Omega_p}\left[B_U\right]^T\left[Df(\omega)\right]\left[B_U\right]dV \\
\left[K_{ss}\right] &= \sum_{e\in\Omega_p}\int_{\Omega_p}\left[B_u\right]^T\left[Dsf(\omega)\right]\left[B_u\right]dV \\
\left\{F_s\right\} &= \sum_{e\in\sum N}\int_{\sum N}\left[N_u\right]^T\left(\left\{f\right\}-h\left\{fn\right\}\right)dS \\
\left\{F_f\right\} &= \sum_{e\in\sum N}\int_{\sum N}\left[N_u\right]^T\left(h\left\{fn\right\}\right)dS
\end{aligned}
\tag{53}
$$

The relationship between the strain, the displacement and the shape functions of the porous media in equation (52) and equation (53) is given by equation (54)

$$
\left[B_u\right]^e = \left[L\right]\left[N_u\right]^e \text{ and } \left[B_U\right]^e = \left[L\right]\left[N_U\right]^e \tag{54}
$$

The concise form of the dynamic equation for the porous media is given by equation (55).

$$
\{-\omega^2[M_{po}]+[K_{po}(\omega)]+j\omega[C_{po}(\omega)]\}\{W_{po}\}=\{F_{po}\} \tag{55}
$$

In equation (55) $[K_{po}(\omega)],[C_{po}(\omega)]$ and $[M_{po}]$ represent the equivalent stiffness, damping and mass matrices for the porous media respectively. The nodal loading vector that acts on the aggregate skeleton of the porous media is illustrated as $\left\{F_{po}\right\}$. In equation (55) $\{W_{po}\}$ vector represents the ratio of the nodal DOF's for the solid and the fluid phase of the porous media and ω represents the angular frequency. In equation (55) the stiffness and the damping matrix are frequency dependent and hence the standard procedures of modal analysis cannot be used for solving the dynamic equation of the porous media. The frequency dependence of the dynamic equation of the porous media given in equation (55) makes the solution computationally expensive as the stiffness and the damping matrices of the porous media have to be calculated at every frequency in frequency range of interest.

2.7 Finite element formulation of the coupled plate-acoustic model

The fully coupled model of the plate and the acoustic domain is shown in Figure 8. In a fully coupled model consisting of the plate and the acoustic domain, both the mediums in contact have a strong coupling at their interface.

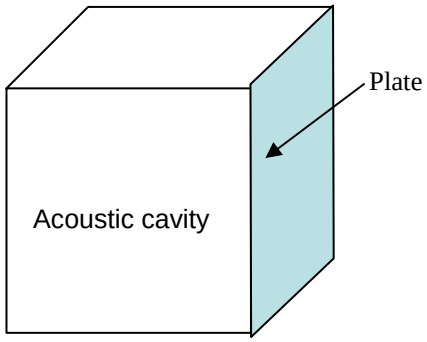

Figure 8. Fully coupled plate and acoustic domain

Rewriting the dynamic equation for the plate domain with a fluid excitation on its surface we have

$$([K_p] - \omega^2[M_p](1+i\xi))\{w\} = \{F_p\} + \{F_e^{pr}\} \tag{56}$$

The fluid pressure vector on the structure $\{F_e^{pr}\}$ obtained by integrating the pressure over the area of contact of the two media is given by

$$\{F_e^{pr}\} = \iint [N']\{n\}\{p\}dS \tag{57}$$

Representing the pressure field inside the acoustic domain in terms of the nodal pressures of the acoustic element we have

$$\{F_e^{pr}\} = \iint [N']\{n\}[N]^T\{p_e\}dS = \left(\iint [N']\{n\}[N]^T dS\right)\{p_e\} \tag{58}$$

On substituting the $\left(\iint [N']\{n\}[N]^T dS\right) = [R_e]$ in equation (58) we have that $\{F_e^{pr}\} = [\mathrm{R_e}]\{p_e\}$. Substituting the value of the $\{F_e^{pr}\}$ in equation (56) we have that the final dynamic equation of the motion for the plate under the influence of fluid pressure in the coupled acoustic cavity and external forces is given by

$$([K_p] - \omega^2[M_p](1+i\xi))\{w\} - [R_e]\{p_e\} = \{F_p\} \tag{59}$$

From the fundamental equation of motion for the acoustic domain derived in Section 2.2, we have that the dynamic equation of motion for the acoustic domain under a structural excitation is given by

$$\left([H] - \frac{\omega^2}{c^2}[Q] \right) \{p_e\} - \rho_o \omega^2 [R_e] = 0 \tag{60}$$

Writing equation (59) and equation (60) in the matrix form we have that the coupled system of the acoustic and the plate domain being excited by a point force on the structural domain is given as

$$\begin{bmatrix} [[K_p] - \omega^2 [M_p](1 + i\xi)] & [K_{fs}] \\ [M_{fs}] & \left([H] - \frac{\omega^2}{c^2}[Q] \right) \end{bmatrix} \begin{Bmatrix} w \\ p_e \end{Bmatrix} = \begin{Bmatrix} F_p \\ 0 \end{Bmatrix}$$
$$[M_{fs}] = \rho o [R_e]^T \tag{61}$$
$$[K_{fs}] = -[R_e]$$

In equation (61) $[M^{fs}]$ and $[K^{fs}]$ are the coupling matrices that capture the transfer of the energy between the structural and the acoustic domain. The other terms in equation (61) have been defined in the prior equations. This equation provides the finite element formulation for a fully coupled model consisting of an acoustic cavity coupled to an externally driven plate, where the forcing function on the plate is given by F_p.

2.8 Finite element formulation of the coupled porous-acoustic model

The fully coupled model of the acoustic and the porous domain is shown in Figure 9.

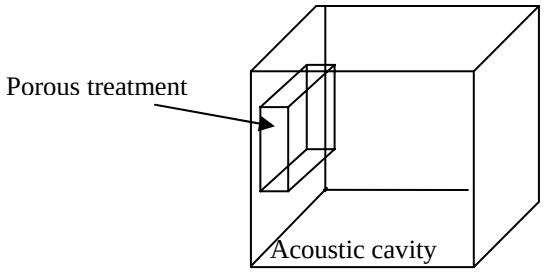

Figure 9. Fully coupled acoustic and porous domain model

The coupled model consists of a rigid walled acoustic cavity having a porous treatment on one of its walls. The coupling conditions between the acoustic and the porous domain at their interface given by Panneton et. al. [18] is of the form

$$\begin{aligned} \{u_a\}^T \{n\} &= ((1-h)\{u\} + h\{U\})^T \{n\} \\ [N_c]^T \{\sigma_s\} &= -(1-h)\, p\{n\} \\ [N_c]^T \{\sigma_f\} &= -(h)\, p\{n\} \end{aligned} \tag{62}$$

Where $[N_c] = \begin{bmatrix} n_x & 0 & 0 & n_y & 0 & n_z \\ 0 & n_y & 0 & n_x & n_z & 0 \\ 0 & 0 & n_z & 0 & n_y & n_x \end{bmatrix}$

In the equation (62) $\{u_a\}$ and p are the unknown normal displacements and pressures at the nodes of the discretized acoustic domain. The stress in the solid phase, the stress in the fluid phase and the porosity of the porous media are represented by σ_s, σ_f and h respectively. The coupling conditions given in equation (62) can be broadly divided into two parts. First equation ensures the continuity of the normal velocity at the interface of the porous and the acoustics domain. The second and the third equations ensure the continuity of the stresses and the pressure at the interface of the acoustic and the porous domain.

The work done at the interface of the acoustic and the porous domain can be assigned to the surface pressure at the interface. Consequently the work done on the porous domain by the acoustic pressure inside the acoustic cavity is given as

$$dW_a = (1-h)\, p\{n\}^T \{u\} + hp\{n\}^T \{U\} \tag{63}$$

The perturbation induced in the acoustics medium due to the vibration in the poroelastic domain along the interface is given by

$$\rho_o \omega^2 (1-h)[C_{sa}]^T \{\bar{u}\} + h[C_{fa}]^T \{\bar{U}\} \tag{64}$$

In equation (64) $[C_{sa}]^T$ captures the interaction between the vibration levels in the skeleton of the porous media and the adjacent acoustic domain. In the equation (64), $[C_{fa}]^T$ couples the vibration levels of the air in the pores of the porous media to the adjacent acoustic domain. Writing the coupling condition and the work done at the

interface of the two mediums in a matrix format given by Panneton et. al. [18] is of the form

$$[C_{pa}] = \begin{bmatrix} (1-h)[C_{sa}] \\ h[C_{fa}] \end{bmatrix} \tag{65}$$

The finite element formulation of the dynamic equation of motion for the fully coupled system consisting of the acoustic and the porous domain is given by

$$\begin{bmatrix} -\omega^2[M_{po}] + j\omega[C_{po}(\omega)] + [K_{po}(\omega)] & -[C_{pa}] \\ -[C_{pa}]^T & 1/\rho_o\omega^2[H] - 1/\rho_o c_o{}^2[Q] \end{bmatrix} \begin{Bmatrix} W_{po} \\ p_e \end{Bmatrix} = \begin{Bmatrix} F_{po} \\ \mathrm{R_e} \end{Bmatrix} \tag{66}$$

This finite element formulation given in equation (66) is used for the numerical modeling of the fully coupled model consisting of the acoustics and the porous media. The terms used in the equation (66) have been explained in the prior sections.

2.9 Finite element formulation of the coupled plate and the porous domain

The fully coupled model consisting of the plate and the porous media is shown in Figure 10.

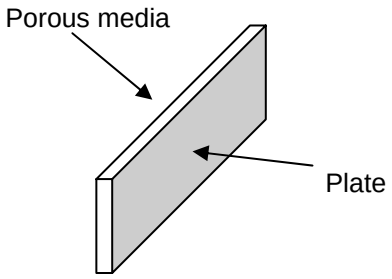

Figure 10. Fully coupled plate and porous domain model

The continuity equations at the interface of the two media given by Panneton et. al. [18] are of the form.

$$u_i = w_i \tag{67a}$$

$$U_n = u_n \tag{67b}$$

In equation (67a) $\{u_i\}$ and w_i represents the nodal displacements vectors of the solid phase of the porous media and the plate respectively. In equation (67b) $\{u_n\}$ and $\{U_n\}$ are the normal components of the solid and fluid phase displacement of the porous media. The coupling condition between the plate and the porous media at their interface can be divided into two major parts. The equation (67a) ensures the continuity of the normal velocity of the plate elements and the skeleton of the porous media. Equation (67b) enforces the elimination of the relative motion between the solid and the fluid phase of the porous media at its interface with the plate elements. The finite element formulation of the dynamic equation of motion for the fully coupled system consisting of the plate and the porous domain is given by

$$\begin{bmatrix} \left[[K_p]-\omega^2[M_p](1+i\xi)\right] & [0] \\ [0] & -\omega^2[M_{po}]+j\omega[C_{po}(\omega)]+[K_{po}(\omega)] \end{bmatrix} \begin{Bmatrix} w \\ W_{po} \end{Bmatrix} = \begin{Bmatrix} F_p \\ F_{po} \end{Bmatrix} \qquad (68)$$

The displacement continuity conditions at the interface of the porous and the plate given in equation (67) are enforced using the Lagrange multipliers given in Cook [21]. This is the reason that we don't have any coupling matrices at the off diagonal positions in equation (68). The procedure of implementation of the Lagrange multipliers to couple the plate and the porous media is explained in the Appendix A. The finite element formulation in equation (68) is used in the development of the numerical model of the fully coupled plate-porous model.

2.10 Finite element formulation of the plate-HG-acoustics coupled model

In this section, the finite element formulation of the fully coupled model of the plate-HG-acoustics assembly will be developed. Combining the finite element formulation of the coupled plate-acoustics model illustrated in section 2.7 and the coupled plate-porous models illustrated in Section 2.9, we have that the FE formulation of the plate-HG-acoustics assembly is given by equation (69)

$$\begin{bmatrix} [K_p]-\omega^2[M_p](1+i\xi) & [0] & [0] \\ [0] & -\omega^2([M_{po}]+[M_m])+j\omega[C_{po}(\omega)]+[K_{po}(\omega)] & [C_{pa}] \\ [0] & -[C_{pa}]^T & 1/\rho_o\omega^2[H_r]-1/\rho_o c_o^2[Q_r] \end{bmatrix} \begin{Bmatrix} w \\ W_{po} \\ p_r \end{Bmatrix} = \begin{Bmatrix} F_p \\ F_{po} \\ R_r \end{Bmatrix} \quad (69)$$

In equation (69) $[H_r]$ and $[Q_r]$ represent the stiffness and the mass matrices of the radiating acoustic domain respectively. The pressure degree of freedom vector and volume displacement in the radiating acoustic domain is represented by $[P_r]$ and $[R_r]$ respectively. The mass in-homogeneities inside the porous layer of the HG blanket have been modeled using the point masses. The location of the point masses in the porous layer is captured in the $[M_m]$ matrix. The effect of these mass insertions in the porous layer is captured by adding $[M_{po}]$ and $[M_m]$ matrices. The rest of the symbols in equation (69) have already been explained in prior sections. The finite element model of the fully coupled plate-HG-acoustic system has been developed on the basis of the mathematical formulation given in equation (69).

2.11 Finite element formulation of the acoustic-plate-HG-acoustic model

In this section, the finite element formulation of the acoustic-plate-HG-acoustic fully coupled model will be discussed. The finite element formulation of the coupled plate and the acoustic domain has been explained in Section 2.7 and the finite element formulation of the plate and the porous domain has been illustrated in the Section 2.9. The mass in-homogeneity of the HG blanket has been modeled as a point mass. The inclusion of these mass in-homogeneities inside the foam layer is captured by adding point masses at the correct rows and columns in the porous mass matrix. This modified mass matrix for capturing the location of the mass inclusions is represented by $[M_m]$. The fully coupled 3D-FE formulation of the acoustic-plate-HG-acoustic is given by equation (70)

$$\begin{bmatrix} 1/\rho_o\omega^2[H_i]-1/\rho_o c_o^2[Q_i] & [K_{fs}] & [0] & [0] \\ [M_{fs}] & \left[[K_p]-\omega^2[M_p](1+i\xi)\right] & [0] & [0] \\ [0] & [0] & -\omega^2([M_{po}]+[M_m])+j\omega[C_{po}(\omega)]+[K_{po}(\omega)] & [C_{pa}] \\ [0] & [0] & -[C_{pa}]^T & 1/\rho_o\omega^2[H_r]-1/\rho_o c_o^2[Q_r] \end{bmatrix} \begin{Bmatrix} p_i \\ w \\ W_{po} \\ p_r \end{Bmatrix} = \begin{Bmatrix} R_i \\ F_p \\ F_{po} \\ R_r \end{Bmatrix} \quad (70)$$

The stiffness and the mass matrix of the incident acoustic domain are represented by $[H_i]$ and $[Q_i]$ respectively. The rest of the terms used in the equation (70) have been explained in the prior sections.

2.12 Finite element formulation of the acoustic-plate-multilayer-acoustic model

In this section, the finite element formulation of the acoustic-plate-multilayer-acoustic assembly will be discussed. The coupling conditions between the multiple porous layers used in the model given by Panneton et. al. [18] is of the form

$$\begin{aligned} &\{u\}_1 = \{u\}_2 \\ &h_1(\{U\}_1 - \{u\}_1)^T\{n\} = h_2(\{U\}_2 - \{u\}_2)^T\{n\} \end{aligned} \quad (71)$$

The first equation in the coupling conditions given by equation (71) ensures the continuity of the solid phase displacement between the two porous media at their interface. The second part of the equation (71) ensures the continuity of the relative motion between the solid and the fluid phase of the two porous media at their interface. These continuity conditions are enforced by using the Lagrange multipliers explained in Appendix A. The finite element formulation of the multiplayer porous media represented by equation (72) is of the form

$$\{-\omega^2[M_{po_M}]+[K_{po_M}(\omega)]+j\omega[C_{po_M}(\omega)]\}\{W_{po_M}\} = \{F_{po_M}\} \quad (72)$$

In equation (72) $[M_{po_M}],[C_{po_M}]$ and $[K_{po_M}]$ represent the global mass, the global damping and the global stiffness matrices of the multilayer porous media respectively. The ratio of the effective solid and fluid phase displacement vector is represented by $\{W_{po_M}\}$. The angular frequency for the dynamic system is given by ω and the effective

forcing on the multilayer is given by $\{F_{po_M}\}$. The finite element formulation of the fully coupled acoustic-plate-multilayer-acoustic model is given by equation (73)

$$\begin{bmatrix} 1/\rho_o\omega^2[H_1]-1/\rho_o c_o^2[Q_1] & [K_{fs}] & [0] & [0] \\ [M_{fs}] & \left[[K_p]-\omega^2[M_p](1+i\xi)\right] & [0] & [0] \\ [0] & [0] & \{-\omega^2[M_{po_M}]+[K_{po_M}(\omega)]+j\omega[C_{po_M}(\omega)]\} & [C_{pa}] \\ [0] & [0] & -[C_{pa}]^T & 1/\rho_o\omega^2[H_r]-1/\rho_o c_o^2[Q_r] \end{bmatrix} \begin{Bmatrix} p_i \\ w \\ W_{po_M} \\ p_r \end{Bmatrix} = \begin{Bmatrix} R_i \\ F_p \\ F_{po_M} \\ R_r \end{Bmatrix} \quad (73)$$

The rest of the terms and expressions used in equation (73) have been explained in the prior sections.

3 Numerical modeling and validation

In this section, the finite element models are developed based on the mathematical formulation illustrated in Chapter 2. The development of the numerical models can be divided into three broad categories. First, the finite element models of the individual components of the studied system shown in Figure 3 will be discussed. Models of the individual components such as the acoustics, the plate and the porous media will be validated by comparing the numerically computed results with the results obtained from the analytical and experimental investigation of the similar models. Second, the 3D-FE

fully coupled models of the plate-DVA assembly and the plate-HG assembly will be developed. These fully coupled models will be validated by comparing the numerically computed response compared with the response obtained from the experimental investigation of the similar geometry. Experimental data will be used for the validation since there are no analytical results available. Third, the validation of the aforementioned models coupled with the radiating acoustic domain will be performed.

3.1 Validation of the FE model of the acoustic domain

In this section, a 3D-FE numerical model of the acoustic domain depicted in Figure 11 a) will be discussed. The configuration of the model comprises of a 1m x 1m x 1m rigid walled rectangular cavity being excited by a unit volume displacement at its corner. The excitation source of the acoustic cavity has been placed at the corner in order to excite all the modes of the cavity. The acoustic particle velocity has been forced to be zero at the boundaries of the numerical model for capturing the rigid boundary condition of the acoustic cavity. The acoustic cavity has been discretized using 1000 hexahedral isoperimetric elements given in Cook [21] with one degree of freedom (DOF) per node corresponding to the acoustics pressure in the rectangular cavity. This mesh density has been found satisfactory for the modeling of the acoustic cavity to the required accuracy in the frequency range of interest. The air inside the cavity is assumed to have a lumped

damping ratio of $\eta_a = 0.001$.The damping matrix of the acoustic cavity is assumed to be proportional to the mass matrix of the cavity.

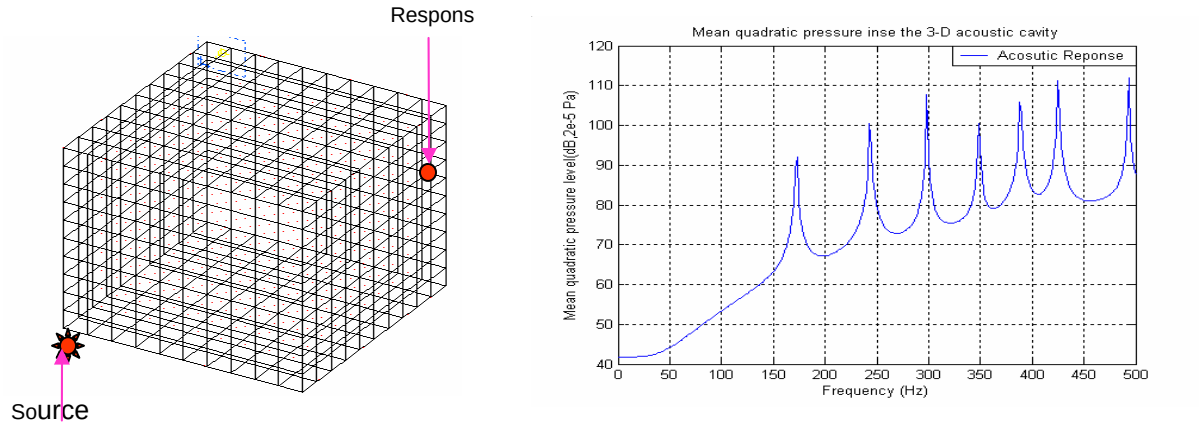

(a) (b)

Figure 11. a) Finite element model of the acoustics cavity having rigid walled boundary condition, b) The response at a point of the acoustic cavity when excited by a volume displacement at the source

The model parameters and material properties for the numerical model have been given in the Table 1. The numerical model of the cavity has been formulated based on equation (25). The numerical model is validated by comparing the numerically computed natural frequencies to the natural frequencies of the cavity computed from the analytical expression given by equation (14). Figure 11 b) depicts the response of the cavity when excited by a volume displacement at a node close to one of the corners of the cavity. Table 2 illustrates the comparison of the natural frequencies obtained from the FE model and the analytical models. As can be seen excellent agreement is observed between the numerically computed natural frequencies and the natural frequencies of the acoustic cavity evaluated from the analytical expression.

Table 1. Model parameters and material properties used in the FE model of the acoustic cavity

Properties	**Value**
Model Parameters	
Number of elements	1000
Boundary condition	Rigid walled
Dimensions	1x1x1 (m)
Material properties	
Density	1.2 kg/ m^3

Speed of sound	343 m/s

Table 2. Comparison between the numerically computed resonance frequency from the finite element model of the acoustic cavity (VAL-FE code) and the resonance frequencies computed from the analytical expression

Modes	Resonance frequency (Analytical)	Resonance frequency (VAL-FE code)	% Error
(1,0,0) etc….	172	171.8	0.1
(1,1,0) etc….	243	243	0
(1,1,1) etc….	298	298	0
(2,0,0) etc….	343	347	1.2
(2,1,0) etc…	388	389	0.3
(2,1,2) etc….	420	425	1.18

3.2 Validation of the Plate model

In this section, a 3D-FE numerical model of the plate domain depicted in Figure 12 a) will be discussed. The configuration of the numerical model comprises of an aluminum plate having dimensions 200 mm x 300 mm and having all its edges clamped and being excited by a point force. The plate has been discretized using 150 rectangular plate elements derived by Yang [17]. The plate element has four degree of freedom (DOF) per node corresponding to the normal displacement$\{w\}$, rotation about the x axis$\{w_x\}$, rotation about the y axis $\{w_y\}$ and the twist in the rectangular plate element$\{w_{xy}\}$. The mesh density has been found to be satisfactory for the modeling of the plate to the required accuracy in the frequency range of interest. The material of the plate is aluminum and is assumed to have a lumped damping ratio of $\eta_s = 0.05$. The damping matrix of the plate is assumed to be proportional to the mass matrix of the plate. The boundary conditions of the numerical model are enforced by setting the displacement of the nodes and the moments on the nodes at the plate edges to be zero.

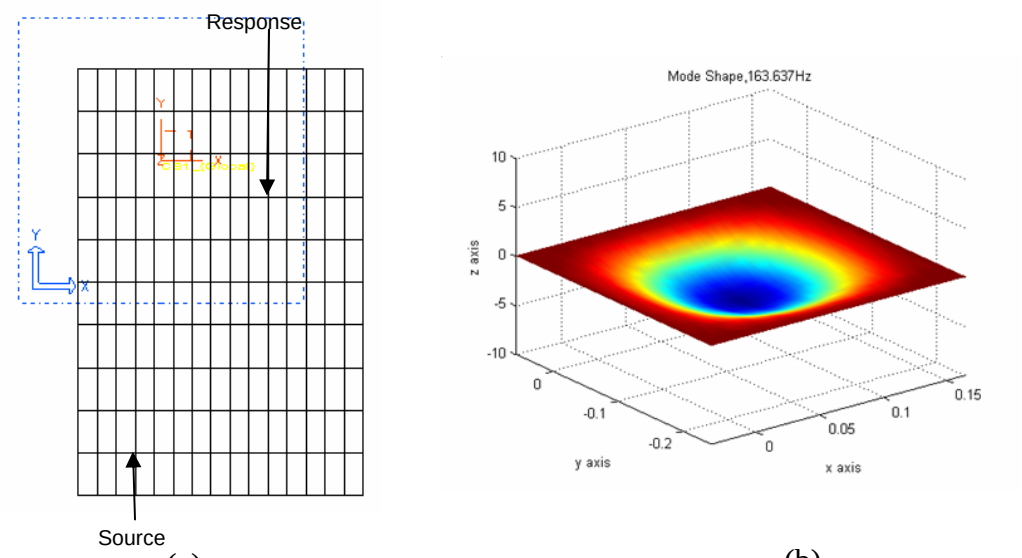

(a) (b)

Figure 12. a) Finite element model of the plate having clamped edges and excited by a point source, b) The (1,1) numerically computed (VLA-FE code) mode shape of the plate

The model parameters and material properties used in the finite element (FE) model of the plate have been given in the Table 3. The numerical model of the plate has been formulated based on equation (44). The numerical model is validated by comparing the natural frequencies obtained from the numerical model with the natural frequencies of the plate computed using ANSYS (a commercially accepted FE code for structural and dynamic analysis). Figure 12 b) depicts (1, 1) mode shape of the plate when excited by a point source. Table 4 illustrates the comparison of the natural frequencies obtained from the VAL-FE code and the resonance frequencies obtained from a similar model in ANSYS.

Table 3. Model parameters and material properties of the finite element model of the plate

Properties	**Value**
Model Parameters	
Number of elements	150
Boundary condition	Clamped -Clamped
Dimensions	200x300 (mm)
Material properties	
Density	7700 kg/ m^3
Young modulus	19.1e10 m/s
Poisson's ratio	0.3

Table 4. Comparison between the numerically computed resonance frequency from the finite element model of the plate (VAL-FE code) and the resonance frequencies computed from modeling a similar plate in Ansys

Modes	Resonance frequency (Ansys)	Resonance frequency (VAL-FE code)	% Error
(1,1)	131	131	0
(2,1)	203	203	0
(1,2)	321	322	0.3
(3,1)	323	324	0.3
(2,2)	387	389	0.5

As seen in Table 4, excellent agreement is observed between the natural frequencies obtained from the VAL-FE code and the frequencies obtained from a similar model in ANSYS.

3.3 Validation of the porous domain model

In this section, a 3D-FE numerical model of the porous domain depicted in Figure 13 a) will be discussed. The configuration of the numerical model for the porous media comprises of a laterally infinite layer of glass wool bonded at its rear end to an impervious rigid wall being excited by a unit amplitude normal plain wave at its front end. The porous media has been discretized using 10 hexahedral elements given in Cook [21]. The hexahedral elements used for the modeling of the porous media follow the Biot theory given in Allard [20] as implemented by Panneton et. al. [18]. The hexahedral elements have eight nodes with six DOF for each node. These six degrees of freedom account for the three displacements of the solid phase $\{u\}$ of the porous media and three displacements of the fluid phase $\{U\}$ of the porous media. To simulate the laterally infinite porous layer in the FE model only the axial microscopic displacements of the solid and the fluid phase of the porous media are considered and the lateral degrees of freedom are set zero.

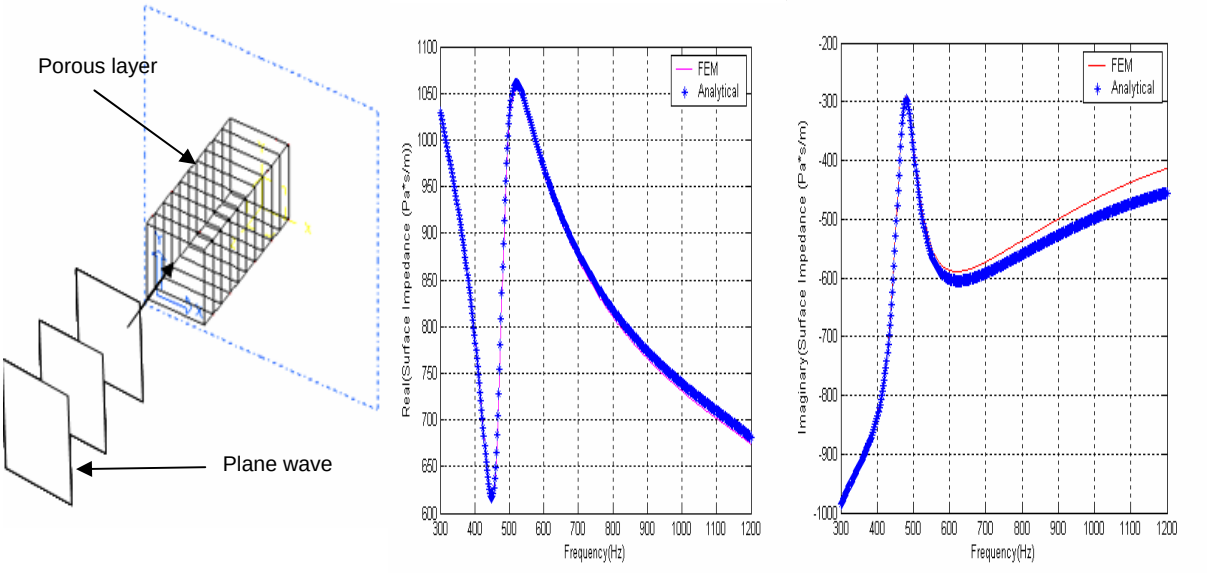

(a) (b) (c)

Figure 13. a) Finite element formulation of a laterally infinite porous layer bonded to a impervious wall at is rear face, b) Comparison of the numerically computed real part of the surface impedance with the real part of the surface impedance given in Allard [20], c) Comparison of the numerically computed imaginary part of the surface impedance with the imaginary part of the surface impedance given in Allard [20]

The model parameters and material properties for the numerical model are given in the Table 5. The numerical model of the porous media has been formulated based on the equation (55). The numerical model of the porous media is validated by comparing the real and imaginary part of the surface impedance of the porous layer from the VAL-FE code to the surface impedance of a similar model of the porous media computed using analytical solution given in Allard [20]. Figure 13 b) and Figure 13 c) depicts the comparison of the real and imaginary part of the surface impedance computed numerically and analytically respectively.

Table 5. Model and material properties of the numerical model of the porous media

Properties	Value
Model Parameters	
Number of elements	10
Boundary condition	Bonded at the rear face
Dimensions	50x50x100 (mm)
Material properties	

Density (ρ_1)	130 kg/ m^3
Young modulus (N)	220e3
Poisson's ratio (ν)	0
Tortuosity (α_∞)	1.06
Flow resistivity (σ)	40000
Porosity (ϕ)	0.99
Atmospheric pressure (P_a)	1.10325e5
Structural damping (η_s)	0.1
Viscous characteristics length (Λ)	56e-6
Thermal characteristics length (Λ')	110e-6

As seen in Figure 13 b) and Figure13 c) excellent agreement is observed between the numerical and analytical evaluation of the real and the imaginary part of the surface impedance of the porous layer.

3.4 Validation of the multilayer porous layer model

The 3D-FE numerical model of multiple porous layers (MPL) depicted in Figure 14 a) consists of the laterally infinite porous layers of blanket, screen, Foam A and Foam B from the front to the rear. The material properties of these porous layers have been tabulated in Table 6 as have been given by Panneton et. al.[18]. MPL is bonded to an impervious rigid wall at the rear face of the foam B and is being excited by a unit amplitude normal plain wave at the front face of the blanket. MPL has been discretized using the hexahedral elements given in Cook [21]. The hexahedral elements used for the modeling of the porous layers in the MPL follow the Biot's theory illustrated in Allard [20] as implemented by Panneton et. al. [18]. The hexahedral elements have eight nodes with six DOF for each node. These six degrees of freedom account for the three displacements of the solid phase $\{u\}$ of the porous media and three displacements of the fluid phase $\{U\}$ of the porous media. To simulate the laterally infinite porous layers in the FE model of the MPL only the axial microscopic displacements of the solid and the fluid phase of the porous layers are considered and the lateral degrees of freedom for both the

solid and the fluid phase of the porous layers are set zero. The blanket, the screen and the foam A were discretized using only one hexahedral element and foam B with two elements.

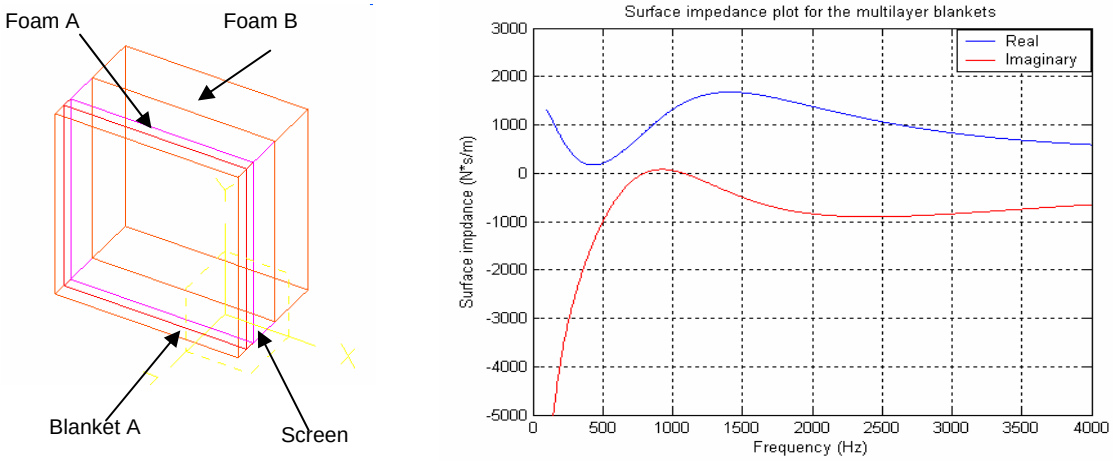

(a) (b)

Figure 14. a) Finite element formulation of the laterally infinite porous layers bonded to a impervious wall at their rear face, b) Numerically computed real and imaginary part of the surface impedance for the multiple porous layers

The model parameters and material properties for the numerical model have been given in the Table 6. The numerical model of the multilayer porous media has been formulated based on equation (55). The numerical model is validated by comparing the real and imaginary surface impedance computed from the VAL-FE code to the surface impedance of a similar model computed by Panneton et. al. [18]. Figure 14 b) depicts the comparison of the real and imaginary part of the surface impedance computed numerically from the VAL-FE code. The numerically computed value of the imaginary and the real surface impedance depicted in Figure 14 b) matches the imaginary and real surface impedance plot computed using a similar model by Panneton et. al. [18] respectively. Efforts have been made to reach R. Panneton for using his figures but he has been unreachable.

Table 6. Model and material properties for the numerical model of the multilayer porous media

Properties	Blanket	Screen	Foam A	Foam B
Model parameters				
Number of elements	1	1	1	2

Boundary condition	Free	Free	Free	Bonded at the rear face
Dimensions	50x50x4 (mm)	50x50x0.8 (mm)	50x50x5 (mm)	50x50x16 (mm)
Material properties				
Density (ρ_1)	41 kg/ m^3	125 kg/ m^3	31kg/ m^3	16 kg/ m^3
Young modulus (N)	110 KN/ m^2	1000 KN/ m^2	55KN/ m^2	18 KN/ m^2
Poisson's ratio (ν)	0.3	0.3	0.3	0.3
Tortuosity (α_∞)	1.18	2.56	2.52	1.98
Flow resistivity (σ)	34000	320e4	87000	65000
Porosity (ϕ)	0.98	0.80	0.97	0.99
Atmospheric pressure (P_a)	1.10325e5	1.10325e5	1.10325e5	1.10325e5
Structural damping (η_s)	0.015	0.1	0.055	0.1
Viscous characteristics length (Λ)	60e-6	6e-6	37e-6	37e-6
Thermal characteristics length (Λ')	87e-6	24e-6	119e-4	121e-6

Excellent agreement is observed on comparing the numerically computed real and imaginary parts of the surface impedance of the multiple layers shown in Figure 14 b) and the real and the imaginary parts of the surface impedance of the system computed in Panneton et. al. [18] using a similar model.

3.5 Validation of the DVA model

In this section, a 3D-FE fully coupled numerical model of the DVA depicted in Figure 15 b) has been validated by comparing the response of the DVA computed using the VAL-FE code with the response evaluated by the experimental investigation of a similar model depicted in Figure 15 a). The DVA consists of a mass layer plate of aluminum attached to a layer of melamine foam.

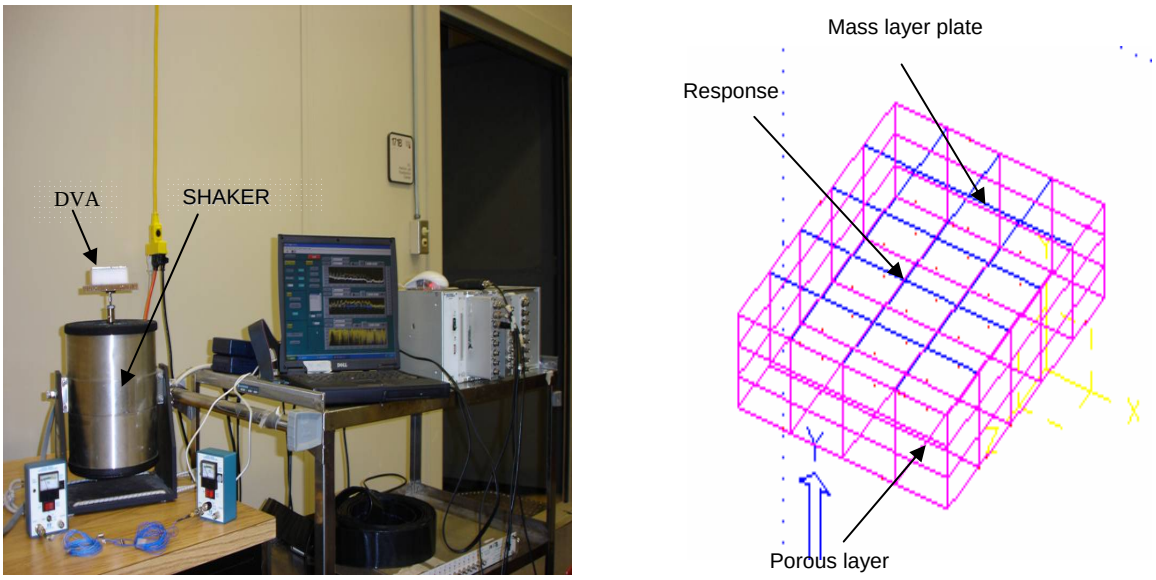

(a) (b)

Figure 15. a) Experimental setup for the DVA validation, b) Numerical model of the DVA validation.

Experimental investigation of the DVA

The experimental setup for the DVA shown in Figure 15 a) consists of a composite plate with a DVA treatment mounted on an electro-dynamic shaker. The bottom surface of the porous layer of the DVA is glued to the composite plate and the top surface is glued to the aluminum mass layer of the DVA. The electro-dynamic shaker driven by the white noise signal excites the composite plate, which excites the base of the DVA glued to it. The transverse acceleration of the composite plate and the transverse acceleration of the mass layer plate of the DVA are measured using light weight accelerometers. The acceleration signals are measured through the spectrum analyzer to calculate the transfer function between the acceleration of the mass layer and the acceleration of the composite plate. The transfer function obtained from the experimental investigation of the DVA is shown in Figure 16 and would be discussed in detail later.

3D-FE model of the DVA

The finite element model of the DVA shown in Figure 15 b) consists of an aluminum mass layer plate covering a layer of melamine foam. The mass layer has been

discretized using 20 rectangular plate elements given in Yang [17] and the porous layer is discretized using 60 hexahedral elements following the finite element (FE) formulation derived in Panneton et. al. [18]. In the absence of the coupling between the mass layer and the porous media, both the meshes have been found to be satisfactory in capturing the dynamics of the porous media and the mass layer plate individually in the frequency range of interest. The coupled numerical model is based on the FE formulation given in equation (68).The model parameters and the material properties of the mass layer and the porous media used in the finite element model of the DVA are given in Table 7. A uniform displacement function of unit amplitude is applied at all the nodes of the base of the DVA model to simulate the forcing function imparted to the base of the DVA in the experimental setup. The numerically computed response is measured at the central node of the mass layer. The transfer function between the measured response of the mass layer and the unit displacement at the base of the DVA is depicted in Figure 16.

Table 7. Model and material properties of the finite element model of the DVA

Properties	**Values**
Model parameters	
Number of elements of the foam	60
Number of elements of the plate	20
Boundary condition of the foam	Bonded at the base
Boundary condition of the plate	Free-Free
Dimensions of the foam	80x100x26 (mm)
Dimensions of the plate	80x100 (mm)
Material properties of the foam	
Density (ρ_1)	8.8 kg/ m^3
Young modulus (N)	258e3 N/ m^3
Poisson's ratio (ν)	0.3
Tortuosity (α_∞)	1.02
Flow resistivity (σ)	32000
Porosity (ϕ)	0.99
Atmospheric pressure (P_a)	1.10325e5

Structural damping (η_s)	0.07
Viscous characteristics length (Λ)	100e-6
Thermal characteristics length (Λ')	130e-6
Material properties of the plate	
Density	2700
Young modulus	7.0e10
Poissions ratio	0.3

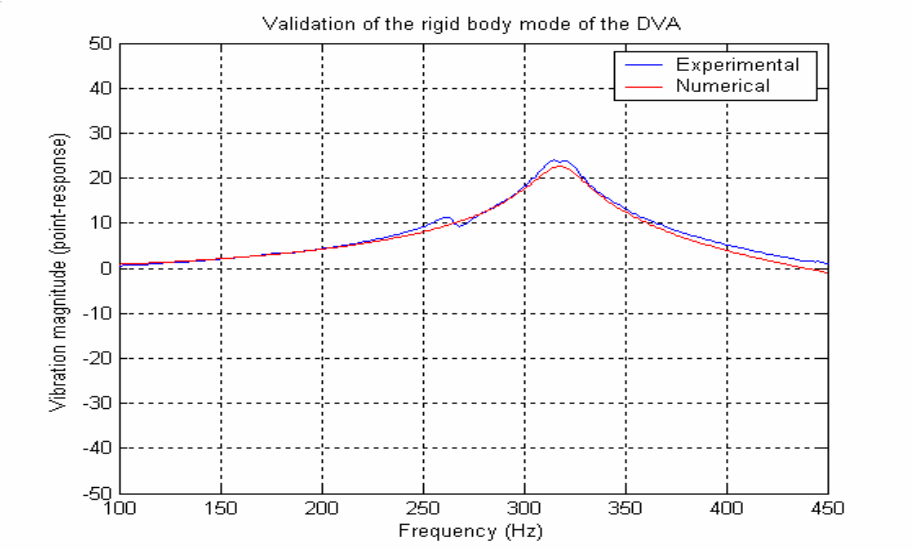

Figure 16 Comparison of the numerically computed (VAL-FE code) response of the DVA with the response of the DVA obtained from the experimental investigation of a similar geometry

Excellent agreement is observed in Figure 16 between the numerically computed response of the DVA using the VAL-FE code and response obtained from the experimental investigation of a similar model shown in Figure 15 a). It can be concluded from the Figure 16 that we are able to capture the magnitude of the response of the DVA at its resonance frequency and are also able to model the distribution of damping of the DVA very effectively with the use of the fully coupled 3D-FE model of the DVA. A further investigation in the response of the DVA shows that the resonance frequency in Figure 16 represents the rigid body mode of the DVA.

3.6 Validation of the HG blankets model

In this section, a 3D-FE fully coupled numerical model of the HG blanket depicted in Figure 17 b) has been validated by comparing the response of the HG blanket computed using the VAL-FE code with the response evaluated by the experimental investigation of a similar model shown in Figure 17 a). The HG blanket consists of a mass in-homogeneity in the form of an steel ball bearing inside a layer of porous media.

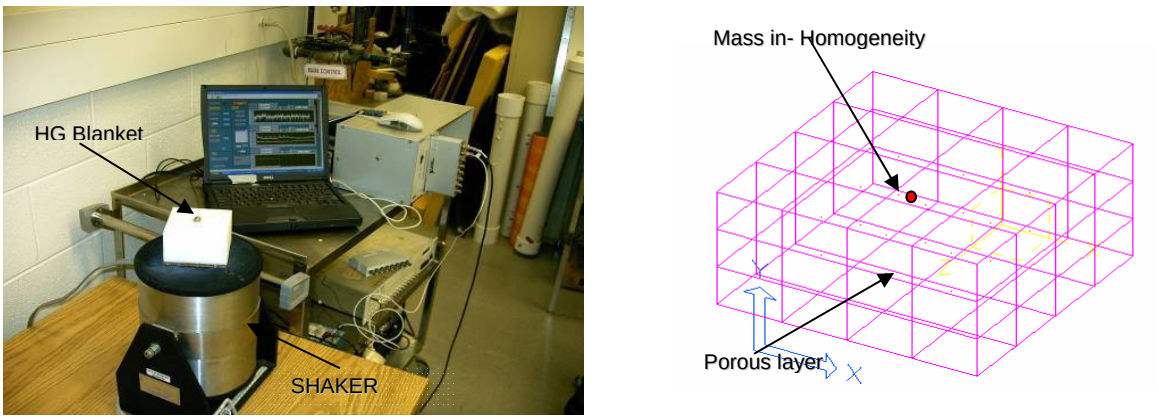

(a) (b)

Figure 17. a) Experimental setup for the validation of the numerical model of the HG blanket, b) Finite element model of the HG blanket

Experimental investigation of the HG blanket

The experimental setup for the HG blanket shown in Figure 17 a) consists of a composite plate with a HG blanket treatment mounted on an electro-dynamic shaker. A mass in-homogeneity is inserted inside the foam but for the illumination purposes the top layer of the HG blanket has been cut off to show the mass in-homogeneity in the experimental set up depicted in Figure 17 a). The bottom surface of the porous layer of the HG blanket is glued to the composite plate. The electro-dynamic shaker driven by the white noise signal excites the composite plate, which excites the HG blanket glued to it. The transverse acceleration of the composite plate and the transverse acceleration of the mass in-homogeneity inside the porous layer of the HG blanket is measured using light weight accelerometers. The acceleration signal are measured by a spectrum analyzer to calculate the transfer function between the acceleration of the mass in-homogeneity and the acceleration of the composite base plate. The transfer function obtained from the

experimental investigation of the HG blanket is shown in Figure 18 and would be discussed later in the section.

3D-FE model of the HG blanket

The finite element model of the HG blanket shown in Figure 17 b) consists of a mass in-homogeneity inserted into a layer of melamine foam. The mass in-homogeneity has been modeled as a point mass and the porous layer is discretized using 60 hexahedral elements following the mathematical formulation derived in Panneton et. al. [18]. In the absence of the coupling between the mass in-homogeneity and the porous media, the mesh density has been found to be satisfactory in capturing the dynamics of the porous layer in the frequency range of interest. The model parameters and the material properties of the mass in-homogeneity and the porous media used in the finite element model of the HG blanket are given in Table 8. A uniform displacement function of unit amplitude is applied at all the nodes at the base of the HG blanket model to simulate the uniform forcing function applied to the base of the HG blanket in the experimental setup. The response is measured at the node where the mass in-homogeneity has been inserted in the porous layer. The transfer function between the measured response of the mass in-homogeneity and the unit displacement at the base of the HG blanket is depicted in Figure 18.

Table 8. Model parameters and material properties of the finite element model of the HG blanket

Properties	Values
Model parameters	
Number of elements of porous media	60
Number of elements of plate	20
Boundary condition of the porous media	Free-Free
Boundary condition of the mass in-homogeneity	Free-Free
Dimensions of the porous media	80x100x26 (mm)
Dimensions of the mass in-homogeneity	Point mass
Material properties of the porous media	
Density (ρ_1)	20 kg/ m^3
Young modulus (N)	28.6e4 N/ m^2
Poisson's ratio (ν)	0.3

Tortuosity (α_∞)	1.7
Flow resistivity (σ)	32000
Porosity (ϕ)	0.99
Atmospheric pressure (P_a)	1.10325e5
Structural damping (η_s)	0.1
Viscous characteristics length (Λ)	50e-6
Thermal characteristics length (Λ')	110e-6
Material properties of the point mass	
Density	2700
Young modulus	7.0e10
Poisson's ratio	0.3

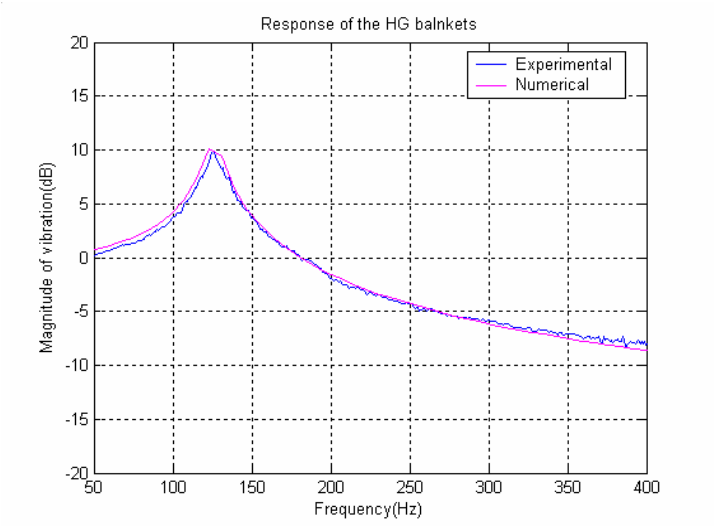

Figure 18. Comparison of the numerically computed (VAL-FE code) response of the DVA with the response of the DVA obtained from the experimental investigation of a similar system

Excellent agreement is observed in Figure 18 between the numerically computed response of the HG blanket using the VAL-FE code and response of the HG blanket obtained from the experimental investigation of a similar model. It can be concluded from the plot in Figure 18 that we are able to match the magnitude of the transfer function at the resonance frequency of the mass in-homogeneity inside the HG blanket and are also able to capture the distribution of the damping of the HG blanket using the

numerical model. This resonance frequency corresponds to the rigid body mode of the HG blanket acting as a single degree of freedom vibration absorber.

3.7 Validation of the coupled plate-acoustic model

In this section, a 3D-FE fully coupled numerical model of the plate and the acoustic domain depicted in Figure 19 b) will be validated. The validation has been achieved by comparing the numerically computed response of the plate and the acoustics domain of the coupled model with the response evaluated by the experimental investigation of a similar model shown in Figure 19 a). The coupled model consists of an aluminum plate clamped at its edges and attached to a rigid walled radiating acoustic cavity.

Experimental investigation of the coupled plate-acoustics model

The experimental setup for the coupled plate acoustics model shown in Figure 19 a) consists of a clamped aluminum plate coupled to a rigid walled radiating acoustic cavity made of medium density fiber bound (MDF). The clamped plate acts as one of the six surfaces of the rigid walled rectangular cavity. An impulse excitation imparted by a hammer is used to drive the plate which radiates sound into the coupled radiating acoustic cavity. The transverse acceleration of the aluminum plate is measured using a light weight accelerometer and the sound pressure fluctuation induced by the vibrating plate inside the coupled radiating acoustic cavity is measured using a small condenser microphone. The excitation signal from the hammer, acceleration signal from the accelerometer and the pressure fluctuation signal from the microphone are collected by the spectrum analyzer. These signals are used to calculate the transfer function between the acceleration of the plate, the sound radiation in the acoustic cavity and the excitation signal of the hammer. The transfer functions of the plate response and the acoustic response obtained from the experimental investigation of the coupled model are shown in Figure 20 and would be discussed later in the section.

3D-FE model of the coupled plate-acoustic model

The finite element model of the coupled plate-acoustic assembly shown in figure 19 b) consists of an aluminum plate clamped at its edges and backed by a rigid walled radiating acoustic cavity. The plate has been discretized using 10x15 rectangular plate

elements given in Yang [17] and the acoustic cavity is discretized using 10x15x3 hexahedral acoustic elements given in Cook [21].

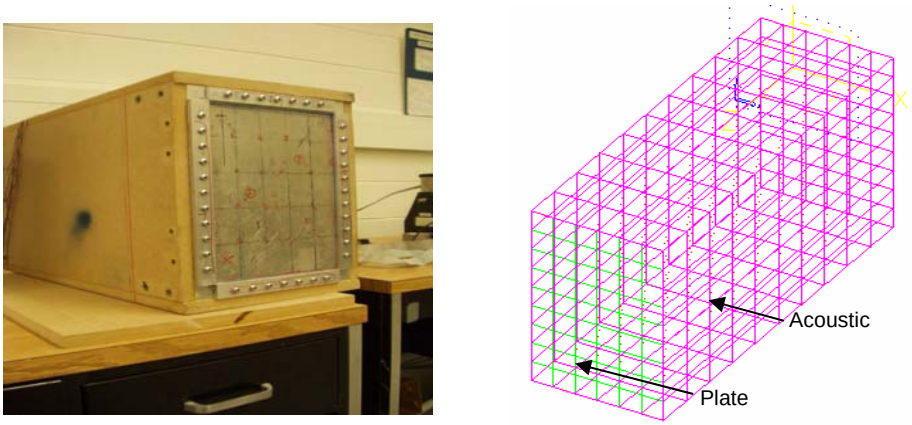

(a) (b)

Figure 19. a) Experimental set up for the validation of the numerical model of the plate-acoustic model, b) Finite Element model of the plate-acoustic model

The plate elements are based on the mathematical formulation given by the equation (44) and the acoustic finite element model is based on the finite element formulation given in equation (25). In the absence of the coupling between plate and the acoustic cavity, the individual mesh densities of the plate and the acoustic domain have been found to be satisfactory in capturing the dynamics of these components in the frequency range of interest. The coupled model of the plate-acoustic assembly is based on the mathematical formulation given in equation (61). The model parameters and the material properties of the plate and the acoustic cavity used in the coupled FE model are given in Table 9. A point force excitation equivalent to the impulse excitation imparted to the aluminum plate in the experiment is used for driving the aluminum plate and the response is measured at the plate and inside the radiating acoustic cavity. The transfer functions between the numerically computed response of the base plate and the point force on the base plate is depicted in Figure 20 a). The transfer function between the measured response of the acoustic cavity and the base plate excitation is shown in Figure 20 b). Figure 20 illustrates a good agreement between the numerically computed response of the coupled FE model computed using the VAL-FE code and its response obtained from the experimental investigation of a similar model shown in Figure 19 a).

Table 9. Model parameters and material properties of the coupled plate-acoustic model

Properties	Values
Model parameters	
Number of elements of acoustic media	270
Number of elements of plate	54
Boundary condition of the acoustic media	Rigid walled cavity
Boundary condition of the plate	Clamped-Clamped
Dimensions of the plate	206x308 (mm)
Dimensions of the acoustic cavity	206x308x597 (mm)
Material properties of the plate	
Density	2700 kg/m(3)
Young modulus	7.0e10
Poisson's ratio	0.3
Material properties of the acoustic domain	
Density	1.2 kg/m(3)
Speed of sound	343
Poisson's ratio	0.0

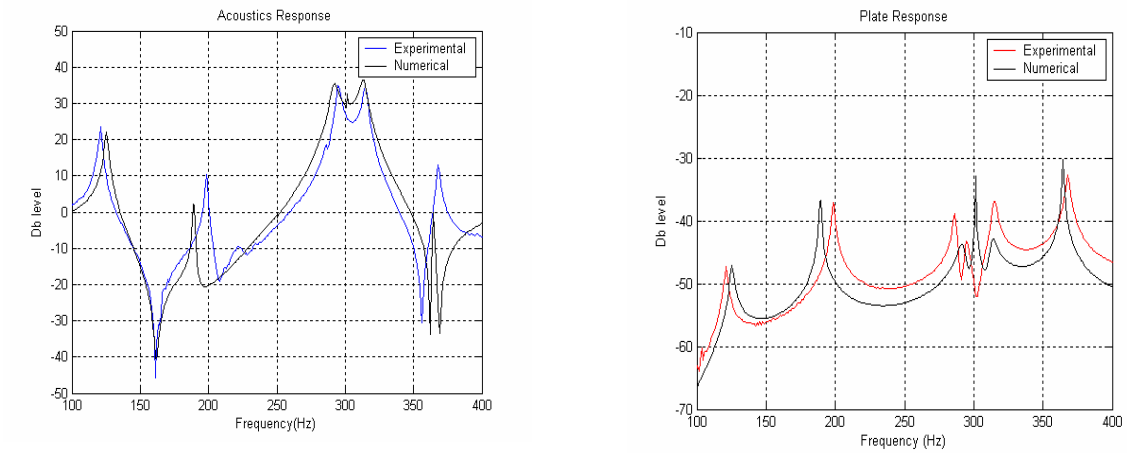

(a) (b)

Figure 20. a) Comparison of the numerically computed plate response with the experimental results, b) Comparison of the numerically computed acoustic response with the experimental results

It can be concluded from the Figure 20 a) that the numerical model is able to capture the magnitude and the distribution of damping of the base plate response in the fully coupled plate-acoustic model over a broad bandwidth of frequency. There is a slight mismatch in the numerically computed response of the plate and the response of the plate obtained from the experimental investigation as shown in Figure 20 a) in the frequency range of 350-400 Hz. This is primarily due to the inadequacy in the mesh density of the plate and the acoustic domains in the coupled model, which reduces the ability of the numerical model to capture the physics of the problem at high frequencies.

Figure 20 b) shows good agreement between the numerically computed acoustic responses with the acoustic response obtained from the experimental investigation of the coupled model. It can be observed from the Figure 20 b) that the acoustic response in the coupled plate-acoustic model is dominated by the dynamics of the plate. The numerical model is able to capture both the magnitude of the acoustic response at the resonance frequencies and the distribution of the damping in the acoustic cavity of the coupled model. There is a mismatch in the numerically computed and experimentally obtained acoustic response at the resonance frequency of 300 Hz, which corresponds to the first mode of the radiating acoustic cavity. This mismatch between the numerically computed result and the result from the experimental investigation of a similar model is primarily due to two reasons. First, the sparse mesh density of the acoustic media reduces the ability of the numerical model to capture the inherent damping inside the acoustic cavity at its resonance frequencies. Second, as the radiating acoustic domain built for the experimental set up is not perfectly airtight any leakage of the SPL's from the acoustic domain would add additional damping to the response of the radiating acoustic domain obtained from the experimental set up.

3.8 Validation of the coupled acoustic-plate-acoustics model

In the following section, a 3D-FE fully coupled numerical model consisting of the incident acoustics domain, the plate and the radiating acoustic cavity assembly will be discussed. The numerical model depicted in Figure 21 b) is validated by comparing the numerically computed response of the coupled model to the response obtained from the experimental investigation of a similar model. The coupled model consists of an incident

acoustic domain coupled to a clamped aluminum plate. The acoustic-plate assembly is in turn coupled to a radiating acoustic cavity.

Experimental investigation of the coupled acoustic-plate-acoustics model

The experimental setup for the coupled acoustic-plate-acoustic model shown in Figure 21 a) consists of a clamped aluminum plate coupled to a rigid walled incident acoustic cavity and a rigid walled radiating acoustic cavity. The walls of the acoustic cavities are made up of medium density fiber bound (MDF). The clamped plate acts as the partition between the two rigid walled rectangular cavities. A volume displacement from a speaker is used as an excitation source of the incident acoustic domain which in turn drives the plate partitioning the two rectangular cavities. The plate excited from the incident acoustic domain radiates sound energy into the coupled radiating acoustic domain. The transverse acceleration of the speaker diaphragms and the transverse acceleration of the aluminum plate are measured using light weight accelerometers. The sound pressure fluctuation in the incident and radiating acoustic domains is measured using small condenser microphones. The acceleration signal from the speaker, acceleration signal from the accelerometer on the plate and the pressure signal from the microphones inside the two acoustic cavities are measured by the spectrum analyzer. The transfer function between the acceleration of the plate and the acceleration of the speaker diaphragm and the transfer function between the sound radiation in the coupled radiating acoustic cavity and the acceleration signal from the speaker diaphragm are computed. These transfer functions obtained from the experimental investigation of the 3D-FE fully coupled model of the acoustic-plate-acoustic assembly are depicted in Figure 22.

3D-FE modeling of the acoustic-plate-acoustic model

The finite element model of the coupled acoustic-plate-acoustic model shown in Figure 21 b) consists of an aluminum plate clamped at its edges driven by a volume displacement in the incident acoustic domain and backed by a radiating rigid walled acoustic cavity. The plate has been discretized using 10x15 rectangular plate elements given in Yang [17]. The incident acoustic cavity is discretized using 10x15x7 hexahedral acoustic elements given in Cooks [21]. The radiating acoustic cavity is discretized using 10x15x10 hexahedral acoustic elements given in Cooks [21].

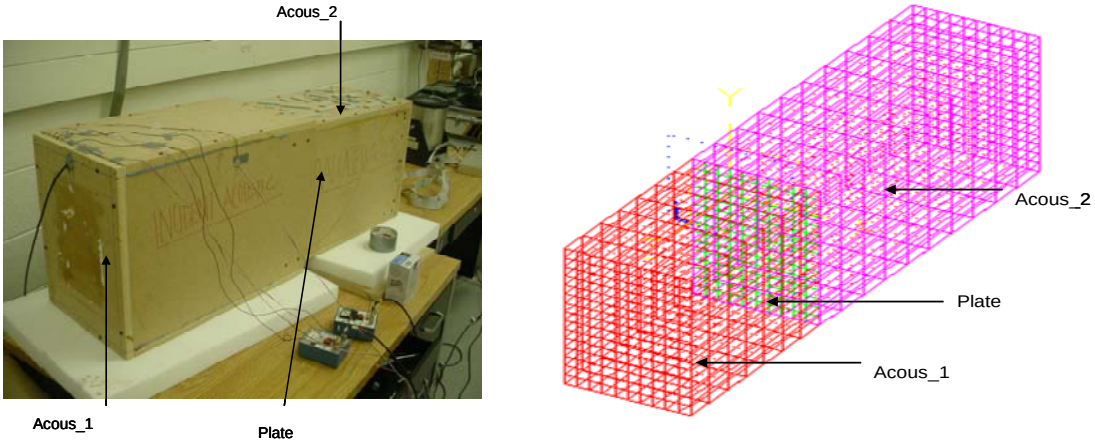

Figure 21. a) Experimental set up for the validation of the numerical model of the acoustic-plate-acoustic assembly, b) Finite element model of the acoustic-plate-acoustic model

The plate elements are based on the finite element formulation given by equation (44) and the acoustic finite elements for the incident and the radiating acoustic domains are based on equation (25). In the absence of the coupling between the plate and the acoustic cavities, the mesh densities of the individual components of the coupled model have been found to be satisfactory in capturing the dynamics of the components in the frequency range of interest. The model parameters and the material properties of the plate and the acoustic cavity used in the coupled acoustic-plate-acoustic assembly are given in Table 9. A volume displacement is imparted to the incident acoustic domain, which is equivalent to the speaker excitation of the incident acoustic domain in the experiment. The response is measured at the plate and inside the radiating acoustic cavity. The numerically computed transfer functions between the measured response of the plate and the volume displacement in the incident acoustic cavity is depicted in Figure 22 a). The numerically computed transfer functions between the measured response of the radiating acoustic cavity and volume displacement in the incident acoustic domain is depicted in Figure 22 b).

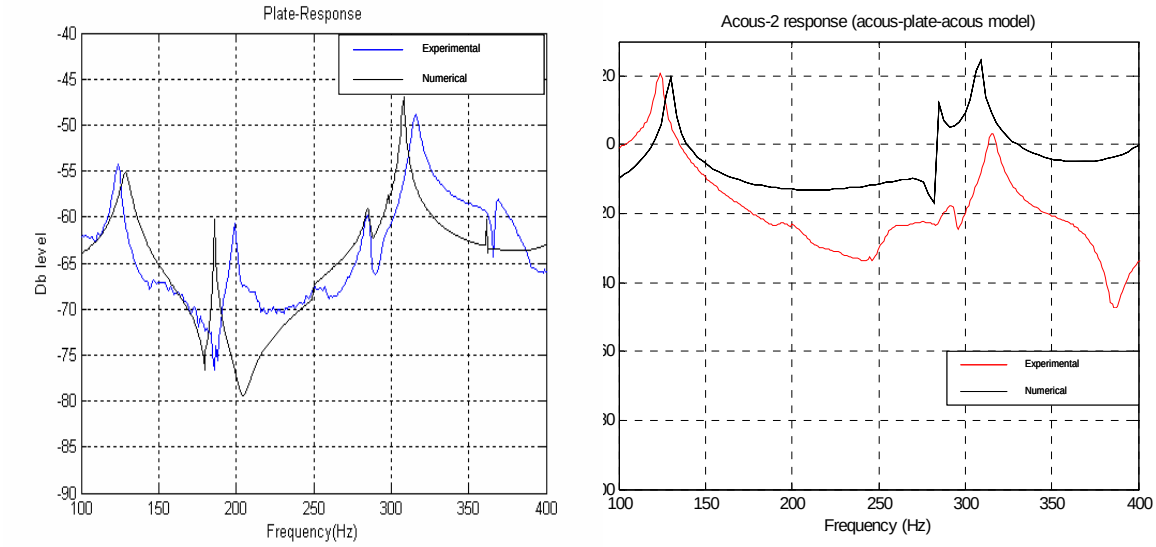

(a) (b)

Figure 22. a) Comparison of the numerically computed plate response with the experimental results for the coupled acoustic-plate-acoustic model, b) Comparison of the numerically computed acoustic response with the experimental results for the acoustic-plate-acoustic model

Figure 22 illustrates a good agreement between the numerically computed response of the coupled 3D-FE model computed using the VAL-FE code and response obtained from the experimental investigation of a similar model shown in Figure 21 a). Figure 22 a) depicts the comparison of the numerically computed response of the plate and the response of the plate obtained from the experimental investigation of the fully coupled model. It can be concluded from the Figure 22 a) that the numerical model is able to capture the magnitude of the dynamics and the distribution of the damping of the plate response in the coupled model. It can be concluded from the Figure 22 a) that though the plate is coupled to an incident and a radiating acoustic domain, no loading effect of these acoustic cavities is observed on the response of the plate in the coupled model. This is due to the fact there is a substantial difference in the impedance of the plate and the impedance of the acoustic domain.

Figure 22 b) depicts the comparison of the numerically computed response of the radiating acoustic cavity and the response of the radiating acoustic cavity obtained from the experimental investigation of the fully coupled model. It can be observed that though the numerical model is able to capture the resonance frequencies of the radiating acoustic domain, it is unable to model the distribution of the damping of the radiating acoustic

domain at the high frequencies. This mismatch between the numerically computed result and the result from the experimental investigation of a similar model is primarily due to two reasons. First, the sparse mesh density of the acoustic media reduces the ability of the numerical model to capture the inherent damping inside the acoustic cavity at its resonance frequencies for such a complex model. Second, as the radiating acoustic domain built for the experimental set up is not perfectly airtight any leakage of the SPL's from the acoustic domain would add additional damping to the response of the radiating acoustic domain obtained from the experimental set up.

3.9 Coupled plate-porous modeling and validation

After the successful validation of the individual models of the plate and the porous media, a 3D-FE fully coupled numerical model of the plate-porous media will be validated. The 3D-FE numerical model of the coupled plate and porous domain model depicted in Figure 23 b) has been validated by comparing the response of the coupled model computed using the VAL-FE code with the response evaluated by the experimental investigation of a similar model given in Figure 23 a). The coupled model consists of an aluminum plate clamped at its edges and attached to a porous layer.

Experimental investigation of the coupled plate-porous model

The experimental setup for the 3D-FE fully coupled plate-porous model shown in Figure 23 a) consists of a clamped aluminum plate coupled to a layer of the foam. An impulse excitation is imparted to the plate by a hammer, which excites the coupled porous media. The transverse acceleration of the aluminum plate is measured using a light weight accelerometer. The excitation signal from the hammer and the acceleration signal from the accelerometer on the base plate are measured by the spectrum analyzer to calculate the transfer function between the acceleration of the response point on the base plate and the excitation signal of the hammer. The transfer function obtained from the experimental investigation of the response point is shown in Figure 24.

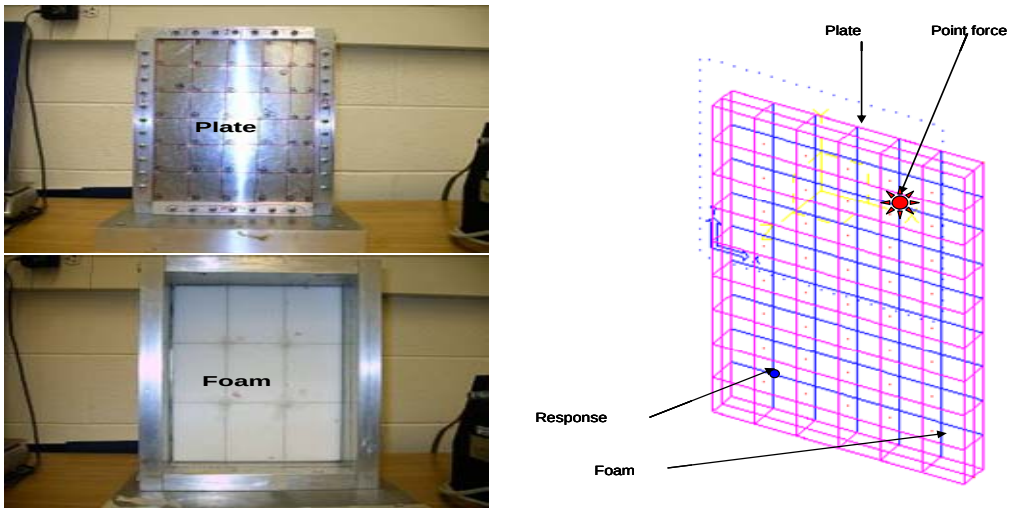

(a) (b)

Figure 23. a) Experimental set up for the validation of the numerical model of the plate-porous assembly, b) Finite element model for the plate-porous assembly

3D-FE modeling of the plate-porous model

The finite element model of the 3D-FE fully coupled plate-porous assembly shown in Figure 23 b) consists of an aluminum plate clamped at its edges backed by a layer of porous media. The plate has been discretized using 9x6 rectangular plate elements given in Yang [17] and the porous media is discretized using 9x6x2 hexahedral elements given by Cooks [21]. The hexahedral elements used for the modeling of the porous layer follow the finite element formulation for the porous media derived by Panneton et. al. [18]. The plate elements are based on the mathematical formulation given by equation (44) and the finite element formulation of the porous media are based on equation (55). In the absence of the coupling between plate and the porous domain, the mesh densities of the components of the model have been found to be satisfactory in capturing the dynamics of the individual components in the frequency range of interest. The coupled model is based on the FE formulation given in equation (68). The model parameters and the material properties of the plate and the porous media used in the numerical model of the plate and the porous domain are given in Table 10. A point force excitation equivalent to the impulse excitation imparted by the hammer to the aluminum plate has been used for driving the clamped plate. The response is measured at the

response nodes on the plate and in the radiating acoustic cavity. The transfer function between the measured response of the plate and the point force on it is depicted in Figure 24.

Table 10. Model parameters and material properties of the numerical model of the plate-porous assembly

Properties	Values
Model parameters	
Number of elements of plate	54
Number of elements of the porous media	108
Boundary condition of the plate	Clamped-Calmped
Boundary condition of the porous media	Free-Free
Dimensions of the plate	206x308 (mm)
Dimensions of the porous media	206x308x26 (mm)
Material properties of the plate	
Density	2700 kg/m(3)
Young modulus	7.0e10
Poisson's ratio	0.3
Material properties of the porous media	
Density (ρ_1)	50 kg/m(3)
Young modulus (N)	220e3
Poisson's ratio (ν)	0.3
Tortuosity (α_∞)	1.7
Flow resistivity (σ)	32000
Porosity (ϕ)	0.99
Atmospheric pressure (P_a)	1.10325e5
Structural damping (η_s)	0.0001
Viscous characteristics length (Λ)	50e-6
Thermal characteristics length (Λ')	110e-6

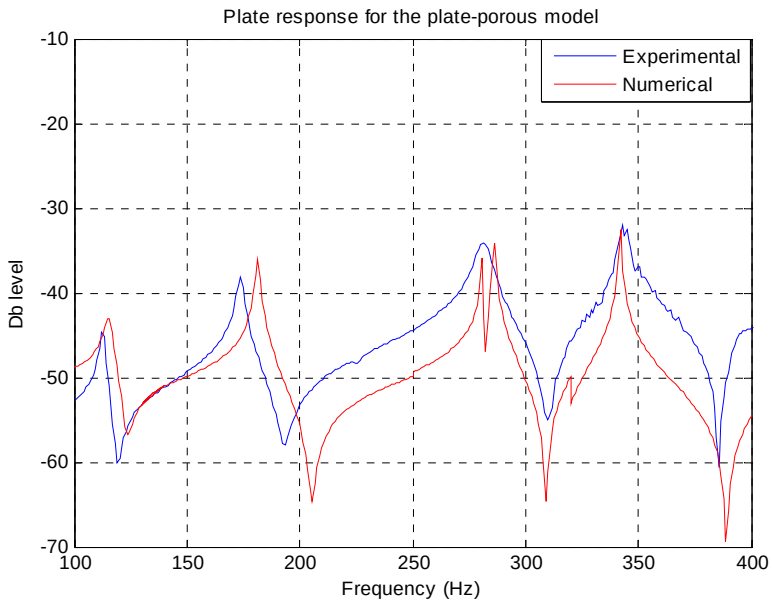

Figure 24 Comparison of the numerically computed (VAL-FE code) response of the plate-porous assembly with the response of the plate-porous assembly obtained from the experimental investigation of a similar system

Figure 24 illustrates a good agreement between the numerically computed plate response of the coupled model computed using the VAL-FE code and the plate response obtained from the experimental investigation of a similar model. It can be concluded that the numerical model is able to model the magnitude of the response of the plate having a porous treatment reasonably well. It can be observed from the Figure 24 that in the numerical prediction there are two resonance frequencies in the frequency range 270-280 Hz as compared to only one in the experimental analysis. This is due to primarily two reasons. First, the high damping in the experimental set up unable the spectrum analyzer to capture the two resonance frequencies. Second, the scarce mesh density of the porous elements used for the modeling of the porous media is not able to capture the damping distribution in this range. These models are extremely complicated as they require modeling the plate, the porous media and the coupling between them. The requirements of the mesh density of the porous media required for modeling the transfer of energy between the elastic and the porous elements is very high, which is restricted by the fact that simulation on the porous media are computationally very expensive.

3.10 Validation of the coupled acoustic-porous model

In this section, the 3D-FE fully coupled numerical model of the acoustic and the porous domain is developed for the validation of the coupling between the porous and the acoustic media. The coupled acoustics-porous FE model depicted in Figure 25 a) has been validated by comparing the response of the coupled model computed using the VAL-FE code with the numerical response of a similar model using the admittance approach as illustrated by Panneton et. al. [18]. The configuration of the coupled model consists of a rigid walled cavity having a partial porous treatment embedded into one of its walls.

3D-FE fully coupled model of the acoustics-porous model

The finite element model of the coupled acoustic-porous assembly shown in Figure 25 a) consists of a rigid walled acoustic cavity having a partial porous treatment embedded into one of its walls. The acoustic cavity has been discretized using 10x10x10 hexahedral elements given in Cook [21] and the porous media is discretized using 8x8x6 hexahedral elements following the finite element formulation derived by Panneton et. al. [18]. The acoustic hexahedral elements are based on the mathematical formulation given by equation (25) and the finite element formulation of the porous media is based on equation (55). In the absence of the coupling between acoustic and the porous domain, the mesh densities of the components have been found to be satisfactory in capturing the dynamics of the individual components in the frequency range of interest. The numerical model of the coupled acoustic-porous assembly is based on the FE formulation given in equation (66). The model parameters and the material properties of the acoustic and the porous media used in the coupled FE model of the acoustic-porous assembly are given in Table 11. A volume displacement of $2.5x10^{-8}\,m^3$ is applied at one of the corner nodes of the acoustic domain. The comparison of the mean quadratic pressure in the acoustic enclosure computed from the numerical model using the VAL-FE code and the mean quadratic pressure of the acoustic domain computed by using the admittance approach as illustrated in Panneton et. al. [18] is given in Figure 25.

Table 11. Model and material properties used in the numerical model of the acoustic-porous assembly

Properties	Values
Model parameters	
Number of elements of the acoustic domain	1000
Number of elements of the porous media	288
Boundary condition of the acoustic domain	Rigid walled cavity
Boundary condition of the porous media	Free on the front surface and fixed on other surfaces
Dimensions of the acoustic cavity	1000x1000x1000 (mm)
Dimensions of the porous media	600x600x76.2 (mm)
Material properties of the acoustic domain	
Density	1.2 kg/ m^3
Speed of sound	343m/s
Poisson's ratio	0.3
Material properties of the porous media	
Density (ρ_1)	30 kg/ m^3
Young modulus (N)	286e3
Poisson's ratio (ν)	0.4
Tortuosity (α_∞)	7.8
Flow resistivity (σ)	25000
Porosity (ϕ)	0.9
Atmospheric pressure (P_a)	1.10325e5
Structural damping (η_s)	0.265
Viscous characteristics length (Λ)	226e-6
Thermal characteristics length (Λ')	226e-6

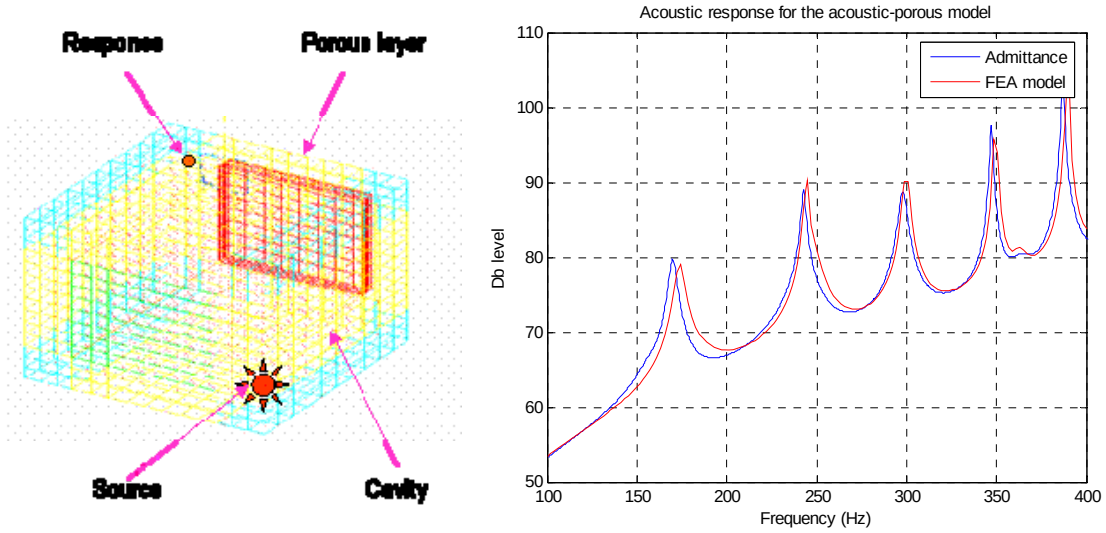

(a) (b)

Figure 25. a) Finite element model for the acoustic-porous assembly, b) Comparison of the numerically computed (VAL-FE code) response of the acoustic-porous assembly with the response of the acoustic-porous assembly obtained from the application of the admittance approach as illustrated in Panneton et. al. [18]

Figure 25 b) illustrates an excellent agreement between the numerically computed mean quadratic pressure of the acoustic enclosures by the VAL-FE code and the mean quadratic pressure computed by using the admittance approach as illustrated in Panneton et. al. [18]. It can be concluded from the Figure 25 b) that the numerical model is able to capture both the magnitude and the distribution of the damping of the acoustic response in the 3D-FE coupled model of the acoustic-porous system. The reason why we have been able to obtain a better validation in spite of the coupling with the porous media is that in this case the validation has been performed by comparing the numerically computed results with the result obtained from applying the admittance approach to the same finite element model. This is why the mesh density is not an issue as it is the same in both the cases.

3.11 Validation of the coupled plate-DVA model

After the successful validation of the individual models of the plate and the DVA, a 3D-FE fully coupled numerical model of the plate-DVA assembly is developed in order to understand the behavior of the DVA when mounted on the plate and also to gauge its

effectiveness of the DVA in controlling the vibration levels of the base plate. The coupled model consists of an aluminum plate clamped at its edges with a DVA mounted on it. The DVA in the coupled model consists of an aluminum mass layer plate covering a layer of melamine foam. The base surface of the porous media of the DVA is glued to the center of the plate and the boundary condition of the mass layer glued to the porous layer of the DVA is free-free. The 3D-FE numerical model of the coupled plate-DVA depicted in Figure 26 b) has been validated by comparing the resonance frequencies of the coupled model computed using the VAL-FE code with the resonance frequencies of the coupled model of the plate-DVA assembly evaluated from the experimental investigation of a similar model shown in Figure 26 a).

Experimental investigation of the coupled plate-DVA model

The experimental setup for the coupled plate-DVA model shown in Figure 26 a) consists of a clamped aluminum plate with a DVA mounted on it. An impulse excitation is used to drive the plate using a hammer, which excites the coupled DVA. The transverse acceleration of the aluminum base plate is measured using a light weight accelerometer. The excitation signal from the hammer and the acceleration signals from the accelerometer on the response point on the base plate are measured through the spectrum analyzer to calculate the transfer function between the acceleration of the response point on the base plate and the excitation signal of the hammer. The resonance frequencies from the transfer functions obtained from the experimental investigation of the coupled plate-DVA model are tabulated in Table 13.

3D-FE modeling of the plate-DVA model

The finite element model of the coupled plate-DVA assembly shown in Figure 26 b) consists of an aluminum base plate clamped at its edges with a DVA treatment on it. The base plate has been discretized using 10x15 and the mass layer plate is discretized using 4x5 rectangular plate elements given in Yang [17] respectively. The porous media of the DVA is discretized using 60 hexahedral porous elements following the mathematical formulation derived in Panneton et. al. [18].

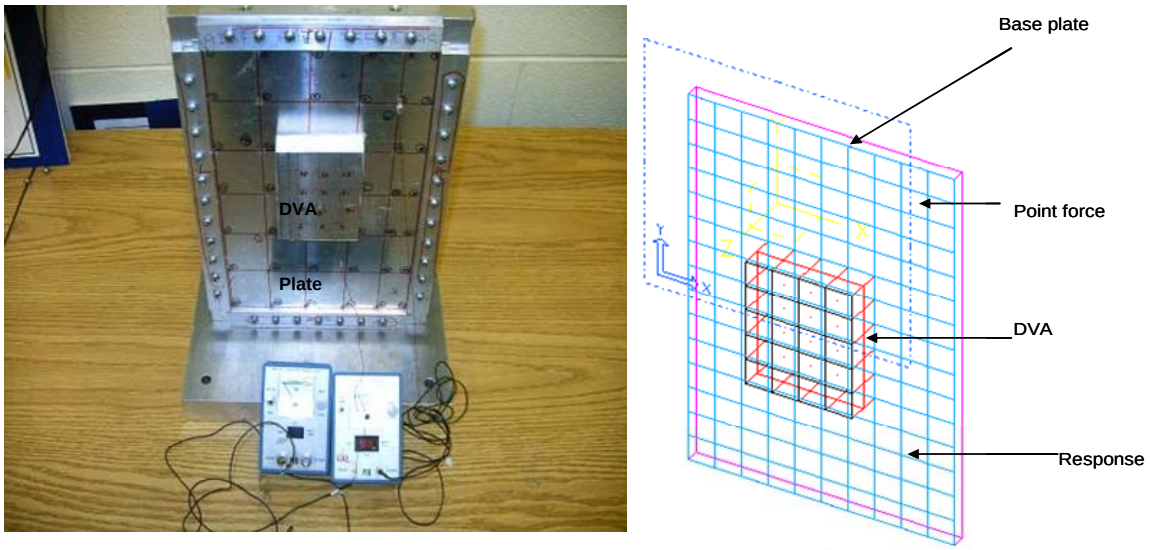

Figure 26. a) Experimental setup for the validation of the FE model of the plate-DVA assembly, b) Finite element model of the plate-DVA assembly

The plate elements used for the modeling of the base plate and the mass layer plate are based on the finite element formulation given by equation (44) and the finite element formulation of the porous media is based on equation (55). In the absence of the coupling between the base plate, the mass layer plate of the DVA and the porous domain of the DVA, the mesh densities of the individual components of the coupled model have been found to be satisfactory in capturing the dynamics of the components in the frequency range of interest. The model parameters and the material properties of the plate and the porous media used in the coupled model of the plate-DVA are given in Table 12. A point force equivalent to the impulse excitation imparted to the base plate with the hammer is used to drive the aluminum plate in the FE model of the plate-DVA assembly. The response is measured at a response point on the base plate. The resonance frequencies from the transfer function between the acceleration of the base plate and the point force on it are tabulated in Table 13.

Table 12. Model parameters and material properties used in the numerical modeling of the plate-DVA model

Properties	Values
Model parameters	
Number of elements of the base plate	150
Number of elements of the mass layer plate	20
Number of elements of the porous media	60
Boundary condition of the base plate	Clamped-Clamped
Boundary condition of the porous media	Free-Free
Boundary condition of the mass layer plate	Free-Free
Dimensions of the base plate	206x308 (mm)
Dimensions of the mass layer plate	80x100 (mm)
Dimensions of the porous media	80x100x26 (mm)
Material properties of the base plate and the mass layer plate	
Density	2700kg/ m^3
Young modulus	7.0e10 Pa
Poisson's ratio	0.3
Material properties of the porous media	
Density (ρ_1)	30 kg/ m^3
Young modulus (N)	286e3
Poisson's ratio (ν)	0.4
Tortuosity (α_∞)	7.8
Flow resistivity (σ)	25000
Porosity (ϕ)	0.9
Atmospheric pressure (P_a)	1.10325e5
Structural damping (η_s)	0.265
Viscous characteristics length (Λ)	226e-6
Thermal characteristics length (Λ')	226e-6

Table 13. Comparison of the resonance frequencies from the experimental and numerical evaluation of the plate-DVA assembly

Modes	Resonance Frequency (Hz) (Experimental)	Resonance Frequency (Hz) (VAL-FE code)	% Error
(1,1)	128	122	4.6
(2,1)	207	207	0
(3,1) low split	295	305	3.36
(3,1) high split	320	317	0.1
(2,2)	372	365	1.88

Table 13 illustrates a good agreement of the numerically computed resonance frequencies of the coupled model of the plate-DVA and the resonance frequencies obtained from the experimental investigation of a similar model shown in Figure 26 a). It can be concluded that the numerical model of the plate-DVA system is able to capture the resonance frequencies obtained from the experimental investigation of the coupled model. The tuned frequency of the DVA in this case is 325 Hz. The effect of the DVA on the base plate can be primarily categorized into three parts. First, for the frequencies of the base plate lower then the tuned frequency of the DVA, the DVA acts as a mass on the base plate and moves in phase with the base structure. This results in the mass effect on the base plate leading to a decrease in the resonance frequencies of the base plate. Second, for the frequency near the tuned frequency of the DVA, the DVA acts as a vibration absorber splitting the resonance mode of the base structure into a lower split frequency and a high split frequency. At the lower split frequency the DVA moves in phase with the base plate and hence acts as mass effect on the base plate. On the other hand at the higher split frequency the DVA moves out of phase with the base plate and hence providing a high level of reactive force on the base structure. Third, for the frequencies above the tuned frequency of the DVA its mass layer moves relative to the base plate. This relative motion of the base plate and the mass layer plate of the DVA with the presence of the foam leads to a passive damping of the vibration levels of the base plate at these frequencies. It can be concluded from the aforementioned analysis that the DVA acts as a true distributed vibration absorber in which it acts as a vibration

absorber at the tuned frequency providing a high amount of reactive force on the base plate and also couples into all the other modes leading to a high level of passive damping at these frequencies.

3.12 Validation of the coupled plate-HG model

After the successful validation of the individual models of the plate and the HG blanket, a 3D-FE fully coupled numerical model of the plate-HG blanket assembly is developed in order to understand the behavior of the HG blanket when mounted on the plate and also to gauge the effectiveness of the HG blanket in controlling the vibration levels of the base plate. The 3D-FE numerical model of the coupled plate-HG assembly depicted in Figure 27 b) has been validated by comparing the response of the coupled model computed using the VAL-FE code with the response evaluated by the experimental investigation of a similar model shown in the Figure 27 a). The coupled model consists of an aluminum plate clamped at its edges with a HG blanket mounted on it. The HG blanket in the coupled model consists of two mass in-homogeneities of 6gms and 4 grams inserted in the porous layer of the HG blanket at the positions shown in the Figure 27 b).

Experimental investigation of the coupled plate-HG blanket model

The experimental setup for the coupled plate HG blanket model shown in Figure 27 a) consists of a clamped aluminum plate with a HG blanket mounted on it. A hammer is used to drive the plate which excites the coupled HG blanket. The transverse acceleration of the aluminum base plate is measured using a light weight accelerometer. The excitation signal from the hammer and the acceleration signal from the accelerometer were measured by the spectrum analyzer to calculate the transfer function between the acceleration of the response point on the base plate and the excitation signal of the hammer. The transfer function of the response point on the base plate of the coupled plate-HG blanket assembly is shown in Figure 28.

3D-FE modeling of the plate-HG blanket model

The finite element model of the coupled plate-HG blanket assembly shown in Figure 27 b) consists of an aluminum plate clamped at its edges with a HG blanket

treatment on it. The plate has been discretized using 6x9 rectangular plate elements given in Yang [17].

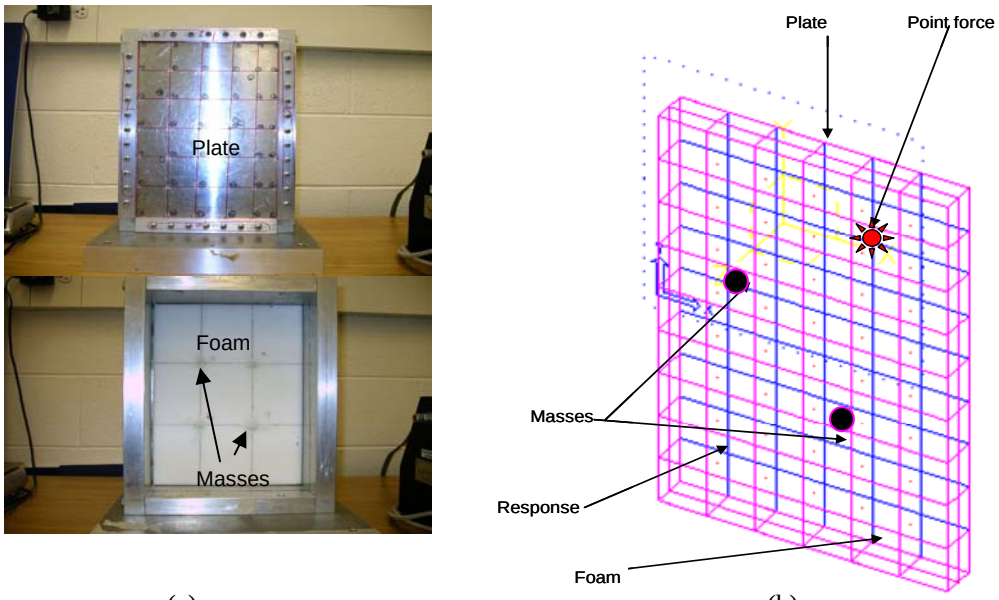

Figure 27. a) Experimental set up for the validation of the numerical model of the plate-HG blanket assembly, b) Finite element model of the plate-HG blanket assembly

The porous media of the HG blanket is discretized using 6x9x2 hexahedral porous elements following the mathematical formulation derived in Panneton et. al. [18]. The mass in-homogeneities inside the porous layer are modeled as point masses. The plate elements are based on the finite element formulation given in equation (44) and the finite element formulation of the porous media are based on equation (55). In the absence of the coupling between the base plate and the HG blanket, the mesh densities of the individual components of the coupled model have been found to be satisfactory in capturing the dynamics of the components in the frequency range of interest. The model parameters and the material properties of the plate, the porous media and the mass in-homogeneity used in the 3D-FE fully coupled model of the plate-HG assembly are given in Table 14. A point force excitation equivalent to the impulse excitation in the experiments is used to drive the aluminum base plate and the response is measured at a response point on the base plate. The transfer function between the measured response of the base plate and the point force on the plate is depicted in Figure 28.

Table 14. Model parameters and the material properties used in the numerical model of the plate-HG blanket assembly

Properties	Values
Model parameters	
Number of elements of plate	54
Number of elements of the HG blanket	108
Boundary condition of the plate	Clamped-Clamped
Boundary condition of the HG blanket	Free-Free
Dimensions of the plate	206x308 (mm)
Dimensions of the HG blanket	206x308x26 (mm)
Number of mass insertions in the HG blanket	2
Material properties of the plate and the mass in-homogeneities	
Density	2700 kg/ m^3
Young modulus	7.0e10
Poisson's ratio	0.3
Material properties of the porous media of the HG blanket	
Density (ρ_1)	50 kg/m(3)
Young modulus (N)	220e3
Poisson's ratio (ν)	0.3
Tortuosity (α_∞)	1.7
Flow resistivity (σ)	32000
Porosity (ϕ)	0.99
Atmospheric pressure (P_a)	1.10325e5
Structural damping (η_s)	0.0001
Viscous characteristics length (Λ)	50e-6
Thermal characteristics length (Λ')	110e-6

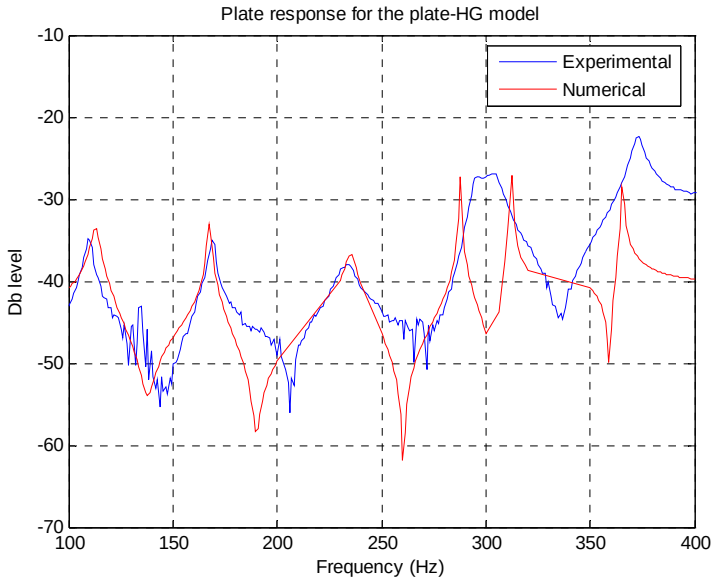

Figure 28 Comparison of the numerically computed (VAL-FE code) response of the plate-HG blanket assembly with the response of the plate-HG blanket assembly obtained from the experimental investigation of a similar system

Figure 28 illustrates a good agreement of the numerically computed plate response of the coupled model of the plate-HG assembly and the plate response obtained from the experimental investigation of a similar model shown in Figure 27 a). It can be concluded that the numerical model of the plate-HG assembly is able to capture the dynamics of the plate and the distribution of damping over a broad frequency bandwidth. There is a slight mismatch in the numerically computed response of the base plate and the experimentally obtained response of the base structure in the frequency range of 275-400 Hz. There are primarily two reasons for the mismatch in the numerical results and the results obtained from the experimental investigation in this frequency range. First, the sparsity in the mesh density reduces the ability of the numerical model to capture the distribution of the damping at higher frequencies. Second, at higher frequencies the geometry of the inserted masses starts to effect the HG blanket response and hence modeling them as point masses reduces the ability of the numerical model to accurately capture the physics behind the interaction between the HG blanket and the base plate.

3.13 Validation of the plate-HG-acoustic numerical model.

In this section, the finite element model consisting of the plate, the HG blanket and the radiating acoustic domain will be discussed. The numerical model shown in Figure 29 b) is validated by comparing the numerically computed response of the plate and the radiating acoustic domain of the coupled FE model with their responses evaluated by the experimental investigation of a similar model shown in Figure 29 a). The coupled model consists of an aluminum plate clamped at its edges with a HG blanket mounted on it and coupled to a radiating acoustic domain. The HG blanket in the coupled model consists of two mass in-homogeneities of 6gms and 4 grams inserted in the porous layer of the HG blanket at the positions shown in the Figure 29 b).

Experimental investigation of the coupled plate-HG-acoustic model

The experimental setup for the coupled plate-HG-acoustic model shown in Figure 29 a) consists of a clamped aluminum plate with a HG blanket mounted on it and coupled to a radiating acoustic domain. An impulse hammer is used to drive the plate-HG blanket assembly, which radiates sound inside the coupled radiating acoustic domain. The transverse acceleration of the aluminum plate is measured using a light weight accelerometer and the sound pressure fluctuations in the radiating acoustic domain are measured by using light weight condenser microphones. The excitation signal from the hammer, the acceleration signal from the accelerometer and the pressure fluctuation reading from the microphones are measured through the spectrum analyzer. These signals are used to calculate the transfer function between the acceleration of the response point on the base plate and the excitation signal of the hammer and the transfer function between the response from the microphones inside the radiating acoustic domain and the excitation signal from the hammer. The transfer function from the experimental investigation of the coupled model is shown in Figure 30.

3D-FE modeling of the plate-HG blanket-acoustic model

The finite element model of the coupled plate-HG-acoustic assembly shown in Figure 29 b) consists of an aluminum plate clamped at its edges with a HG blanket treatment on it. The plate has been discretized using 6x9 rectangular plate elements given in Yang [17].

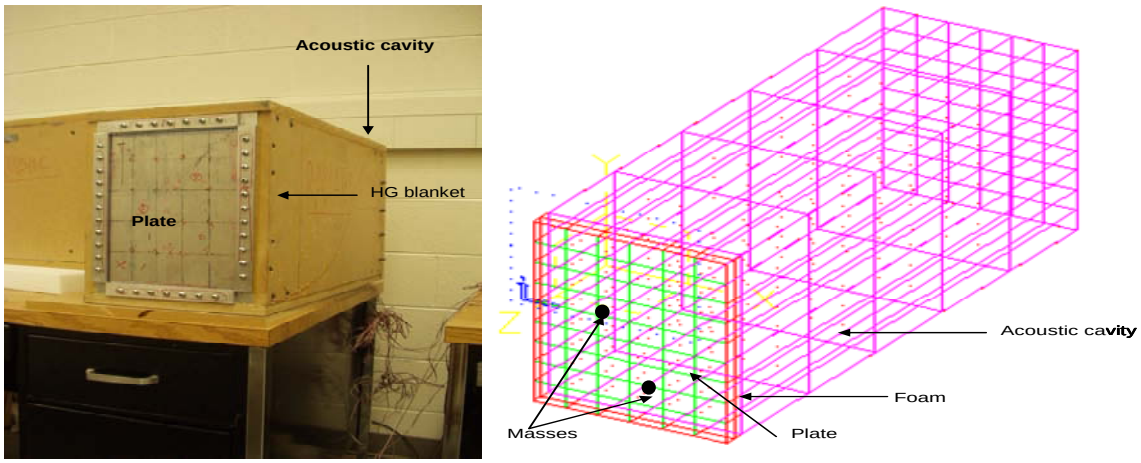

(a) (b)

Figure 29 (a) Experimental set up for the validation of the plate-HG blanket-acoustic numerical model (b) Finite element model of the plate-HG blanket-acoustic assembly

The porous media of the HG blanket is discretized using 6x9x2 hexahedral porous elements following the finite element formulation derived by Panneton et. al. [18]. The mass in-homogeneities inside the porous layer are modeled as point masses. The plate elements are based on the finite element formulation given in equation (44) and the finite element formulation of the porous media is based on equation (55). In the absence of the coupling between the base plate, the HG blanket and the radiating acoustic domain, the mesh densities of the individual components of the coupled model have been found to be satisfactory in capturing the dynamics of the components in the frequency range of interest. The model parameters and the material properties of the plate, the porous media of the HG blanket, the mass in-homogeneity in the HG blanket and the radiating acoustic domain used in the coupled model are given in Table 15. A point force excitation equivalent to the impulse excitation imparted to the aluminum base plate in the experiments is used to drive the aluminum plate in the 3D-FE model. The response is measured at the response point on the base plate and the response nodes in the radiating acoustic domain.

Table 15. Model parameters and the material properties used in the numerical model of the plate-HG blanket-acoustic assembly

Properties	Values
Model parameters	
Number of elements of plate	54
Number of elements of the HG blanket	108
Number of elements of the acoustic domain	270
Boundary condition of the plate	Clamped-Clamped
Boundary condition of the acoustic domain	Rigid walled cavity
Dimensions of the plate	206x308 (mm)
Dimensions of the HG blanket	206x308x26 (mm)
Dimension of the acoustic cavity	206x308x597 (mm)
Number of mass insertions in the HG blanket	2
Material properties of the plate and the mass in-homogeneities	
Density	2700 kg/ m^3
Young modulus	7.0e10
Poisson's ratio	0.3
Material properties of the porous media of the HG blanket	
Density (ρ_1)	50 kg/m(3)
Young modulus (N)	220e3
Poisson's ratio (ν)	0.3
Tortuosity (α_∞)	1.7
Flow resistivity (σ)	32000
Porosity (ϕ)	0.99
Atmospheric pressure (P_a)	1.10325e5
Structural damping (η_s)	0.0001
Viscous characteristics length (Λ)	50e-6
Thermal characteristics length (Λ')	110e-6
Material properties of the radiating acoustic domain	
Density	1.2 kg/m(3)
Speed of sound	343

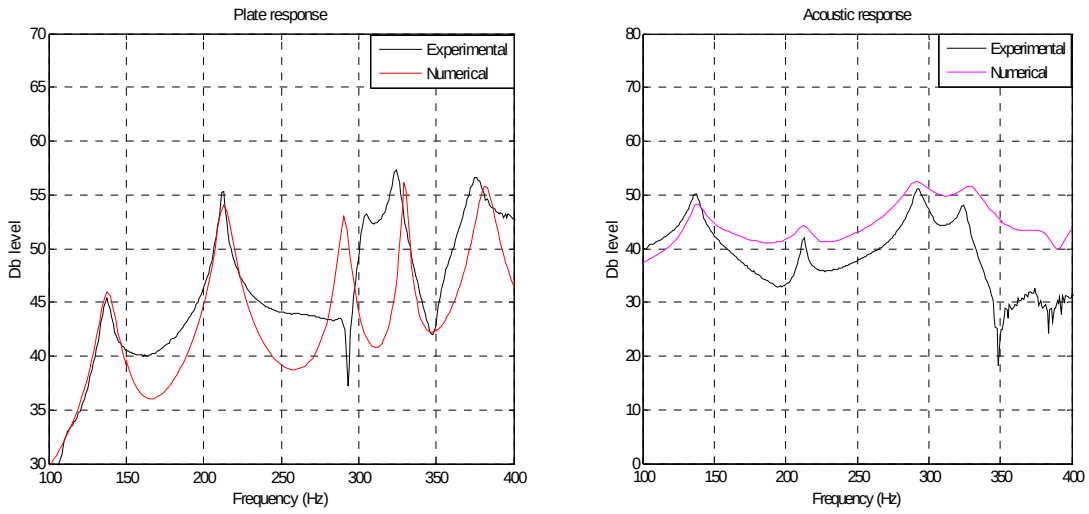

(a) **(b)**

Figure 30. a) Comparison of the numerically computed plate response of the coupled model with the plate response from the experimental investigation of a similar model, b) Comparison of the numerically computed acoustic response of the coupled model with the acoustic response from the experimental investigation of a similar model

The transfer function between the measured response of the plate and the point force on the base plate is depicted in Figure 30 a). The transfer function between the measured response of the radiating acoustic domain and the point force on the plate is depicted in Figure 30 b). Figure 30 illustrates a good agreement of the numerically computed plate response of the coupled model of the plate-HG-acoustic assembly and the plate response obtained from the experimental investigation of a similar model shown in Figure 29 a). It can be concluded that the numerical model of the coupled plate-HG-acoustic assembly is able to capture both the dynamics and the distribution of the damping in the plate and the acoustic cavity. The numerical model though is able to capture the damping distribution in the base plate response, is unable to capture it in the acoustic response at the higher frequencies. This is primarily due to two reasons. First, the mesh density used for the discretization of the acoustic cavity is sparse, which reduces the capability of the numerical model to capture the damping distribution of the acoustic cavity at higher frequencies. Second, as the radiating acoustic domain built for the experimental set up is not perfectly airtight and any leakage of the SPL's from the acoustic domain would add additional damping to the response of the radiating acoustic domain obtained from the experimental set up.

3.14 Validation of the acoustics-plate-HG-acoustic model

In this section, the finite element model consisting of the plate, the HG blanket and the acoustic domains will be discussed. The numerical model shown in Figure 31 b) is validated by comparing the numerically computed resonance frequencies of the plate and the radiating acoustic domain with their responses evaluated by the experimental investigation of a similar model shown in Figure 31 a). The coupled model consists of an incident acoustic domain coupled to an aluminum plate clamped at all its edges. The aluminum plate has a HG blanket mounted on it and coupled to a radiating acoustic domain. The HG blanket in the coupled model consists of two mass in-homogeneities of 6gms and 4 grams inserted in the porous layer of the HG blanket at the positions shown in the Figure 31 b).

Experimental investigation of the coupled acoustic-plate-HG blanket-acoustic model

The experimental setup for the coupled acoustic-plate-HG-acoustic model shown in Figure 31 a) consists of an incident acoustic domain coupled to a clamped aluminum plate with a HG blanket mounted on it. The assembly of the acoustic-plate-HG is then coupled to a radiating acoustic domain. A speaker is used to drive the incident acoustic domain, which drives the plate-HG blanket assembly. This vibrating plate-HG assembly radiates sound inside the coupled radiating acoustic domain. The transverse acceleration of the aluminum plate and the speaker diaphagram is measured using a light weight accelerometer and the sound pressure fluctuations in the radiating acoustic domain are measured by using light weight condenser microphones. The acceleration signal from the accelerometers and the pressure fluctuation reading from the microphones is measured through the spectrum analyzer to calculate the transfer functions between the acceleration of the response point on the plate and the acceleration signal from the speaker and the transfer function between the response from the microphones and the acceleration signal from the speaker excitation signals. The experimentally obtained resonance frequencies of fully coupled acoustic-plate-HG-acoustic model are tabulated in Table 17.

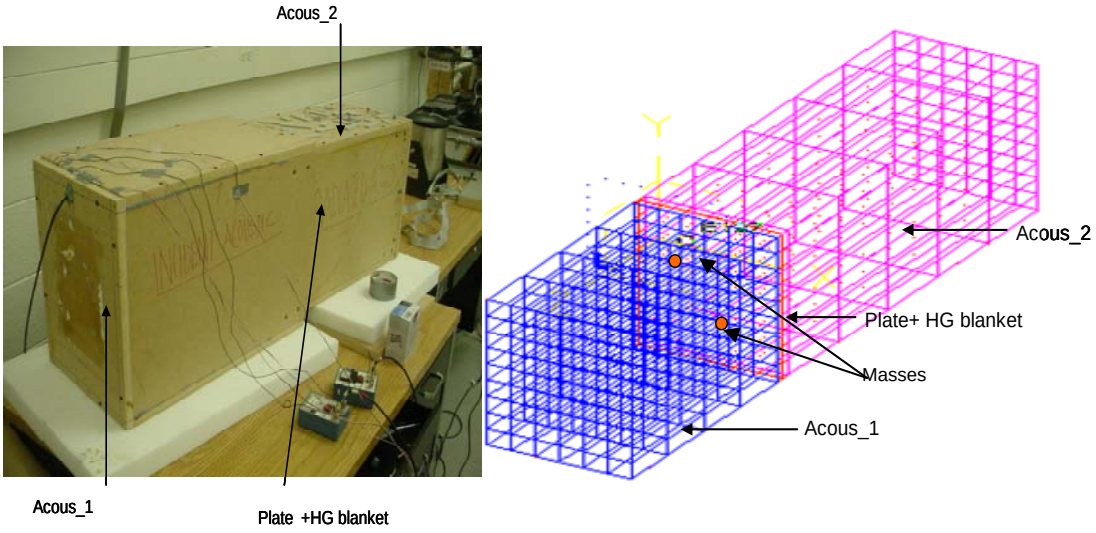

Figure 31. a) Experimental set up for the validation of the numerical model for the acoustic-plate-HG blanket-acoustic assembly, (b) finite element model of the acoustic-plate-HG blanket-acoustic assembly

3D-FE modeling of the acoustic-plate-HG blanket-acoustic model

The finite element model of the coupled acoustic-plate-HG-acoustic assembly shown in Figure 31 b) consists of an incident acoustic domain coupled to an aluminum plate clamped at its edges with a HG blanket treatment on it. The assembly of the acoustic-plate-HG is then coupled to a radiating acoustic domain. The plate has been discretized using 6x9 rectangular plate elements given in Yang [17]. The porous media of the HG blanket is discretized using 6x9x2 hexahedral porous elements following the finite element formulation derived by Panneton et. al. [18]. The incident acoustic domain is discretized using 6x9x4 hexahedral elements given in Cook [21]. The radiating acoustic domain is discretized using 6x9x5 hexahedral elements given by Cook [21]. The mass in-homogeneities inside the porous layer are modeled as point masses. The plate elements are based on the finite element formulation given in equation (44) and the finite element formulation of the porous media is based on equation (55). The acoustic hexahedral elements are based on the finite element formulation given in equation (25). In the absence of the coupling between the incident acoustic domain, the base plate, the HG blanket and the radiating acoustic domain, the mesh densities of the individual components of the coupled model have been found to be satisfactory in capturing the dynamics of the components in the frequency range of interest.

Table 16. Model parameters and the material properties used in the numerical model of the acoustic-plate-HG blanket-acoustic assembly

Properties	Values
Model parameters	
Number of elements of plate	54
Number of elements of the HG blanket	108
Number of elements of the acoustic domain	270
Boundary condition of the plate	Clamped-Clamped
Boundary condition of the HG blanket	Free-Free
Boundary condition of the acoustic domain	Rigid walled cavity
Dimensions of the plate	206x308 (mm)
Dimensions of the HG blanket	206x308x26 (mm)
Dimension of the acoustic cavity	206x308x597 (mm)
Number of mass insertions in the HG blanket	2
Material properties of the plate and the mass in-homogeneities	
Density	2700 kg/ m^3
Young modulus	7.0e10
Poisson's ratio	0.3
Material properties of the porous media of the HG blanket	
Density (ρ_1)	50 kg/m(3)
Young modulus (N)	220e3
Poisson's ratio (ν)	0.3
Tortuosity (α_∞)	1.7
Flow resistivity (σ)	32000
Porosity (ϕ)	0.99
Atmospheric pressure (P_a)	1.10325e5
Structural damping (η_s)	0.0001
Viscous characteristics length (Λ)	50e-6
Thermal characteristics length (Λ')	110e-6
Material properties of the porous media of the incident and radiating acoustic domain	
Density	1.2 kg/m(3)
Speed of sound	343
Poisson's ratio	0.0

The model parameters and the material properties of the plate, the porous media of the HG blanket, the mass in-homogeneity in the HG blanket and the acoustic cavities used in the coupled model are given in Table 16. A volume displacement excitation equivalent to the speaker excitation is imparted to the incident acoustic domain in the numerical model and the response is measured at response point on the plate and the response nodes inside the radiating acoustic domain. The transfer function between the measured response of the plate and the volume displacement of the incident acoustic domain and the transfer function between the measured response of the radiating acoustic domain and the volume displacement of the incident acoustic domain are computed. The numerically computed resonance frequencies of fully coupled acoustic-plate-HG-acoustic model are tabulated in Table 17.

Table 17. Comparison of the numerically computed resonance frequencies for the fully coupled acoustic-plate-HG-acoustic with the resonance frequencies of the coupled model obtained from the experimental investigation of a similar model

Resonance Frequency (Hz) (Experimental)	Resonance Frequency (Hz) (VAL-FE code)	% Error
136	138	1.45
205	215	4.6
285	295	3.39
320	335	4.48
375	385	2.66

It can be concluded from Table 17 that the numerically computed resonance frequencies of the fully coupled FE model of the acoustic-plate-HG-acoustic assembly are in good agreement with the resonance frequencies of the coupled model obtained from the experimental investigation of a similar model. It can be concluded form the Table 17 that the numerical model is able to capture resonance frequencies of the fully coupled 3D-FE model of the acoustic-plate-HG-acoustic assembly.

NOTE:

The numerical model for the acoustic-plate-HG-acoustic assembly is very complicated and takes about 200-250 Hrs to simulate. It is due to these factors that the attempt to validate the transfer functions of the plate and the radiating acoustic domain has not been successful.

4 Numerical study and predictions

The purpose of this chapter is to perform parametric studies on the controlling parameters of the noise control devices (NCD's) such as the DVA's, the HG blankets and the multiple porous layers (MPL) blankets. First the effect of the variation of the material and geometric properties of the individual components on the response of the NCD's is studied. Second, parametric studies are performed on the fully coupled numerical models to estimate the effect of the change in the controlling parameters of these NCD's on the vibration response of the elastic structure and radiated acoustic pressure inside the coupled acoustic domain. These parametric studies give us a deep insight in the working of these noise control devices and also help us to develop advanced designs.

4.1 Parametric studies on the DVA's

Distributed vibration absorbers (DVA's) have been used in this study as a noise control device. They have a tremendous potential to control the vibrations response of the base structure leading to a reduction in the sound radiated by these base structures into the coupled radiating acoustic domains. In spite of their promising sound attenuation characteristics, little is known about the actual mechanism by which it is achieved. To gain an insight in their functioning, a 3D-FE model of the DVA has been validated and parametric studies have been performed on this model. In this section a detailed understanding of the behavior of the DVA's under varied conditions and configurations will be analyzed in order to enable us to develop advanced designs for this vibration absorber.

4.1.1 3D-FE model for the DVA

The finite element model of the DVA shown in Figure 32 consists of a mass layer covering a layer of melamine foam. The mass layer has been modeled as a plate discretized into 20 plate elements given in Yang [17] and the porous layer is discretized using 60 hexahedral elements following the mathematical formulation derived in Panneton et. al. [18]. The coupling between the plate and the porous elements is captured by ensuring the continuity of normal displacement between the plate and the porous elements using the Lagrange multipliers, which are explained in Appendix A. In the

absence of the coupling between the mass layer and the porous media, the mesh density has been found to be satisfactory in capturing the dynamics of both the individual components in the frequency range of interest. The model parameters and the material properties of the mass layer and the porous media used in the finite element model of the DVA are given in Table 7. A uniform displacement function of unit amplitude is applied at all the nodes at the base of the 3D-FE model of the DVA. The numerical response is measured at the center node of the mass layer plate of the DVA. This 3D-FE model has been used for the conducting the parametric studies on the DVA to gain an insight in the physics behind their functionality.

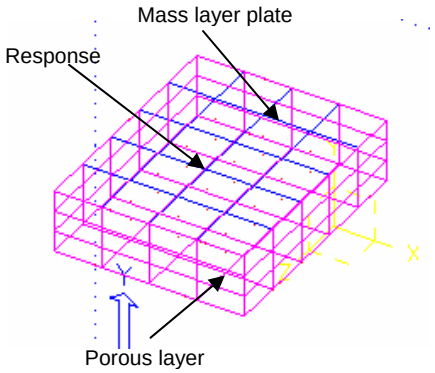

Figure 32. Finite element model of the DVA having a mass layer covering the foam layer

Three parametric studies were performed on the DVA's. First, the change in the response of the DVA on varying the damping of the foam by changing the shear modulus loss factor was compared to change in the response of the DVA encountered by varying the damping properties of the mass layer plate. This study would provide us an understanding of the source of the damping capabilities of the DVA. Second, the change in the response of the DVA was studied on changing the thickness of the foam layer. The objective of this parametric study was to understand as to what is the effect of the change of the thickness of the foam on the tuned frequency of the DVA. In the third parametric study, the effect of the change in the stiffness distribution of the foam layer of the DVA on the response of the mass layer plate of the DVA was studied. The results obtained from the aforementioned studies have been analyzed to gain an insight in the behavior of the DVA under varied material properties and geometrical configuration.

4.1.2 Effect of the variation in the damping properties of the foam and the mass layer

In the following section the finite element model of the DVA is used for predicting the variation in the response of the DVA due to the change in the damping properties of the foam. The numerical model of the DVA consisting of a mass layer covering a porous layer is shown in Figure 32. The variations in the material properties for the parametric study have been tabulated in Table 18. The variation in the numerically computed responses of the DVA with varied damping characteristics have been illustrated in Figure 33.

Table 18. Variations in the material properties and the thickness of the foam layer of the DVA

Simulation	Original	Modified -1	Modified -2	Modified-3
Parametric study -I				
Case –I				
Damping ratio of plate	0.1	0.001	0.1	0.1
Case-II				
Loss factor of the foam	0.065	0.065	0.0065	0.16
Parametric study -II				
Thickness of the Foam layer	26	48	37	-

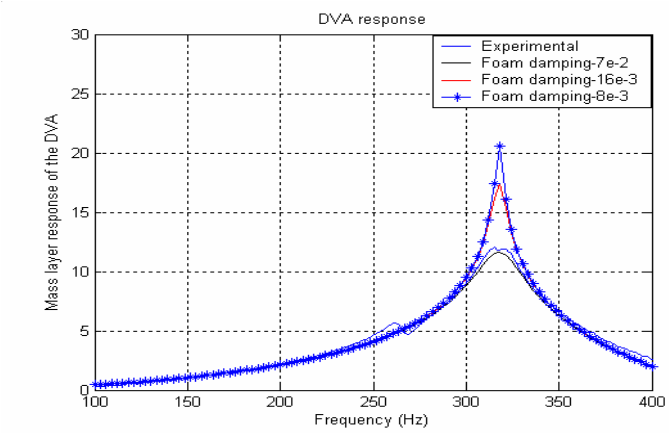

Figure 33. Results from the first parametric study on the DVA, where the damping properties of the porous media were modified by changing the shear modulus loss factor and the mass layer damping

Figure 33 represents the results obtained from the first parametric study on the DVA. In this parametric study the damping characteristics of the DVA was varied in three ways. First, the damping properties of the foam were varied by decreasing the shear

modulus loss factor by 10 times but keeping the mass layer plate damping unchanged. Second, the damping property of the mass layer of the DVA was reduced by 100 times and the foam damping was not modified. Third, the damping of the mass layer plate is kept unchanged but the damping of the foam is changed by modifying the shear modulus loss factor. It can be observed from the Figure 33 that the loss factor of the foam has a major effect on the response of the DVA as compared to the damping ratio of the mass layer. This is a lumped damping term, which is universally used to numerically model the physics of the damping of the structural part of the foam layer. The damping capability of the foam due to the loss factor is affected by the shear modulus (N) of the foam hence it can be concluded that stiffer foam will have better damping capabilities as compared to limp foam for the same loss factor. This provides the understanding that in case we require the passive damping from the DVA to be more then we should increase the stiffness of the foam layer of the DVA.

4.1.3 Effect of the variation in the thickness of the foam layer

In the following section, the finite element model of the DVA is used for predicting the variation in the response of the DVA due to the change in the thickness of the foam layer of the DVA. The numerical model of the DVA consisting of a mass layer covering a porous layer is shown in Figure 32. The variations in the thickness of the foam for this parametric study have been tabulated in Table 18. The variation in the response of the DVA with varying thickness of the porous layer has been illustrated in Figure 34.

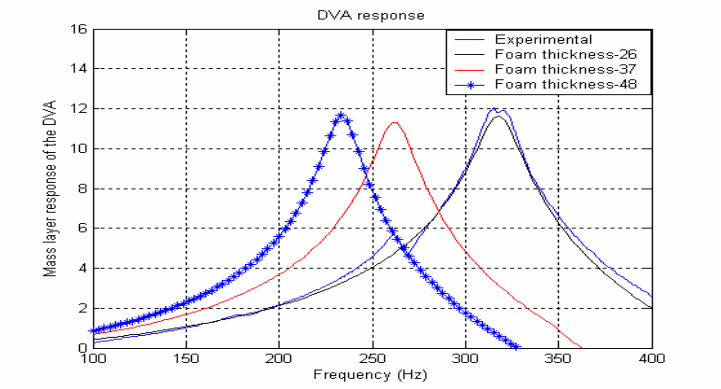

Figure 34. Results from the second parametric study on the DVA, where the thickness of the foam layer is modified

Figure 34 illustrates the results obtained from the second parametric study on the DVA, where the thickness of the porous layer is increased from its original size. It can be observed from the Figure 34 that increasing the thickness of the foam layer leads to a reduction in the resonance frequency of the DVA. It can be concluded that in case we have to tune the DVA to a high frequency mode of the base structure the thickness of the foam layer should be reduced. This provides us the ability to tune the fundamental frequency of the DVA to reduce the vibration levels of the efficient radiator modes of the base structure.

4.1.4 Effect of the variation in the stiffness distribution pattern of the foam layer

In the following section, the finite element model of the DVA is used for predicting the variation in the response of the DVA on changing the stiffness distribution pattern of the foam layer of the DVA from a symmetric to an asymmetric pattern. The stiffness distribution of the foam layer has been made asymmetric by reducing the stiffness of half of the elements of the foam layer by 40%. Figure 32 shows the numerical model of the DVA consisting of a mass layer covering a layer of foam. The comparison of the numerically computed response of the DVA with symmetric and asymmetric stiffness pattern of the foam layer has been illustrated in Figure 35. The result obtained from the aforementioned study was analyzed to gain an insight in the behavior of these DVA's under the varied stiffness pattern and also to estimate the relative position of the resonance frequency of the rigid-body mode and the rocking mode of the DVA.

Figure 35 represents the change in the DVA response due to a change in the stiffness distribution of the foam layer of the DVA. It can be observed from Figure 35 that under asymmetric stiffness distribution, there is an increase in the number of resonance modes of the DVA. These increased resonance modes of the DVA represent the rigid body mode and the rocking mode of the mass layer plate of the DVA. This provides us with an opportunity to tune these multiple resonances of the DVA to target multiple modes of the base structure. It can also be concluded that under non-uniform stiffness condition the rigid body mode occurs prior to the rocking mode. In addition to this we see a marked variation in the response of the rigid body mode of the DVA for the

asymmetric stiffness case when compared to the symmetric stiffness case. This is due to an overall decrease in the effective stiffness of the porous layer of the DVA in the asymmetric case leading to a reduction of the resonance frequency of the rigid body mode. The conclusion drawn from the aforementioned study is that in case we want to improve the effectiveness of the DVA as a vibro-acoustic attenuation device, we can design the extent of the non-uniformity of the stiffness of the foam to tune the multiple modes of the DVA to target the efficient radiator modes of the base structure.

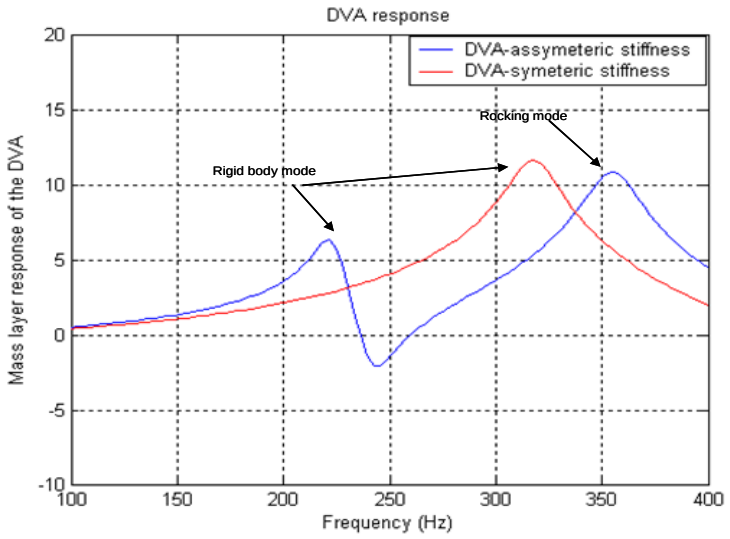

Figure 35. Comparison of the DVA response for the case when the stiffness of the porous media is following a symmetric pattern with the DVA response for the case when the stiffness of the porous media is having an asymmetric pattern

4.2 Parametric studies on the HG blankets

HG blankets have been used in this study as a noise control device. They have a tremendous potential to control the vibrations response of the base structure hence reducing the sound radiated by these base structures into the coupled radiated acoustic domains. To gain an insight in their functioning 3D-FE models of the HG blankets have been validated and parametric studies have been performed on them. In this section a detailed understanding of the behavior of these blankets under varied conditions and configurations would be done in order to enable us to develop customized solution to the vibration and sound problems by developing advanced designs for these blankets.

4.2.1 3D-FE model of the HG blankets

The finite element model of the HG blanket shown in Figure 36 consists of a mass in-homogeneity inserted in a layer of melamine foam. The mass in-homogeneity has been modeled as a point mass and the porous layer is discretized using 60 hexahedral elements following the mathematical formulation derived in Panneton et. al. [18]. In the absence of the coupling between the mass in-homogeneity and the porous media, the mesh density has been found to be satisfactory in capturing the dynamics of the porous layer in the frequency range of interest. The model parameters and the material properties of the mass in-homogeneity and the porous media used in the finite element model of the HG blanket are given in Table 8. A uniform displacement function of unit amplitude is applied at all the nodes at the base of the HG blanket model. The response is measured at the node where the mass in-homogeneity has been inserted in the porous layer. This 3D-FE model has been used for conducting the parametric studies on the HG blankets to understand the effect of the change in the material properties of the foam and mass of the in-homogeneity on the response of the HG blankets. Three parametric studies were performed on the HG blankets. First, the damping of the foam of the HG blanket was varied by decreasing the characteristic viscous and thermal characteristics frequencies and by decreasing the shear modulus loss factor of the foam. The objective of this parametric study is to understand the relative importance of the viscous induced and the stiffness induced damping in the foam layer of the HG blanket. Second, different mass in-homogeneities of 10gms, 5gms and 20gms were used to understand the effect of the change in the mass of the in-homogeneity on the passive damping characteristics and the fundamental frequency of the HG blanket. The third parametric study analyzed the change in the response of the HG blanket caused by numerically modeling the geometrical configuration of the inserted mass rather then modeling it as a point mass. The results obtained from the aforementioned studies have been analyzed to gain an insight in the behavior of the HG blankets.

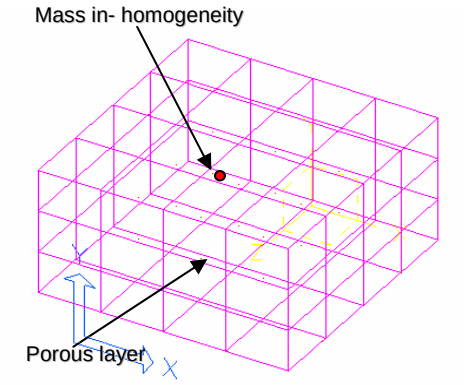

Figure 36. Finite element model of the HG blanket having a point mass in-homogeneity

4.2.2 Effect of the variation in the damping characteristics of the foam layer

In the following section the finite element model of the HG blanket is used for predicting the variation in the response of the HG blankets due to the variation in the damping characteristics of the foam layer of the HG blanket. The numerical model of the HG blanket consisting of a porous layer having a point mass inside it is shown in Figure 36. The variations in the damping characteristics of the foam layer of HG blanket for the parametric study have been tabulated in Table 19. The variation in the numerically computed responses of the HG blankets with varied damping characteristics have been illustrated in Figure 37.

Table 19 Variation in the material properties and mass of the in-homogeneity in the HG blanket

Simulation	Original	Modified-1	Modified-2	Modified-3
Case –I				
Viscous characteristics frequency	48763.13	80	48763.13	96e3
Thermal characteristics frequency	26605.19	52	26605.19	52e3
Case-II				
Loss factor	0.08	0.08	0.008	0.02
Mass in-homogeneity	10	5	20	-----

Figure 37 represents the results obtained from the first parametric study on the HG blanket. In this parametric study the damping characteristics of the foam of the HG blanket was varied in two ways. First, the damping properties of the foam were varied by decreasing the viscous and the thermal characteristics frequency (changing the viscous

damping) but keeping the shear modulus loss factor unchanged. Second, the damping properties of the foam were modified by decreasing the loss factor of the foam keeping the viscous and the thermal characteristics frequency unchanged. Third, all the viscous characteristics frequency, the thermal characteristics frequency and loss factor of the foam layer were modified.

It can be observed from the Figure 37 that the shear modulus loss factor has a major effect on the damping capabilities of the HG blanket as compared to the viscous damping, which is dependent on the viscous and the thermal characteristic frequency. The loss factor of the foam is a lumped damping term that is universally used to numerically model the damping mechanism of the structural part of the porous layer. Based on the numerical modeling, we can conclude that stiffer foam will have better damping capabilities since the damping capability of the foam due to the lumped loss factor is controlled by the shear modulus (N) of the foam. It can be further suggested from the study that in order to increase in the passive damping of the HG blanket one should concentrate on increasing the stiffness of the structural part of the foam rather then concentrating on increasing the viscosity of the structural component of the foam.

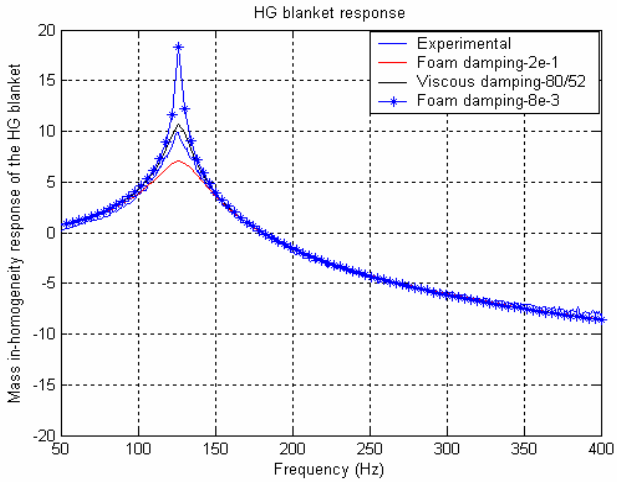

Figure 37. Effect of the change in the damping of the foam layer on the response of the HG blanket

4.2.3 Effect of the variation in the mass of the mass in-homogeneity

In the following section, the finite element model of the HG blanket is used for predicting the variation in the response of the HG blankets due to the variation in the mass of the in-homogeneity inside the foam layer of the HG blanket. The numerical

model of the HG blanket consisting of a porous layer and having a point mass inside it is shown in Figure 36. The variations in the mass of the in-homogeneity inside the foam layer of HG blanket for the parametric study have been tabulated in Table 19. The variation in the numerically computed responses of the HG blanket with the change in the mass in-homogeneities has been illustrated in Figure 38.

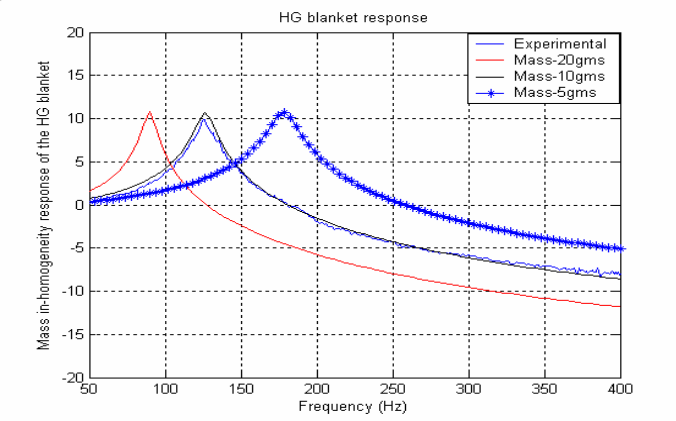

Figure 38. Results from the second parametric study on the HG blanket, where the mass of in the inserted in-homogeneity is varied from 10gms to 5gms, to 20gms

Figure 38 illustrates the results obtained from the second parametric study on the HG blanket, where the mass of the inserted in-homogeneity are varied from 10gms to 5gms and 20gms. It can be observed from the Figure 38 that the reduction in the mass of the in-homogeneity leads to an increase in the resonance frequency and an increase in the mass leads to a decrease in the fundamental frequency of the HG blanket.

4.2.4 Effect of mass in-homogeneity modeling

In the following section, the finite element model of the HG blanket is used for predicting the variation in the response of the HG blanket on modeling the mass in-homogeneity by taking its geometrical configuration into account rather then modeling it as a point mass. Figure 39 shows the numerical model of the HG blanket consisting of a porous layer having a mass in-homogeneity being modeled as a point mass and a block mass respectively. The comparison of the numerically computed responses of the HG blanket with mass in-homogeneity being modeled as a block and as a point mass has been illustrated in Figure 40.

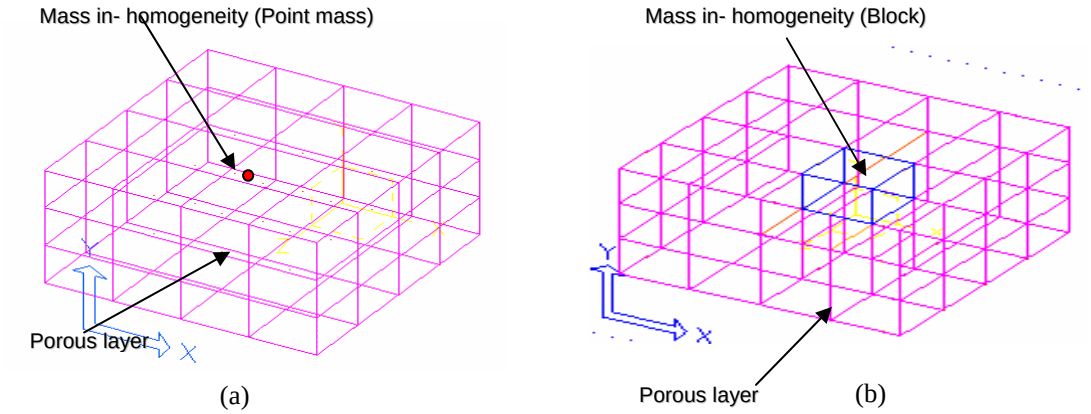

Figure 39. a) Finite element model of the HG blanket having the mass in-homogeneity as a point mass, b) Finite element model of the HG blanket having the mass in-homogeneity as a block mass

The parametric study comprised of changing the modeling of the mass in-homogeneity from a point mass to a block mass keeping the material properties of the foam layer unchanged. The result obtained from the aforementioned study shown in Figure 40 has been analyzed to gain an insight in the behavior of these HG blankets under varied modeling configurations and also to estimate the degree of accuracy of the numerical model of the HG blanket, when the mass in-homogeneity is modeled as a point mass.

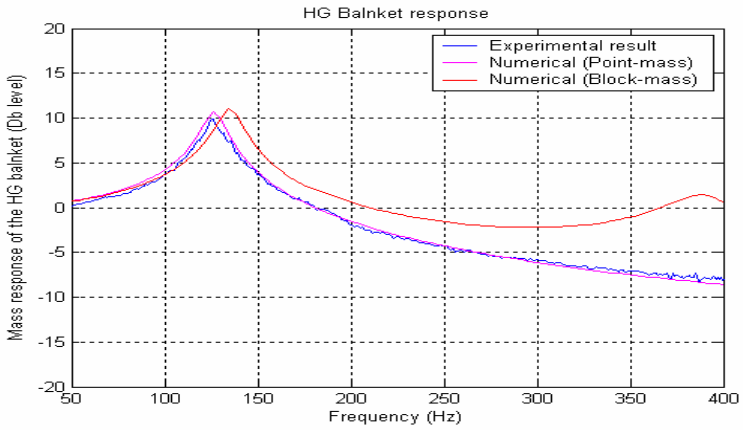

Figure 40. Effect on the HG blanket response on numerically modeling the mass in-homogeneity

Figure 40 depicts the comparison of the HG blanket response for the case when the mass inserted is modeled as a point mass with the HG blanket response for the case when the mass in-homogeneity is modeled as a bock mass having a finite volume and shape. In this parametric study the method of modeling the mass in-homogeneity has

been modified to understand the effect of taking into account the geometric configuration of the mass inserted into the porous media on the response of the HG blankets. It can be observed from the Figure 40 that the first resonance response for both the point mass case and the block mass case is approximately the same. This is the resonance which corresponds to the rigid body mode of the inserted mass, which is identical for both the modeling techniques. In addition, there is a marked variation in the response of the HG blanket for the block mass case at higher resonance frequency when compared with the point mass case. This is evident from the fact that the point mass model is unable to capture the resonance occurring at 390Hz whereas the block mass model can. This can be due to the interaction between the geometry of the mass in-homogeneity and the surrounding foam, which excites vibration in another degree of freedom of the inserted mass. The conclusion drawn from the aforementioned study is that in case we want to improve the prediction accuracy of the 3D-FE model of the HG blanket at the higher frequency, we should model the HG blanket taking into consideration the geometrical configuration of the inserted mass in-homogeneity.

4.3 Parametric study on the 3D-FE fully coupled Plate-DVA assembly

After understanding the physics behind the functionality of the DVA by performing parametric studies on its 3D-FE numerical model, parametric studies were performed on the fully coupled plate-DVA model in order to analyze the effect of the variation in the properties of the DVA on the base plate response. Two parametric studies were performed on the 3D-FE fully coupled numerical model of the plate-DVA assembly. In the first parametric study, the effect of the change in the material of the mass layer of the DVA on the vibration levels of the base structure was studied. In the second parametric study, the effect of the asymmetric stiffness distribution of the foam layer of the DVA on the vibration attenuation of the base structure was analyzed.

4.3.1 3D-FE model of the plate-DVA assembly

The fully coupled finite element model of the plate-DVA assembly in Figure 41 comprises of an aluminum plate clamped at its edges and having a DVA treatment at its center. The base plate has been discretized using 10x15 rectangular plate elements given in Yang [17]. The mass layer covering the foam layer of the DVA has been discretized

using 20 plate elements given in Yang [17]. The porous layer of the DVA is discretized using 60 hexahedral porous elements following the finite element formulation derived by Panneton et. al. [18]. The plate elements are based on the finite element formulation given in equation (44) and the finite element formulation of the porous media is based on equation (55). The coupling between the base plate and the porous layer of the DVA has been modeled by ensuring the continuity of the normal displacements at the interface of the porous and the structural elements. This coupling is captured using the Lagrange multipliers, which is explained in Appendix A. In the absence of the coupling between the base plate and the DVA, the mesh densities of the individual components of the fully coupled FE model have been found to be satisfactory in capturing the dynamics of the individual components in the frequency range of interest. The model parameters and the material properties of the plate, the mass layer and the porous layers of the DVA are given in Table 12. A point force excitation is imparted to the aluminum base plate in the fully coupled FE model and the mean quadratic velocity of the base plate is measured.

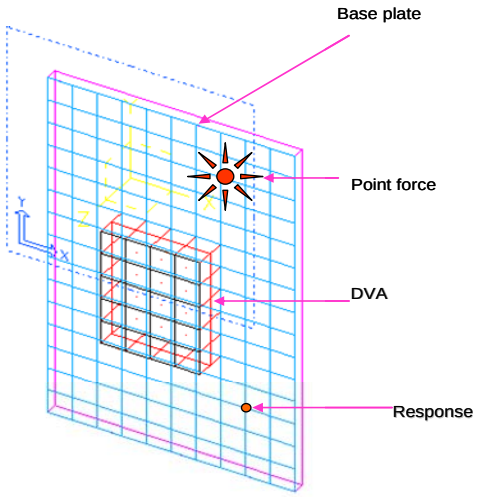

Figure 41. Finite element (FE) model of the plate-DVA assembly used for parametric study

4.3.2 Effect of the change in the material properties of the mass layer plate of the DVA

In this section, the effect of the change in the material of the mass layer plate of the DVA on the vibration levels of the base structure is analyzed. Figure 41 depicts the numerical model of the plate-DVA assembly used in the parametric study. The numerical model primarily consists of a clamped aluminum plate having a DVA treatment at its

center. The change in the material properties of the mass layer plate of the DVA for the parametric study has been tabulated in Table 20. The vibration levels of the base plate are measured in terms of its mean quadratic velocity, which is an average measure of the normal velocities of all the nodes of the base plate. The comparison of the numerically computed mean quadratic velocity of the base plate for the varied material properties of the mass layer of the DVA from aluminum to steel has been illustrated in Figure 42.

Table 20. Variation in the material properties of the mass layer of the DVA

Simulation	Original	Modified
Modulus of elasticity of the mass layer	7.0e10	19.5e10
Poisson's ratio of the mass layer	0.3	0.3
Density of the mass layer	2700	7700
Thickness of the mass layer	0.794e-3	0.794e-3

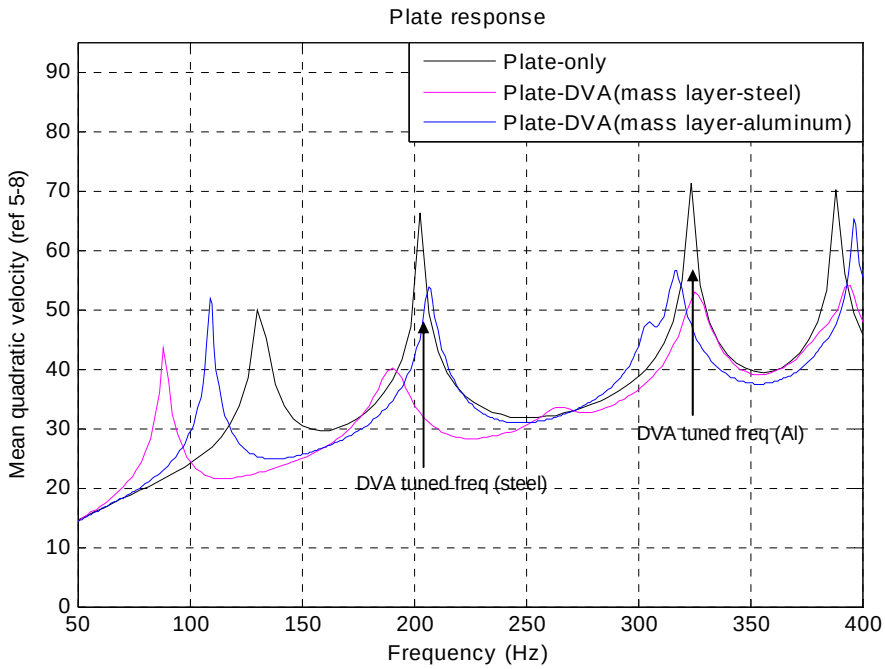

Figure 42. Comparison of the mean quadratic velocity of the base plate with no treatment , for the case when the mass layer of the DVA is made of aluminum and for the case when the when the mass layer of the DVA is made of steel

Figure 42 compares the mean quadratic velocity of the base plate, with and without the DVA treatment on it and also the compares the two with the response of the

base plate when the material of the mass layer of the DVA is changed from aluminum to steel. The mass effect of the DVA on the base plate has been explained in Section 3.11.

The effect of change in the material of the mass layer plate of the DVA from aluminum to steel shown in Figure 42 has two prominent effects on the base structure. First, in the case of the steel mass layer plate the DVA is tuned to the second mode (205 Hz) of the base structure as compared to the third mode (325 Hz) in the case of aluminum mass layer plate. It can be concluded from the aforementioned, by varying the material of the mass layer plate we can change the tuned frequency of the DVA to tune it to a desired mode of the base structure. This provides us with the capability to target efficient radiators of sound. Second, it can be observed that due to an increase in the effective mass of the mass layer plate of the DVA from the aluminum to steel there is a further decrease in the vibration levels of the base structure and a decrease in all its resonance frequencies. This phenomenon can be attributed to the high mass effect of the steel mass layer plate of the DVA on all the modes of the base structure.

4.3.3 Effect of the change in the stiffness distribution pattern of the foam layer of the DVA

In the following section, the finite element model of the plate-DVA assembly shown in Figure 41 consisting of the plate with a DVA treatment at its center is used for performing the second parametric study on the plate-DVA assembly. This study involves predicting the variation in the mean quadratic velocity of the base plate by varying the stiffness distribution of the foam layer of the DVA from being symmetric to asymmetric. In the parametric study, the stiffness of the porous media of the foam layer is changed from that of a symmetric nature to the one of an asymmetric nature by reducing the stiffness of the half the elements of the foam layer of the DVA by 65%. The mean quadratic response of the base plate in the coupled model is measured for both the cases of the porous layer having symmetric and asymmetric stiffness distribution. The comparison of the transfer function between the measured mean quadratic velocity of the base plate and the point force on the plate for both the cases is depicted in Figure 43.

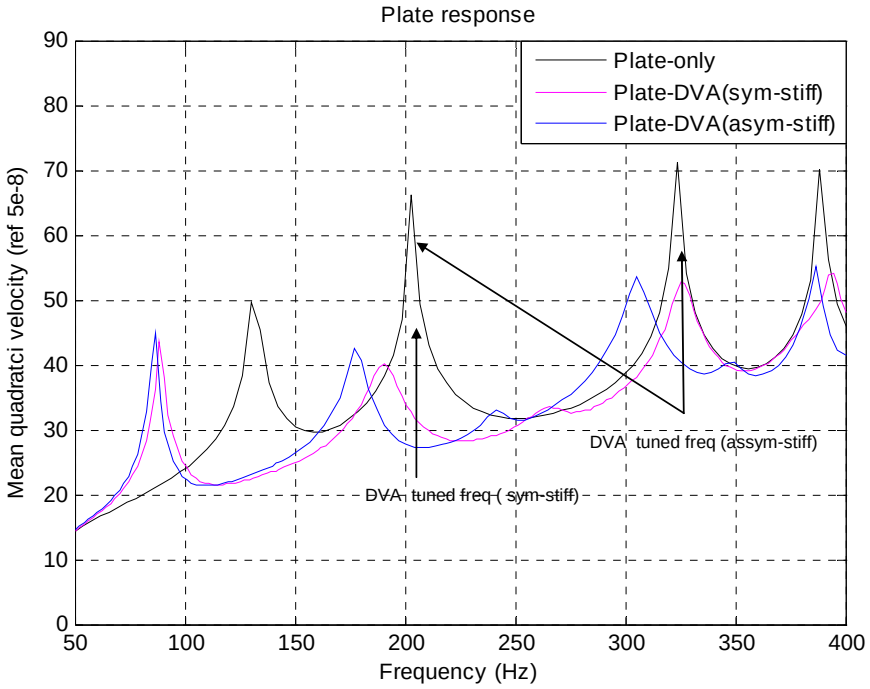

Figure 43. Comparison of mean quadratic velocity of the base plate for the case of no treatment , for the case when the stiffness of the porous layer of the DVA is symmetric and for the case when the stiffness of the porous layer is asymmetric`

It can be observed from the Figure 43 that for the case when the stiffness of the porous layer is symmetric, there is a broad band reduction of the base plate response due to the DVA treatment on it. This is due to the ability of the DVA to act as a vibration absorber at the tuned frequency of the DVA and also to couple into all the major modes of the base plate providing a high reactive force over the whole frequency bandwidth.

The change in the stiffness distribution of the foam layer from one of symmetric nature to an asymmetric nature has two prominent effects on the base structure vibration levels. First, the DVA having the asymmetric stiffness distribution of its foam layer has its resonance frequencies tuned to the second (205 Hz) and the third mode (325 Hz) of the base structure hence acting as a tuned vibration absorber for two distinct frequencies of the base structure. Second, all the resonance frequencies of the plate-DVA system is reduced for the case when the foam layer of the DVA is having an asymmetric stiffness distribution when compared to the symmetric stiffness distribution case. This is primarily due to the fact that there is an effective decrease in the stiffness for the asymmetric case as compared symmetric case. It can be concluded from the aforementioned study that

with the introduction of assymetricity in the stiffness of the foam layer of the DVA we would be able to tune the resonance frequencies of the DVA to multiple resonance frequencies of the base structure. This would enable us to enhance the effectiveness of the DVA in controlling the vibration levels of the base structure for a wide frequency broadband.

4.4 Parametric study on the 3D-FE fully coupled model of the plate-HG-acoustics assembly

In this section, parametric studies on the fully coupled 3D-FE plate-HG-acoustic assembly were performed in order to gain an insight in the interaction of the HG blanket with the structural and acoustic media. Two parametric studies were performed on the 3D-FE fully coupled numerical model of the plate-HG-acoustics assembly. In the first parametric study, the effect of the increasing the depths of the mass in-homogeneity inside the foam layer of the HG blanket on the vibration levels of the base plate and the sound pressure levels (SPL's) inside the radiating acoustic domain was studied. In the second parametric study, the effect of the change in the location of the inserted masses inside the foam layer of the HG blanket on the vibration levels of the base plate and the SPL's inside the radiating acoustic domain was analyzed.

4.4.1 3D-FE fully coupled model of the plate-HG-acoustic assembly

The fully coupled finite element model of the plate-HG-acoustic assembly depicted in Figure 44 comprises of an aluminum plate clamped at its edges having a HG blanket treatment on it and coupled to a radiating acoustic domain. The plate has been discretized using 6x9 rectangular plate elements given in Yang [17]. The porous layers of the HG blanket is discretized using 6x9x3 hexahedral porous elements following the finite element formulation derived by Panneton et. al. [18]. The radiating acoustic cavity is discretized using 6x9x5 acoustic hexahedral elements given in Cook [21]. The plate elements are based on the finite element formulation given in equation (44) and the finite element formulation of the porous media is based on equation (55). The finite element model of the acoustic cavity is based on the mathematical formulation given in equation (25). In the absence of the coupling between the plate, the porous media and the acoustic cavity, the mesh densities used for the modeling of these components has been found to

be satisfactory in capturing the dynamics of these individual components in the frequency range of interest. The model parameters and the material properties of the plate, the porous layers of the HG blanket and the radiating acoustic domain are given in Table 16. A point force excitation is imparted to the aluminum plate in the fully coupled FE model and the mean quadratic response is measured on the plate and inside the radiating acoustic domain. The coupling between the base plate and the porous layer of the HG blanket in the coupled model has been modeled by ensuring the continuity of the normal displacements at the interface of the porous and the structural elements. This coupling is captured using the Lagrange multipliers, which has been explained in detail in Appendix A. In the numerical model of the plate-HG-acoustic assembly the face-2 is the plane of the porous layer adjacent to the base plate and the face-4 is the plane of the porous layer closer to the free surface of the HG blanket. The face-2 of the porous media is on greater depths as compared to the face-4 of the porous media.

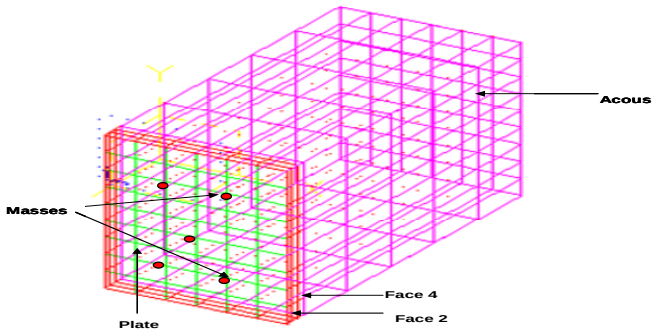

Figure 44. Finite element model of the plate-HG-acoustics assembly having five masses at five different locations on face-4 consisting of 2 weighing 5gms, 2 weighing 8gms and one weighing 3gms which are later shifted to the same positions but at face- 2

4.4.2 Effect of the change in the depth of the mass in-homogeneities

In the following section, the 3D-FE numerical model of the plate-HG-acoustic assembly is used for predicting the variation in the mean quadratic response of the base plate and the radiating acoustic domain by positioning of the mass in-homogeneities at different depths in the HG blankets. The numerical model under study is shown in Figure 44 consisting of mass in-homogeneities at different depths in the porous layer. The

numerically computed mean quadratic response of the base plate and the radiating acoustic domain for different positioning depths of the mass in-homogeneities has been illustrated in Figure 45 (a) and Figure 45 (b) respectively.

The FE model of the assembly shown in Figure 44 consists of 5 masses placed at five different locations on the face-4 (this is the plane of the porous media nearer to the free surface of the HG blanket). This in-homogeneity is of different masses such as 3gms, 2x5gms and 2x8gms. Figure 45 depicts the effect of the shifting the five masses from the face-4 to face-2 on the mean quadratic response of the base plate and the radiating acoustic domain.

It can be observed from the Figure 45 a) and Figure 45 b) that there is a change in the effective attenuation zone of the HG blanket from a low frequency bandwidth (125-210 Hz) to a high frequency bandwidth (200-300 Hz) on shifting the mass in-homogeneities from the face-4 to face-2. This is because there is an increase in the fundamental resonance frequencies of the inserted masses when their position is modified from the face-4 to face-2.

From the aforementioned observation, we can conclude that for developing HG blankets for high frequency attenuations the mass in-homogeneities should be inserted at greater depths and nearer to the base structure. On the other hand for designing the HG blanket for a lower frequency effective bandwidth the masses should be inserted near the free surface of the HG blanket. It can be concluded from the parametric study that these numerical models provide us a tool in calculating the right insertion depths and location of the mass insertions inside the HG blanket to attack specified modes of the base structure. In addition to the capabilities of targeting multiple efficient radiation modes of the base structure, the mass insertions also leads to an increase in the passive damping characteristics of the HG blankets in the region of its tuned frequency. This is evident from the fact that the resonance and off resonance mean quadratic response of the base plate and the radiating acoustic cavity are less when treated with the HG blanket as compared to the case when the base plate is treated with a homogeneous foam blanket. It can be concluded from the aforementioned observation that the mass insertions generate an effective bandwidth for the HG blanket in which the mass in-homogeneities reduces

the vibration response of the targeted modes of the base structures and also cause an increase in the passive damping of the porous layer of the HG blanket.

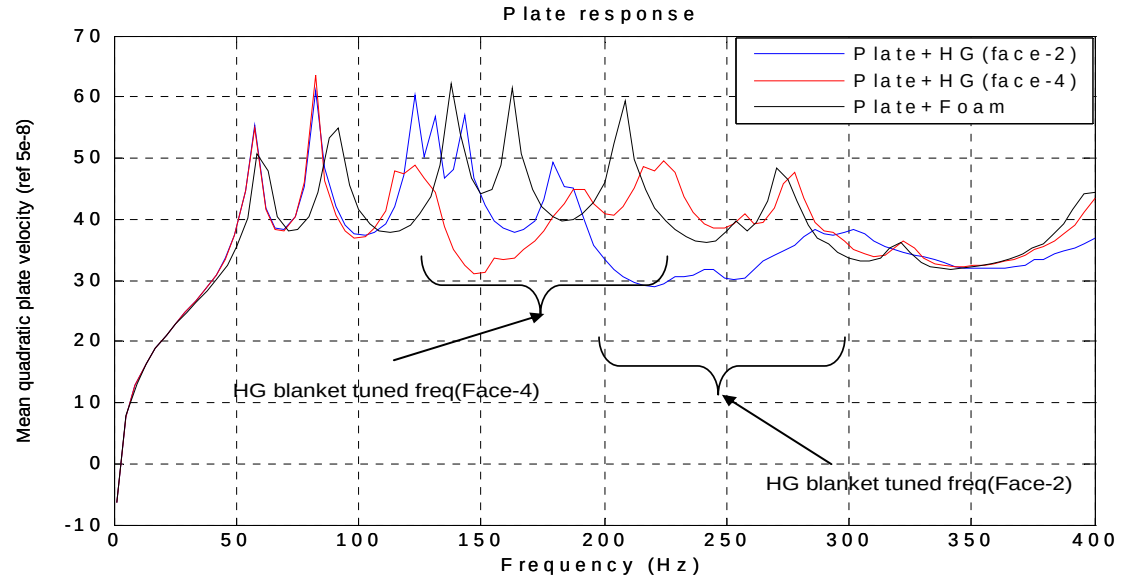

(a)

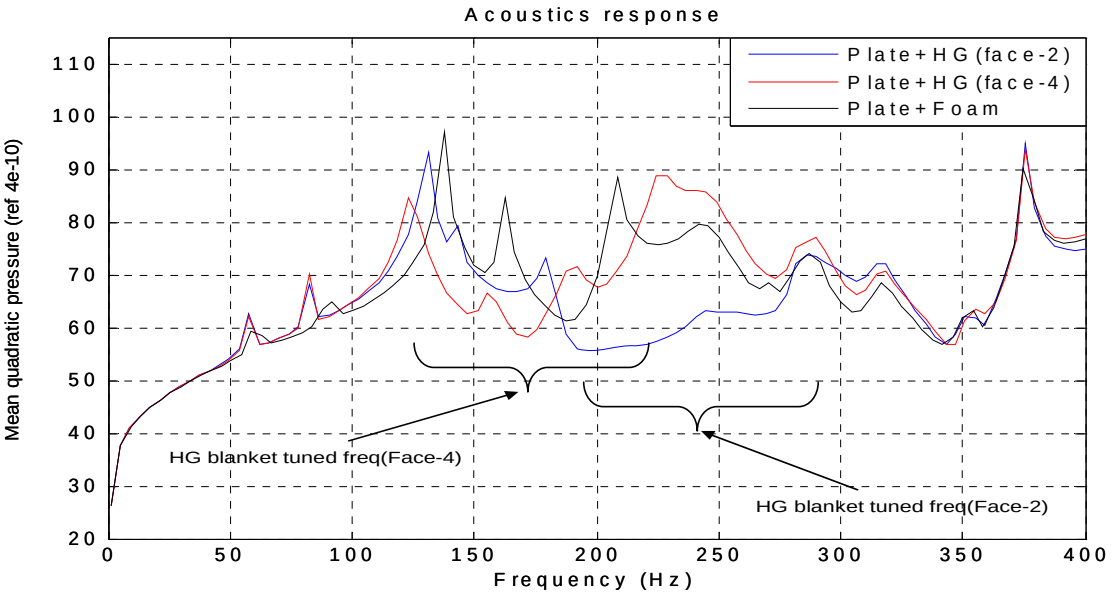

(b)

Figure 45. a) Comparison of the mean quadratic response of the base plate for the case when there are no masses in the HG blanket with the case when the masses were placed on the face 4 and face 2 of the porous media, b) Comparison of the mean quadratic pressure inside the radiating acoustic domain for the case when there are no masses in the HG blanket with the case when the masses were placed on the face 4 and face 2 of the porous media.

4.4.3 Comparison of design location and design depth .vs. random location and design depth

In the following section, the 3D-FE numerical model of the plate-HG-acoustic assembly is used to study the effect of the positioning of the mass in-homogeneity on the mean quadratic response of the base plate and the radiating acoustic domain. The numerical model under study is shown in Figure 44. The comparison of the numerically computed mean quadratic response of the base plate and inside the radiating acoustic domain for the case of the designed location and designed depth (Test case-I) and for the case of the random location and designed depth (Test case -II) has been illustrated in Figure 46 a) and Figure 46 b) respectively. The description of these test cases is given in Table 21.

Table 21. Description of the test cases for the parametric studies on the Plate-HG-acoustic assembly

Test case	Location	Depth
Test case-I		
Designed	yes	yes
Random		
Test case-II		
Designed		yes
Random	yes	

The 3D-FE model of the assembly used in the parametric study is shown in Figure 44. This parametric study entails the placement of the mass in-homogeneities at different locations and on different depths of the porous media. In each of these test cases the HG blanket has been designed to target three efficient radiators of the base structure and has been tuned to an effective frequency bandwidth of 125-210 Hz. After obtaining the mean quadratic response of the base plate and inside the radiating acoustic domain for the Test case-I, a random number generator was used to randomly select the positions of these point masses and place them at designed depths (Test case-II) to target the same the modes of the base structure. The comparison of the measured mean quadratic response of the base plate and inside of the radiating acoustic domain for both the test cases is depicted in Figure 46 a) and Figure 46 b) respectively.

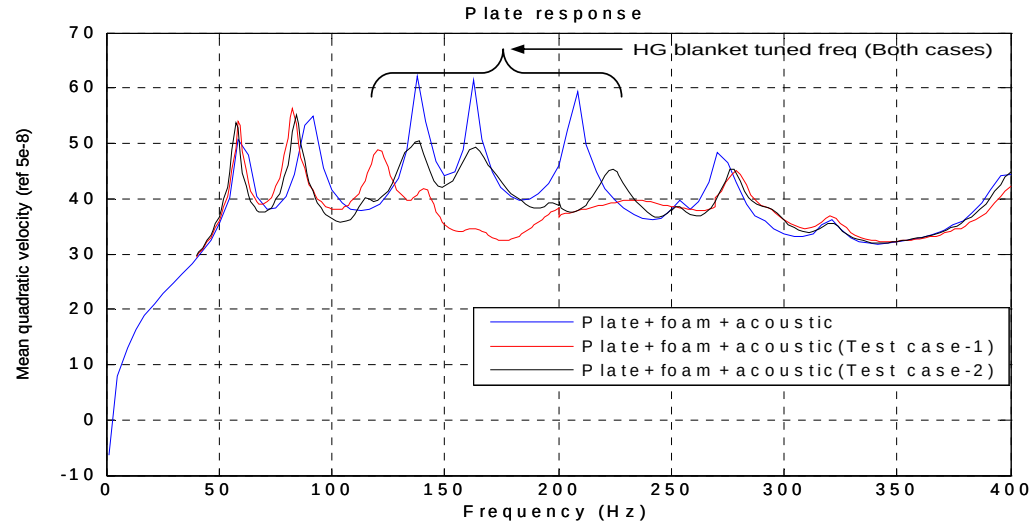

(a)

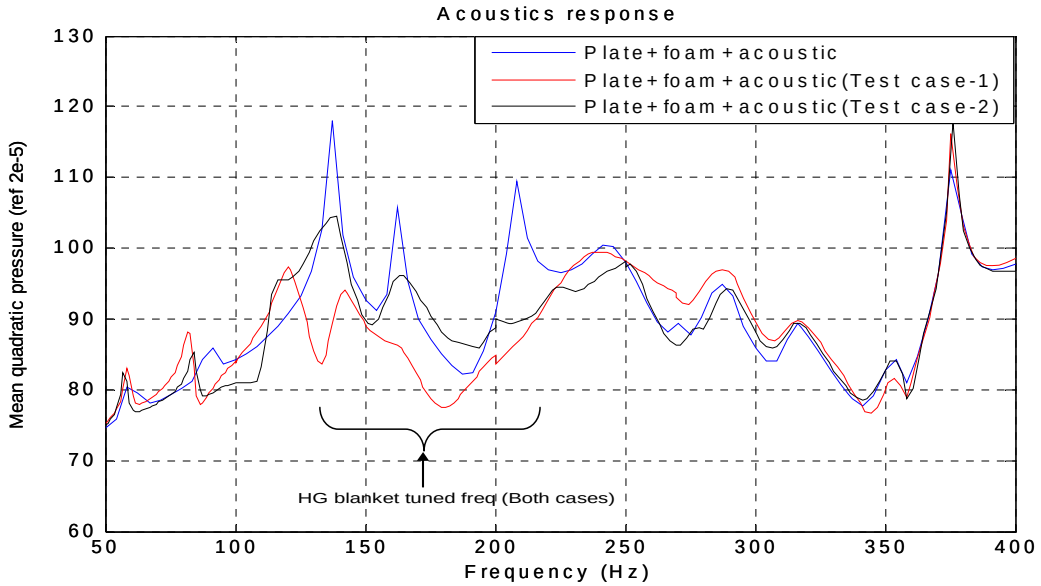

(b)

Figure 46. a) Comparison of the mean quadratic response of the base plate for the case when the base plate is having a foam treatment , a designed location and designed depth (Test case-I) HG blanket treatment and a random location and designed depth (Test case-II) HG blanket treatment, b) Comparison of the mean quadratic pressure inside the radiating acoustic domain for the case when the base plate is having a foam treatment , a designed location and designed depth (Test case-I) HG blanket treatment and a random location and designed depth (Test case-II) HG blanket treatment

It can be observed from Figure 46 that the mean quadratic response of both the base plate and the radiating acoustic domain is less for the Test case-I as compared to the Test case-II. This can be attributed to the fact that in case of less modally dense base structures such as the small plate used in this numerical model, we have a clear

understanding of the efficient radiating modes of the base structure and their corresponding mode shapes. This makes it relatively easier for us to compute the correct location and depths for the mass in-homogeneities for optimizing the vibro-acoustic attenuation capabilities of the HG blankets. On the other hand, for the modally dense base structures the deterministic evaluation of the modal frequencies and their corresponding mode shapes is computationally expensive. It is due to this reason that in the case of modally dense base structures it is desirable to use the random allocation of the mass in-homogeneities in order to optimize the performance of the HG blankets.

4.5 Parametric study of the fully coupled numerical model of the Plate-Multilayer-Acoustics assembly

In this section, parametric studies were performed on the fully coupled plate-MPL-acoustics numerical model in order to analyze the effect of varying the material properties and geometric configuration of the MPL blankets on their vibro-acoustic attenuation capabilities. The parametric study involves replacing a continuous foam blanket with multiple foam blankets (MPL) having different material properties keeping the thickness of the treatment on the base plate unchanged.

The numerical model consisting of a multiple layer treatments is shown in Figure 47. The coupled finite element model used in this study consists of an aluminum plate clamped at its edges with a MPL blanket mounted on it and coupled to a radiating acoustic domain. The MPL blanket used in the 3D-FE models consists of three different foam layers foam A, foam B and foam C. The comparison of the numerically computed mean quadratic response of the base plate and the radiating acoustic domain of these models has been illustrated in Figure 48 a) and Figure 48 b) respectively.

3D-FE model of the plate-MPL-acoustic assembly

The fully coupled finite element model of the coupled plate-MPL-acoustic assembly shown in Figure 47 consists of an aluminum plate clamped at its edges with different MPL treatment on it and coupled to a radiating acoustic domain. The plate has been discretized using 6x9 rectangular plate elements given in Yang [17]. Each of the different porous layers of the MPL blanket is discretized using 6x9x2 hexahedral porous elements following the finite element formulation derived by Panneton et al. [18]. The

radiating acoustic cavity is discretized using 6x9x5 acoustic hexahedral elements given in Cook [21]. The plate elements are based on the finite element formulation given in equation (44) and the finite element formulation of the porous media is based on equation (55). The finite element model of the acoustic cavity is based on the mathematical formulation given in equation (25). In the absence of the coupling between the base plate, the MPL and the radiating acoustic domain, the mesh densities of the individual components of the coupled model have been found to be satisfactory in capturing the dynamics of the individual components in the frequency range of interest. The coupling between the base plate and the porous layer of the MPL in the coupled model has been captured by ensuring the continuity of the normal displacements at the interface of the porous media of the MPL blanket and the structural elements of the base plate using the Lagrange multipliers given in Appendix A.

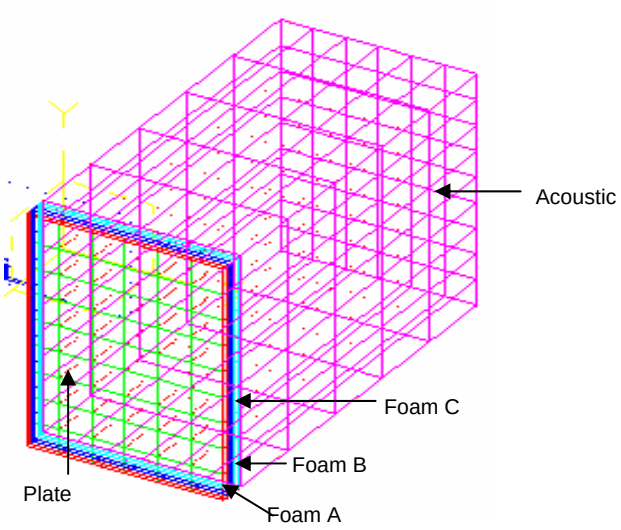

Figure 47. a) Finite element model of the plate-MPL-acoustic assembly where MPL consists of foam A ,foam B and foam C respectively.

In the parametric study the effect of the variation in the material properties and the geometrical configuration of the MPL blanket on the mean quadratic response of the base plate and the radiating acoustic domain is analyzed. Three geometric configurations of the MPL blankets have been used. In the first study, the MPL blanket consists of a 45 mm thick layer of foam A. In the second parametric study, the MPL blanket consists of a 22.5 mm thick layer of foam A and a 22.5 mm thick layer of foam B and the MPL blanket used in the third study consists of a 15 mm thick layer of foam A, foam B and

foam C. The material properties of the porous layers used in these MPL blankets are given in Table 22. A point force excitation is imparted to the aluminum base plate in the fully coupled FE model and the mean quadratic response is evaluated on the base plate and inside the radiating acoustic domain.

Table 22. Model parameters and material properties for the foam A, foam B and foam C

Properties	Foam A	Foam B	Foam C
Number of elements	108	108	108
Boundary condition	Coupled to the plate	Bonded at the sides	Bonded at the sides
Density	31kg/ m^3	16 kg/ m^3	30 kg/ m^3
Young modulus	55KN/ m^2	18 KN/ m^2	28.6 KN/ m^2
Poisson's ratio	0.3	0.3	0.3
Tortuosity	2.52	1.98	7.8
Flow resistivity	87000	65000	25000
Porosity	0.97	0.99	0.90
Atmospheric pressure	1.10325e5	1.10325e5	1.10325e5
Structural damping	0.055	0.1	0.27
Viscous characteristics length	37e-6	37e-6	226e-6
Thermal characteristics length	119e-4	121e-6	226e-6

Figure 48 a) represents the comparison of the mean quadratic velocity of the base plate with different MPL blankets treatment on it. Figure 48 b) presents the comparison of the mean quadratic pressure inside the radiating acoustic domain with the different MPL blankets treatment of the base plate. It can be observed from the Figure 48 that there is a decrease in all the resonance frequencies of the base plate for the case when the base plate is treated with foam (A+B) when compared to the plate response for the case when the base plate is treated with foam (A). On the other hand there is an increase in all the resonance frequencies of the base plate for the case when the MPL consists of all three foam layers (A+B+C) in the MPL treatment. This can be attributed to the relative efficiency of the coupling of the collective stiffness effect and the mass effect of the porous layers with the modes of the base structure. Figure 48 depicts a reduction in the

vibration levels of the base plate and SPL's in the radiating acoustic cavity due to multiple porous layer treatment when compared to the same thickness of uniform treatment. In addition, it can be concluded from the aforementioned observations that the use of porous layers having different material properties will lead to higher damping properties when compared to the use of a continuous foam layer of the same thickness.

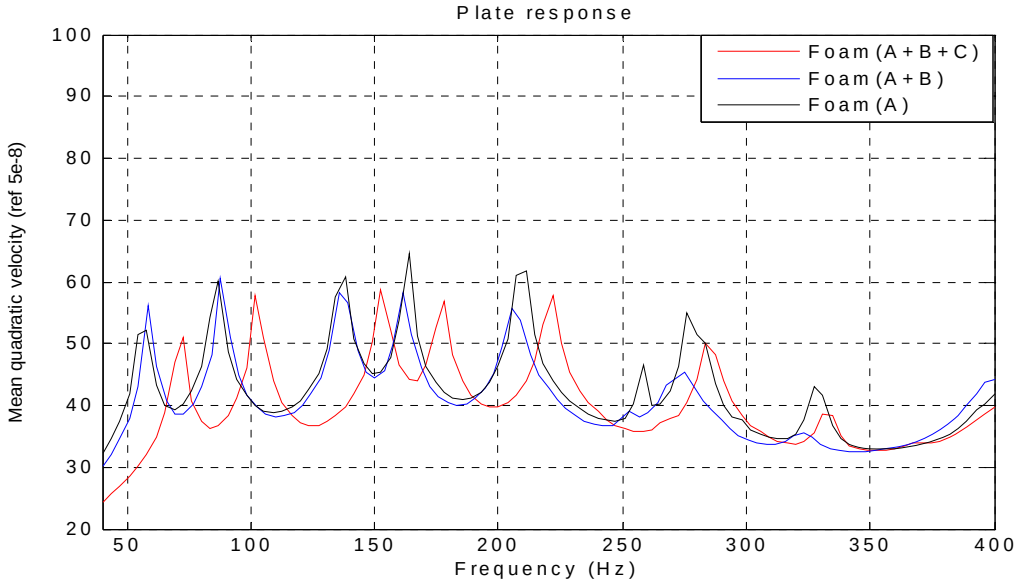

(a)

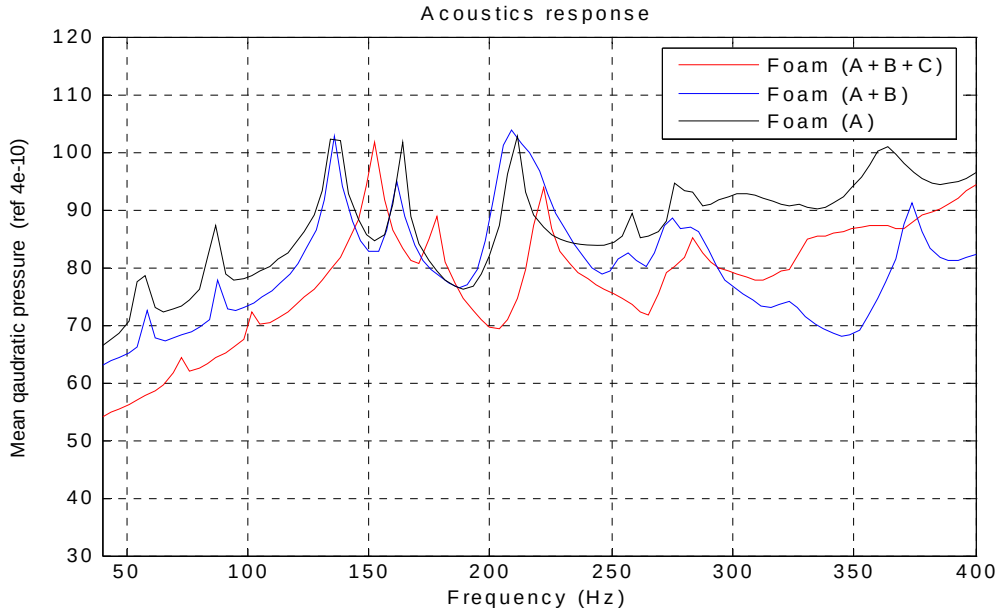

(b)

Figure 48. a) Plate response for different MPL used in the plate-MPL-acoustic model, b) Acoustic response for different MPL used in the plate-MPL-acoustics model

5 *Conclusions and Future work*

The goal of this chapter is to review and summarize the results of this thesis and to present some suggestions for the future work. First, the effectiveness of the various noise and vibration control devices (NCD's) such as the DVA's, the HG blankets and the multi-porous layers (MPL) would be discussed. Second, suggestions would be made for further improvements in the modeling and designing of these devices to achieve optimum performance from them.

5.1 Conclusions

In this section, the final conclusions on the relative effectiveness of these noise and vibration control devices would be discussed from a holistic perspective.

DVA's

In chapter 3 the finite element models of the DVA and the 3D-FE fully coupled model of the plate-DVA assembly has been validated. These fully coupled models were later used in the Chapter 4 for conducting parametric studies on the controlling parameters of the DVA to understand the physics behind their functionality. It was seen from the parametric studies conducted on the DVA that resonance frequency of the DVA is dominated by the stiffness and the thickness of the foam layer and also that the magnitude of the response of the mass layer of the DVA at the resonance is primarily dominated by the loss factor of the foam rather then the damping ratio of the mass layer.

The parametric studies on the plate-DVA assembly indicated that the DVA acts as a true distributed vibration absorber as it splits the targeted mode shape of the base structure and also couples into all the modes of the plate leading to an effective vibration attenuation over a broad band of frequency bandwidth. These are the prime reasons due to which the DVA's show a great potential in controlling vibration levels of the base structures in the experimental studies. In addition to the aforementioned, the numerical modeling also helps us to understand the effect of the asymmetric stiffness of the porous layer of the DVA on the vibration response of the base structure. The numerical modeling of the DVA's and the fully coupled plate-DVA assembly provides us the ability to develop customized DVA's for vibro-acoustic attenuation problems.

HG blankets

In chapter 3 the finite element models of the HG blankets and the 3D-FE fully coupled model of the plate-HG-acoustic assembly has been validated. These fully coupled models were later used in the Chapter 4 for conducting parametric studies on the controlling parameters of the HG blankets to understand the physics behind their functionality. It was seen from the parametric studies conducted on the HG blankets that resonance frequency of the HG blankets is dependent upon the mass of the in-homogeneity and the shear modulus of the foam layer of the HG blanket. It can also be concluded that the damping capabilities of the HG blankets is primarily influenced by the value of the shear modulus loss factor rather then the viscous damping of the porous media. In addition, it can be concluded that the modeling of the mass in-homogeneity as a point mass gives reasonably accurate results at low frequencies but as the target frequencies of the HG blankets increases the geometric configuration of the mass in-homogeneity starts to effect the response of the HG blankets. This observation calls for the numerical modeling of the mass in-homogeneity when designing the HG blankets to target high frequency modes of the base structure.

The studies conducted on the fully coupled plate-HG-acoustic 3D-FE model indicates that as the depth of the mass in-homogeneity increases it leads to an increase in the effective bandwidth of the HG blanket. It can be concluded from the aforementioned observation that for designing the HG blankets to target high frequency response of the base structure the mass in-homogeneities of the HG blankets should be placed at a greater depth from the free surface. In addition, it has been observed from the parametric studies on the fully coupled plate-HG-acoustic model that for relatively less modally dense base structures the vibro-acoustic attenuation capabilities of the HG blankets having the mass in-homogeneities at designed location and designed depths is superior as compared to the case in which the mass insertions are placed randomly but at designed depths. This is due to the fact that in the less modally dense base structures the deterministic computation of the resonance frequencies and their corresponding mode shapes of the base structure is computationally feasible. This provides us the ability to find the optimum location of the mass insertions in the porous media for optimal performance of the HG blanket. On the other hand the deterministic estimation of the modal resonance frequency and their

corresponding mode shapes for a modally dense base structure is computationally expensive and cumbersome. This is the reason that the random allocation of the masses in the HG blankets becomes necessary for the vibration attenuation of the high modal density base structure.

Multi porous layer (MPL)

In this section, conclusions are drawn from the results obtained from the multiple porous layers treatment on the base structures. It can be concluded that the shift of the resonance frequencies of the base plate is dependent upon the relative coupling strength of the collective mass and collective stiffness effect of the MPL blanket with the modes of the base plate. In addition, it can be observed that the use of more foam layers of the porous media as compared to one homogenous porous layer on the base structure keeping the thickness of the treatment unchanged causes increased damping characteristics, which leads to reduced vibration response of the base structure. The MPL blankets although result in a broad band attenuation of the vibration levels of the base structure can not be used as a improvised vibration absorber as they cannot be tuned to a particular resonance frequency of the base structure. The primary source of the reduction of the vibrations levels of the base structure and the SPL's in the radiating acoustic domain due to the MPL blanket treatment is the interaction of the passive damping of the porous layers of the MPL blankets with the structural and acoustic media.

Overall perspective on the noise control devices

In this thesis, the noise and vibration control devices such as the DVA, the HG blankets and the MPL blankets have been shown to have great potential to reduce the vibration response of the base structures and the sound radiated by them into the coupled radiating acoustic domain. In spite of the good performance of these devices in controlling the sound radiation from the base structure, each one of them has its own advantages that can be used for specific vibro-acoustic applications. Distributed vibration absorbers (DVA's) are good for attaining broad band attenuation as they couple into all the modes of the base structure but their effectiveness in reducing the vibration levels of the multiple resonance frequencies of the base structure is limited. This is primarily due to the limited resonance frequencies of the DVA. On the hand, the heterogeneous blankets (HG blankets) are very effective in reducing the vibration levels of the multiple

efficient radiating structural modes. This is due to the fact that multiple mass in-homogeneities inside the foam layer of the HG blanket can be tuned to different resonance frequencies of the base structure. The dynamics of the HG blankets only couples into the modes of the base structure for which they are designed and hence the effect of the HG blanket on the other modes of the base structure is primarily restricted to the mass, the stiffness and the passive damping effect of the foam layer of the HG blanket. The multiple porous layer blankets (MPL blankets) treatment on the other hand is primarily good for improving the effectiveness of a single porous layer treatment by substituting the thickness of the porous layer treatment with a bunch of thin porous layers having different material properties. The MPL blankets are primarily used as a broad band attenuation device rather then an improvised vibration absorber as they don't have the capability to target any particular resonance frequency.

The various noise control devices discussed in the thesis such as the DVA, the HG blanket and the MPL blankets have shown great promise in reducing the vibration response of the base structure and reducing the sound radiated by them into the coupled radiating acoustic domain. Each of these devices have their own strong points and limitations and the numerical models developed in the thesis provides a tool to exploit the strong points of these devices to come up with customized solutions for the vibro-acoustic attenuation problems.

5.2 Recommended future Work

A number of suggestions for the future work are as follows:

Development of the advanced models for the plate-DVA-acoustics and acoustic-plate-DVA-acoustics assembly

The DVA has been shown both experimentally and numerically to be a promising noise and vibration control device. The future work on them would entail the validation of the 3D-FE fully coupled numerical models of the plate-DVA-acoustic and acoustic-plate-DVA-acoustic assembly. These modes will be validated by comparing the numerically computed results from these models with the results obtained from the experimental studies on the models having similar geometries. This would be followed by performing parametric studies on these fully coupled models for optimizing the design

of the DVA to maximize the sound attenuation in the coupled radiating acoustic domain. These parametric studies would also enable us to investigate the contribution of the mass layer plate vibration to the SPL's inside the radiating acoustic domain, which would enable the development of the mass layer designs to minimize the sound radiated by them.

Parametric studies on the acoustic-plate-NCD's-acoustic models

Further improvements in the validation of the acoustic-plate-NCD's-acoustic models by comparing the numerically computed results from these coupled models with the results obtained from experimental investigation of similar models can be achieved. This could be followed by conducting parametric studies on these models. The results from these studies would enable us to understand the difference between the effectiveness of these NCD's under airborne and structural excitations. These studies would also lead to optimized designs of these NCD's for maximum transmission losses under the airborne excitation of the structures.

Develop hybrid vibration absorbers DVA\HG blankets

It can be concluded from the discussion in the thesis that the DVA treatment on the base structure leads to broad band attenuation due to its capability to couple into all the mode of the base structure. The HG blankets on the other hand do not couple into all the modes of the base structure but are extremely effective in targeting multiple resonance efficient radiator mode shapes of the base plate. Numerical models in the future could be used for developing a hybrid vibration absorber which has both the capability of the coupling into all the modes of the base structure and also be able to specifically and effectively target the efficient radiators of sound of the base structure.

Develop 3D-FE models by modeling the inserted mass in-homogeneities.

The parametric studies conducted on the HG blankets have shown that though the modeling of the mass in-homogeneity as a point mass in the FE model gives reasonably accurate results at low frequencies but as the target frequency of the HG blanket increases the geometrical configuration of the inserted masses starts playing a significant role in capturing of the HG blanket response. In future fully coupled numerical models of the plate-HG, the plate-HG-acoustic and the acoustic-plate-HG-acoustic assemblies can be developed taking into consideration the geometric configuration of the mass in-

homogeneities. Studies performed on these models would enable optimizing the design of the HG blankets for targeting the high resonance frequency modes of the base structure.

Accelerate computation

In order to provide faster optimization and to solve large scale vibro-acoustic problems, increased computational efficiency of the code is required. In the future there could be effort on increasing the computational efficiency of the code. This can be done by computationally parallelizing the code.

6 References

[1]H.Frahm. Device for damping vibration of bodies. US patent 989958, 1911.

[2]S.Esteve. Control of sound transmission into payload fairing using distributed vibration absorbers and Helmholtz resonators. PhD thesis, Virginia Polytechnic Institute and State University, 2004.

[3]J.P Den Hartog. *Mechanical Vibrations*. McGraw-Hill, fourth edition,1956.

[4] M.A Franchek, M.W. Ryan, and R.J. Bernhard. Adaptive passive vibration control. *Journal of Sound and Vibration*, 189(5):565-585,1995.

[5] S. J. Huang and R. J. Lian. A dynamic vibration absorber with active vibration control. *Journal of Sound and Vibration*, 178(3): 323-335 ,1994.

[6]M.Yasuda, R. Gu, O.Nishihara, H. Matsuhisa, K. Ukai, and M.kondo. Development of anti-resonance enforced active vibration absorber system. *JSME International Journal*, 39(3):464-469, 1996.

[7]J.Q. Sun, M.R. Jolly, and M. A. Norris. Passive, adaptive and active tuned vibration absorbers – a survey. *ASME Journal of Vibration and Acoustics*, 117:234-241 ,1995.

[8] Y.M. Huang and C.R. Fuller. The effects of dynamic absorber on the forced vibration of a cylinder shell and its coupled interior sound field. *Journal of Sound Vibration* , 200(4):401-418 ,1997.

[9]Y.M. Huang and C. R. Fuller. Vibration and noise control of the fuselage via dynamic absorbers. *ASME Journal of Vibration and Acoustics*, 120:496-502 , 1998.

[10]C. R. Fuller , J. P. Maillard, M.Mercadal, and A. H. vonFlotow. Control of aircraft interior noise using globally detuned vibration absorbers. *Journal of Sound Vibration*, 203:745-761 , 1997.

[11]A. S. Joshi and R. S. Jangid. Optimum parameters of multiple tuned mass dampers for base-excited damped systems. *Journal of Sound Vibration*, 202(5):657-667 , 1997.

[12]T. Aida , S. Toda , N.Ogawa, and Y. Imada. Vibration control of beams by beam-type dynamic vibration absorbers. *ASCE Journal of Engineering Mechanics* , 118(2):248-258, 1992.

[13]T. Aida, K.Kawazoe and S. Toda. Vibration control of plates by plate-type dynamic vibration absorbers. *ASME Journal of Vibration and Acoustics* , 117:332-338 , 1995.

[14]P.Cambou. A Distributed Active Vibration Absorber (DAVA) for active-passive vibration and sound radiation control. Master's thesis, Virginia Polytechnic Institute and State University, 1998.

[15] S. Estève and M. Johnson. Reduction of sound transmitted into a composite cylinder using Distributed Vibration Absorbers and Helmholtz Resonators. *Journal of the Acoustical Society of America*, 112(6), 2840-2848, (2002).

[16]Lawrence E. Kinsler, Austin R.Frey, Alan B. Coppens, James V. Sanders. *Fundamentals of Acoustics*, Jhon Wiley & Sons, fourth edition, 2000.

[17]T.Y. Yang. *Finite element structural analysis*, Prentice Hall , 2nd edition, 1986

[18] R. Panneton and N. Atalla. An efficient finite element scheme for solving the three-dimensional poroelasticity problem in acoustics. *Journal of Acoustical Society of America* .101(6):3287-3298 , 1997.

[19] D. L. Jhonson, J. Koplik, and L. M. Schwartz. *New pore-size parameter characterizing transport in porous media.* Phys. Rev. Lett. 57, 2564-1979 , 1986.

[20]J. F. Allard. *Propagation of sound in porous media*. Elsivier Applied Science , 2nd edition ,1993.

[21] R. Cook, D. Malkus, M. Plesha, R. Witt. Concepts and applications of finite element analysis. Jhon Willey & Sons Inc, 4nd edition ,2001.

Appendix A

Lagrange multipliers for enforcing the constraints

The maximum and the minimum of a function having 2 or more variables that are not independent but must satisfy a prescribed relation can be found by the application of the Lagrange multipliers to the maxima problem. In the case of the structural analysis the function under consideration is the potential energy represented by $\prod_p$, the function variables are the degree of freedom of the system under study represented by $\{D\}$ and the prescribed relation between the degree of freedom are the multiple point constraints. The unknown in this case are the degrees of freedom $\{D\}$ and the Lagrange multipliers used for enforcing the constraints between the degrees of freedom.

The constraint equation relating the degrees of freedom given by Cook [21] is of the form

$$[C]\{D\} - \{Q\} = \{0\} \tag{74}$$

In equation (74) $[C]$ and $\{Q\}$ are the matrices of the constants and $\{D\}$ represent the degrees of freedom of the system.

The potential energy expression given in Cook [21] is of the form

$$\prod_p = \frac{1}{2}\{D\}^T [K]\{D\} - \{D\}^T \{R\} \tag{75}$$

On multiplying $[\lambda]^T$ to the equation (74) and adding it to the left side of the equation (75)

$$\prod_p = \frac{1}{2}\{D\}^T [K]\{D\} - \{D\}^T \{R\} + \{\lambda\}^T ([C]\{D\} - [Q]) \tag{76}$$

In the equation (76) $\{D\}$ and $\{\lambda\}^T$ are the unknowns and the rest of the terms of the equation have been explained in the discussion of the prior equations.

To evaluate the maximum or the minimum of the potential energy expression given in equation (76) with respect to the unknowns of the expression we have

$$\partial \prod_p / \partial\{D\} = 0 \text{ and } \partial \prod_p / \partial\{\lambda\} = 0 \tag{77}$$

Writing the differential formulation of the maxima and the minima of the potential energy in the matrix form given by Cook [21] is of the form

$$\begin{bmatrix} K & C^T \\ C & 0 \end{bmatrix} \begin{Bmatrix} D \\ \lambda \end{Bmatrix} = \begin{Bmatrix} R \\ Q \end{Bmatrix} \tag{78}$$

In the equation (78) $\{\lambda\}$ can be termed as the force in the system due to the constraints on its degree of freedoms.

The use of Lagrange multipliers in enforcing the constraints between the degrees of freedom of a system leads to an increase in the number of unknown in the system leading to an increase in the order of the system to be solved and hence can only be used for the system in which the numbers of constraints are less. On the other hand in this procedure of enforcing the constraints between the degrees of freedom of a system the stiffness matrix remains unchanged when the constraints are applied therefore the constraints can be changed without the refactoring of the [K] matrix. This is of vital importance for the systems on which there are multiple constraints on the same variables of the system. The Lagrange multipliers have been used in this thesis for enforcing the continuity of displacement between the porous and the plate media at their interface.

Vitae

Ashwini Gautam was born on November 7, 1979 in Merrut ,India. After graduating from the high school in 1996, he enrolled in the Jamia Millia Islamia Faculty of Engineering and Technology. After the completion of the undergraduate studies he worked for Jupiter No Break Systems Ltd. in India. His projects during the work experience involved the development of the advanced diesel generating sets for salient application of the industry. In 2004, Ashwini joined the Vibration and Acoustics Laboratories at Virginia Tech, where he started his master's under the guidance of the Dr. Chris R. Fuller. His project involved the design of advanced noise control devices using the finite element approach. Ashwini has been employed in Cummins and his work profile would involve the structural and acoustic analysis of the diesel engines.